universität wien

MASTERARBEIT / MASTER'S THESIS

Titel der Masterarbeit / Title of the Master's Thesis

„Heavy Jet Mass with Massive Quarks“

verfasst von / submitted by

Christopher Lepenik, BSc

angestrebter akademischer Grad / in partial fulfilment of the requirements for the degree of

Master of Science (MSc)

Wien, 2016 / Vienna, 2016

Studienkennzahl lt. Studienblatt / degree programme code as it appears on the student record sheet:	A 066 876
Studienrichtung lt. Studienblatt / degree programme as it appears on the student record sheet:	Masterstudium Physik UG2002
Betreut von / Supervisor:	Univ.-Prof. Dr. André H. Hoang

Abstract

In this thesis we investigate the effects of massive primary quark production in the process $e^+e^- \to$ hadrons, using an event-shape variable called "heavy jet mass" (HJM). We calculate the cross section with respect to this observable up to N^{2}LL accuracy, including non-perturbative effects and renormalon subtractions. First we perform the fixed order QCD calculation with massive quarks at next to leading order in the strong coupling constant α_s and discuss the problem of large logarithms in the dijet region. To resum these logarithms we introduce soft-collinear effective theory (SCET), an effective field theory well suited for the region of interest where just jets of collinear particles and soft radiation are present in the final state. The part of the cross section described by SCET, called the "singular contribution", can be factorized into several functions, describing the dynamics at the different characteristic energy scales present in the dijet region. This formula is used to resum the large logarithms by applying a renormalization group evolution for each factor. To obtain accurate predictions we also implement non-singular contributions, which are not described by leading order SCET and become important for large HJM values, and non-perturbative corrections to account for hadronization, which is especially important for small HJM values. Furthermore, we carry out renormalon subtractions to improve perturbative convergence. We then check the convergence of our results and examine bottom mass effects by comparing our results for massive and massless bottom quark pair production at different energies. This is done for the tagged bottom cross section as well as for all-flavor production.

Zusammenfassung

In dieser Arbeit benutzen wir die Event-shape Variable "Heavy Jet Mass" (HJM), um die Effekte von massiver primärer Quarkproduktion im Prozess $e^+e^- \to$ Hadronen zu untersuchen. Wir berechnen den Wirkungsquerschnitt bezüglich dieser Observable mit der Genauigkeit N^{2}LL, wobei wir auch nicht-perturbative Effekte und die Subtraktion des führenden Renormalons miteinbeziehen. Zuerst führen wir die fixed-order QCD Rechnung mit massiven Quarks in erster Ordnung in der starken Kopplungskonstante α_s durch und diskutieren das Problem der großen Logarithmen in der 2-Jet Region. Um diese großen Logarithmen zu resummieren, führen wir die soft-collinear effective theory (SCET) ein, eine effektive Feldtheorie, welche gut geeignet ist um die Phasenraumregion, in der die großen Logarithmen auftreten und in welcher nur Jets von kollinearen Teilchen und niederenergetische Strahlung im Endzustand vorhanden ist, zu beschreiben. Der Teil des Wirkungsquerschnitts welcher von SCET beschrieben wird, auch "singuläre Beiträge" genannt, kann in mehrere Funktionen faktorisiert werden. Diese Funktionen beschreiben die Dynamik an den unterschiedlichen charakteristischen Energieskalen, welche in der 2-Jet Region auftreten. Diese Faktorisierungsformel wird verwendet um die großen Logarithmen zu resummieren, indem für jeden Faktor eine Renormierungsgruppen-Evolution angewendet wird. Um exakte Vorhersagen zu erhalten, implementieren wir auch die nicht-singulären Beiträge, welche nicht durch die führende Ordnung in SCET beschrieben werden und besonders wichtig für hohe HJM-Werte sind. Weiters inkludieren wir nicht-perturbative Korrekturen, welche der Hadronisierung Rechnung tragen und besonders für niedrige HJM-Werte von Bedeutung sind, und Renormalon-Subtraktionen, welche die störungstheoretische Konvergenz stark verbessern. Anschließend testen wir die Konvergenz unserer Ergebnisse und untersuchen Bottom Quark Masseneffekte, indem wir unsere Ergebnisse für massive und masselose Bottom Quark Paar Produktion bei unterschiedlichen Energien vergleichen. Wir tun dies für den tagged Bottom Wirkungsquerschnitt, sowie für die Produktion aller Flavor.

Contents

Chapter 1

Introduction

Today we are living in an era of precision physics, in which continuously increasing accuracy at collider experiments requires high precision calculations to do a proper analysis of experimental data and discover potential deviations from standard model predictions.

In this context quantum chromodynamics (QCD), the quantum field theory of strong interactions, is especially interesting for phenomenological as well as theoretical reasons. In high energy processes, where strongly interacting particles are created, the measured final states are often found in the form of (hadronic) jets, which are objects containing highly boosted particles, collineated in specific directions. Due to this fact, a very popular set of observables to test QCD are event shapes, which measure the geometric form of final state particles [1, 2] and therefore can be used to study jet properties like the distribution of their broadening. This gives not only important hints to understand basic features of QCD, but also allows to perform very precise determinations of the strong coupling constant α_s due to the high sensitivity of event shapes to this fundamental constant [1, 2].

For this purpose often the process $e^+e^- \to$ hadrons is considered, since no parton distribution functions are involved and theoretical predictions are especially clean. Some popular event shapes used in this context are thrust, C parameter, and heavy jet mass, which belong to the class of "2-jet event shapes", i.e. they give a minimal or maximal value if the final state consists of only two pencil-like back-to-back jets.

It is observed that fixed order QCD calculations contain logarithmic contributions which become large close to the dijet region and spoil the perturbative expansion in α_s, since corrections of higher orders are not necessarily small. This is of course a big problem, since it leads to bad convergence and poor quality of predictions. The origin of this problem is the existence of a strong hierarchy between the characteristic scales which affect the dynamical process in this region of phase space, manifesting in logarithms containing fractions of these widely separated scales. To cure this, one has to resum the logarithms to all orders.

A very convenient way of doing this is by using "soft-collinear effective theory" (SCET) [3–9], an effective field theory well suited for the dijet region, which makes the relevance of different scales explicit at the Lagrangian level. It can be shown that the part of the cross section described by SCET (called the singular contribution) factorizes into distinct functions, where each describes the dynamics at one characteristic scale. For these functions, separate renormalization group evolutions can be derived, which individually resum the corresponding logarithms [10–12].

In the past many sudies concerning event shape distributions in e^+e^- collisions have been carried out for massless quark production. For center of mass energies Q that are much larger than the quark mass m (e.g. LEP energies with respect to the bottom quark) this is a valid approximation, since mass effects are suppressed by factors of m/Q and give only small corrections. Nevertheless, the full mass dependence plays an important role in some phenomenological studies and, making predictions with higher and higher accuracy, detailed information about mass dependencies of various event shapes should be known at some point.

Considering recent studies, full mass corrections were included in the thrust analysis in [10] and leading order mass effects were considered in the heavy jet mass analysis in [13] using a Monte Carlo approach, where it was pointed out that the full form of mass corrections should be examined at some point. In context of a recent precise α_s determination from C parameter distributions in [14], which assumed massless quarks, the exact massive contribution at NNLL order was derived in [15], which gave hints that this assumption is valid at least to this accuracy.

In this thesis we examine the full primary quark mass dependence of the heavy jet mass cross section for $e^+e^- \to$ hadrons. To do so we derive this quantity with massive primary quarks at order α_s, including NNLL resummation, non-perturbative corrections, and renormalon subtractions.

This thesis is organized as follows. In chapter 2 we introduce event shapes in more detail. In particular, we discuss the heavy jet mass and related quantities.

In chapter 3 we calculate the massive heavy jet mass cross section in fixed order QCD up to order α_s, which was not known analytically before. At the end we point out the problem of large logarithms and consequently the importance of log resummation.

To set up the theoretical basis for resummation, we give a short introduction to soft-collinear effective theory in chapter 4 and prove factorization of the singular heavy jet mass cross section in chapter 5.

In chapter 6 we collect all ingredients for our final result of the heavy jet mass cross section, which is used in our analysis. This includes in particular the calculations of the functions that appear in the factorized cross section, the solution of their renormalization group equations to resum the contained logarithms up to NNLL, the determination of the non-singular part, the non-perturbative corrections via a model function convolution, and details concerning the renormalon subtractions.

Finally, in chapter 7 we analyze our results and draw first conclusions. We check convergence and the impact of bottom mass induced corrections at different energies. At the end, all-flavor production is considered, where again the size of mass related contributions is investigated.

Chapter 2

Event-Shapes and the Heavy Jet Mass

In this chapter we will explore event-shapes and their usage, especially the definition and basic properties of the heavy jet mass (HJM). In connection to this observable, a very short introduction to the popular event-shape "thrust" is given and different definitions of hemispheres are discussed.

"Event-shapes", also called "shape variables", are observables which can be used to measure the geometric form of final state particles in collider experiments, especially in e^+e^- collisions and deep inelastic scattering [1, 2]. Since these event-shapes are very sensitive to strong interaction dynamics, they are often used to determine the strong coupling constant α_s via fitting theoretical predictions to experimental data.

Since the probability of a quark radiating soft or collinear gluons is enhanced, the objects observed in a detector are mostly soft radiation and "jets", which are objects consisting of highly boosted collinear particles. Since event-shapes measure the global geometric properties of an event, the characteristics of jets, and consequently of QCD, can be explored by studying their distributions.

One of the most popular event-shapes is called "thrust" [16], which is defined as

$$T := \max_{\vec{n}} \frac{\sum_i |\vec{n} \cdot \vec{p}_i|}{\sum_i |\vec{p}_i|}, \tag{2.1}$$

where the sum runs over all final state particles with momenta $\vec{p}_i$, and $\vec{n}$ is a unit vector which is chosen so that the whole expression is maximized. Very often the parameter $\tau = 1 - T$ is used (also called thrust most of the times), which is minimal for a 2-jet event with thin pencil-like jets, and maximal for a spherical final state. Event-shapes which are minimal or maximal for a 2-jet event are called "2-jet event-shapes". It should be also noted that the region of an event-shape distribution, which is associated with a dijet event is called the "peak region", while the regions further away are called the "tail" and "far-tail region". This naming becomes obvious when looking at the shape of the distribution as in subsection 6.8.

The direction of $\vec{n}$ which maximizes T is called the thrust axis. In a 2-jet event, it coincides with the jet axis up to power suppressed corrections related to soft radiation. The plane perpendicular to the thrust axis divides the event into two hemispheres, which can be used to define other event-shapes like the invariant mass of the left and right hemisphere (indicated with subscripts l and r respectively) [1, 17]

$$\rho_{l,r} := \frac{\left(\sum_{i\in\mathcal{H}_{l,r}} p_i\right)^2}{\left(\sum_i E_i\right)^2}, \tag{2.2}$$

where $\mathcal{H}_i$ denotes the respective hemisphere. Note that this is the usual definition of hemispheres used in experiments [18], in contrast to other types as explained at the end of this section.

The heavy jet mass, which we will consider in this theses, is defined as the heavier of the two hemisphere masses [1, 17], so

$$\rho := \max(\rho_l, \rho_r). \tag{2.3}$$

Since the invariant mass of a hemisphere is minimal for exclusively collinear particles, and the heavy jet mass is by definition the heavier one, a minimal value for ρ forces also the light hemisphere to consist of a pencil-like jet. Consequently, like thrust, heavy jet mass is a 2-jet event-shape. On the other hand it can be shown that the maximal value of ρ for arbitrary many particles is not a spherical configuration as it is for thrust [19].

It is clear that for massless particles ($m = 0$) the minimal value of the heavy jet mass is

$$\rho_{\text{min}}^{m=0} = 0. \tag{2.4}$$

Considering massive primary quarks, the basic situation for the minimal value is analogous and thus

$$\rho_{\text{min}} = \hat{m}^2, \tag{2.5}$$

where

$$\hat{m} := \frac{m}{Q}. \tag{2.6}$$

It is easy to show that for three massless particles (corresponding to $\mathcal{O}(\alpha_s)$) $\rho^{(3),m=0} = \tau^{(3),m=0}$, thus the maximal value for this setting is

$$\rho_{\text{max}}^{(3),m=0} = \frac{1}{3}, \tag{2.7}$$

as for thrust. For 2 massive primary quarks the value is

$$\rho_{\text{max}}^{(3)} = \frac{1}{3}\left(5 - 4\sqrt{1 - 3\hat{m}^2}\right), \tag{2.8}$$

as we will see in section 3.4. Finding the final state configuration corresponding to the maximal value of the heavy jet mass for arbitrary many particles is a very interesting kinematic and geometric problem. The value for the massless case is expected to be near [19]

$$\rho_{\text{max}}^{m=0} = 0.477, \tag{2.9}$$

while a situation including massive primary quarks has not been considered yet. Since the exact value of ρ_{max} is not important for the results in this thesis, this problem will be investigated in future works.

For completeness it should be noted that there are two different definitions of heavy jet mass in the literature [19], which are only equal for three massless particles. In contrast to the definition given above, which will be used in our analysis, the other one defines the hemispheres not through the thrust axis but by minimizing the hemisphere mass sum [20–22]

$$\mathcal{H}_{l,r} : \min_{\mathcal{H}_l, \mathcal{H}_r} (\rho_l + \rho_r), \tag{2.10}$$

which is in fact the way hemispheres were originally introduced theoretically [20]. In this case the maximal value for arbitrary many massless particles is 1/3, as shown in [21]. For three massless particles, both hemisphere definitions are equivalent.

For further theoretical considerations regarding heavy jet mass differential cross sections with massless particles we refer to [17, 23–25], while a more extensive analysis can be found in [13].

Chapter 3

Fixed-Order Calculation

In this chapter we will present the $\mathcal{O}(\alpha_s)$ fixed order QCD calculation of the $\mathrm{e}^+\mathrm{e}^- \to q\bar{q}$ differential cross section with respect to the heavy jet mass (HJM) with massive primary quarks. We ignore the masses of the incoming electron-positron pair, since energies much higher than the electron mass scale are considered. QED loop effects are omitted as well, since in the considered energy range $\mathcal{O}(\alpha_{em}) \sim \mathcal{O}(\alpha_s^2)$.

After some general considerations we calculate the Born cross section, and the virtual and real radiative contributions at $\mathcal{O}(\alpha_s)$.

The virtual contribution is proportional to a delta function and can be obtained from the total virtual cross section. For the real radiation contribution the calculation in $d = 4 - 2\varepsilon$ dimensions is very complicated and, as it turns out, not necessarily needed. To get the full result, we first calculate the real radiation contribution to the cross section in $d = 4$ dimensions, which is not properly regularized and is valid only in the region $\rho > \rho_{min}$. The structure at $\rho = \rho_{min}$ is determined afterwards in a second calculation in the soft limit and $d = 4 - 2\varepsilon$ dimensions.

At the end we will shortly discuss the problem of large logarithms, which shows the need of resummation e.g. by using effective field theory methods. In order to have a complete description of the cross section, we use the factorized SCET cross section to resum large logs in the dijet region, as well as the non-singular contributions, which can be extracted from the full QCD result and are important away from the dijet region. This will be done in later chapters.

3.1 General Considerations and Leptonic Part

Let us start by noting some properties of the cross section which simplify the calculation.

The general formula of a cross section for the process $e^+e^- \to X$ in $d = 4 - 2\varepsilon$ space-time dimensions reads

$$\sigma = \frac{\tilde{\mu}^{-2\varepsilon}}{2Q^2} \int \left(\prod_{i\in X} \frac{\mathrm{d}^{d-1}p_i}{(2\pi)^{d-1}} \frac{1}{2p_i^0} \right) (2\pi)^d \delta^{(d)} \left(q - \sum_{i\in X} p_i \right) \left| \mathcal{M}(e^+e^- \to X) \right|^2, \tag{3.1}$$

where Q is the center of mass energy, p_i is the momentum of the i^{th} final state particle, k_1 and k_2 are the momenta of the electron and positron, and $q = k_1 + k_2$ is the momentum of the virtual γ or Z with $q^2 = Q^2$.

We use dimensional regularization to regularize the amplitude $\mathcal{M}$ as well as the phase space integration. The factor

$$\tilde{\mu}^2 := \mu^2 \frac{\mathrm{e}^{\gamma_E}}{4\pi}, \tag{3.2}$$

is the renormalization scale used in the $\overline{\text{MS}}$ scheme. Note that a factor $\tilde{\mu}^{-2\varepsilon}$ was added in Eq. (3.1) to obtain the right energy dimensions when expanding in $\varepsilon \ll 1$. Of course in the limit $\varepsilon \to 0$ the final result is independent of this scale.

At $\mathcal{O}(\alpha_{\text{em}})$ the amplitude can be written in the factorized form

$$\mathcal{M} = \frac{i4\pi\alpha\tilde{\mu}^{2\varepsilon}}{Q^2}\Bigg\{\left[\left(Q_eQ_f + \frac{v_ev_f}{1-\hat{m}_Z^2}\right)\langle X|\mathcal{J}_v^\mu|0\rangle + \left(\frac{v_ea_f}{1-\hat{m}_Z^2}\right)\langle X|\mathcal{J}_a^\mu|0\rangle\right]\bar{v}(k_1)\gamma_\mu u(k_2) + \left[\left(\frac{a_ev_f}{1-\hat{m}_Z^2}\right)\langle X|\mathcal{J}_v^\mu|0\rangle + \left(\frac{a_ea_f}{1-\hat{m}_Z^2}\right)\langle X|\mathcal{J}_a^\mu|0\rangle\right]\bar{v}(k_1)\gamma_\mu\gamma_5 u(k_2)\Bigg\}, \tag{3.3}$$

with $\alpha \equiv \alpha_{\text{em}}$, Q_f the charge of the produced fermion, Q_e the charge of the incoming lepton, and $\hat{m}_Z := m_Z/Q$ is the mass of the Z boson divided through the center of mass energy. The v_i and a_i factors arise from the Z coupling and read

$$v_i := \frac{T_{3,L}^f - 2Q_i\sin^2\theta_W}{\sin\theta_W}, \qquad a_i := -\frac{T_{3,L}^i}{\sin(2\theta_W)}, \tag{3.4}$$

where θ_W is the weak mixing angle, and $T_{3,L}^i$ is the weak isospin of the incoming lepton and the outgoing fermion respectively. The quark current reads $\mathcal{J}_i^\mu(x) = \bar{\psi}(x)\Gamma_i^\mu\psi(x)$ with $\Gamma_v^\mu := \gamma^\mu$ for the vector, and $\Gamma_a^\mu := \gamma^\mu\gamma_5$ for the axial current.

When squaring the amplitude and averaging over the lepton spins, the following structures have to be considered:

$$\begin{aligned}
s_{\mu\nu}^{(1)} &:= \frac{1}{4}\sum_{\text{spins}}\left[\bar{v}(k_1)\gamma_\mu u(k_2)\right]^\dagger\left[\bar{v}(k_1)\gamma_\nu u(k_2)\right] = \frac{1}{4}\text{Tr}\left[\not{k}_2\gamma_\mu\not{k}_1\gamma_\nu\right] \\
&= g_{\mu\alpha}g_{\nu\beta}(k_1^\beta k_2^\alpha + k_1^\alpha k_2^\beta) - g_{\mu\nu}\frac{Q^2}{2}, \\
s_{\mu\nu}^{(2)} &:= \frac{1}{4}\sum_{\text{spins}}\left[\bar{v}(k_1)\gamma_\mu\gamma_5 u(k_2)\right]^\dagger\left[\bar{v}(k_1)\gamma_\nu\gamma_5 u(k_2)\right] = \frac{1}{4}\text{Tr}\left[\not{k}_2\gamma_\mu\not{k}_1\gamma_\nu\right] = s_{\mu\nu}^{(1)}, \\
s_{\mu\nu}^{(3)} &:= \frac{1}{4}\sum_{\text{spins}}\left[\bar{v}(k_1)\gamma_\mu\gamma_5 u(k_2)\right]^\dagger\left[\bar{v}(k_1)\gamma_\nu u(k_2)\right] = -i\epsilon_{\alpha\nu\beta\mu}k_1^\alpha k_2^\beta, \\
s_{\mu\nu}^{(4)} &:= \frac{1}{4}\sum_{\text{spins}}\left[\bar{v}(k_1)\gamma_\mu u(k_2)\right]^\dagger\left[\bar{v}(k_1)\gamma_\nu\gamma_5 u(k_2)\right] = -s_{\mu\nu}^{(3)}.
\end{aligned} \tag{3.5}$$

Since we are not interested in the directions of the final state jets with respect to the beam axis, we average the expressions in (3.5) with respect to the direction of the incoming leptons. This simplifies the subsequent calculations considerably.

To figure out the averaged expressions, we choose the most general ansatz

$$l_{\mu\nu}^{(i)} := A^{(i)}\frac{q_\mu q_\nu}{Q^2} + B^{(i)}g_{\mu\nu}, \tag{3.6}$$

and derive the unknown coefficients $A^{(i)}$ and $B^{(i)}$ via demanding

$$\int\frac{\text{d}^{d-2}\Omega}{\Omega_{\text{tot}}^{d-2}}s_{\mu\nu}^{(i)} \stackrel{!}{=} l_{\mu\nu}^{(i)}, \tag{3.7}$$

where

$$\Omega_{\text{tot}}^{d-2} = \Omega_{\text{tot}}^{2-2\varepsilon} = (4\pi)^{1-\varepsilon}\frac{\Gamma(1-\varepsilon)}{\Gamma(2-2\varepsilon)}, \tag{3.8}$$

is the $(d-2)$-dimensional total solid angle.

Since $s^{(3)}_{\mu\nu}$ and $s^{(4)}_{\mu\nu}$ are antisymmetric, the respective A and B are zero. On the other hand, the solutions for $s^{(1)}_{\mu\nu}$ and $s^{(2)}_{\mu\nu}$ are

$$\begin{aligned} A^{(1,2)} &= -B^{(1,2)} = Q^2 \frac{1-\varepsilon}{3-2\varepsilon}, \\ \Rightarrow l^{(1,2)}_{\mu\nu} &\equiv l_{\mu\nu} = Q^2 \frac{1-\varepsilon}{3-2\varepsilon} \tilde{l}_{\mu\nu}, \end{aligned} \tag{3.9}$$

with

$$\tilde{l}_{\mu\nu} := \frac{q_\mu q_\nu}{Q^2} - g_{\mu\nu}. \tag{3.10}$$

Using these results, the squared amplitude can be written in the form

$$\begin{aligned} |\mathcal{M}|^2 = &\int \frac{\mathrm{d}^{d-2}\Omega}{\Omega^{d-2}_{\text{tot}}} \frac{1}{4} \sum_{\text{spins}} \frac{16\pi^2\alpha^2\tilde{\mu}^{4\varepsilon}}{Q^4} \Big\{ \left[c_{vv} \langle X|\mathcal{J}^\mu_v|0\rangle + c_{va} \langle X|\mathcal{J}^\mu_a|0\rangle\right] \bar{v}(k_1)\gamma_\mu u(k_2) \\ &+ \left[c_{av} \langle X|\mathcal{J}^\mu_v|0\rangle + c_{aa} \langle X|\mathcal{J}^\mu_a|0\rangle\right] \bar{v}(k_1)\gamma_\mu\gamma_5 u(k_2) \Big\}^2 \\ = &\frac{16\pi^2\alpha^2\tilde{\mu}^{4\varepsilon}}{Q^4} \Big\{ (c^2_{vv} + c^2_{av}) \langle X|\mathcal{J}^\mu_v|0\rangle^2 + (c^2_{va} + c^2_{aa}) \langle X|\mathcal{J}^\mu_a|0\rangle^2 \Big\} l_{\mu\nu}, \end{aligned} \tag{3.11}$$

where the coefficients c_{ij} can be read off from Eq. (3.3). Note that the square means $(\mathcal{O}^\mu)^2 = \mathcal{O}^{\dagger\mu}\mathcal{O}^\nu$ for simplicity of notation, and that there is no vector-axial mixing due to the symmetry of the averaged spin structures. In the squared hadronic matrix element spin and color sums are implied.

Consequently the final form of the cross section at leading order in the electroweak coupling constant α for arbitrary final state particles is

$$\sigma = \tilde{\mu}^{-2\varepsilon} \sum_X \int \mathrm{d}\Pi_X \, (2\pi)^d \delta^{(d)}(q - P_X) \sum_{i=a,v} L^i_{\mu\nu} H^{i,\mu\nu}, \tag{3.12}$$

$$H^{i,\mu\nu} := \left\langle 0 \middle| \mathcal{J}^{\dagger\,\mu}_i \middle| X \right\rangle \left\langle X \middle| \mathcal{J}^\nu_i \middle| 0 \right\rangle, \tag{3.13}$$

where $\mathrm{d}\Pi_X = \prod_{i\in X} \frac{\mathrm{d}^{d-1}p_i}{(4\pi)^{d-1}} \frac{1}{2p^0_i}$, and $H^{i,\mu\nu}$ is the hadronic tensor. The leptonic tensor is defined as

$$\begin{aligned} L^v_{\mu\nu} &:= c^{v,\varepsilon}_{\text{lep}} \tilde{l}_{\mu\nu} := \frac{8\pi^2\alpha^2\tilde{\mu}^{4\varepsilon}}{Q^4} \left(\frac{1-\varepsilon}{3-2\varepsilon}\right) (c^2_{vv} + c^2_{av}) \tilde{l}_{\mu\nu}, \\ L^a_{\mu\nu} &:= c^{a,\varepsilon}_{\text{lep}} \tilde{l}_{\mu\nu} := \frac{8\pi^2\alpha^2\tilde{\mu}^{4\varepsilon}}{Q^4} \left(\frac{1-\varepsilon}{3-2\varepsilon}\right) (c^2_{va} + c^2_{aa}) \tilde{l}_{\mu\nu}, \end{aligned} \tag{3.14}$$

with

$$\begin{aligned} c^2_{vv} + c^2_{av} &= Q^2_e Q^2_f + \frac{v^2_f (v^2_e + a^2_e)}{(1-\hat{m}^2_Z)^2 + \left(\frac{\Gamma_Z}{m_Z}\right)^2} + \frac{2Q_e Q_f v_e v_f (1-\hat{m}^2_Z)}{(1-\hat{m}^2_Z)^2 + \left(\frac{\Gamma_Z}{m_Z}\right)^2}, \\ c^2_{va} + c^2_{aa} &= \frac{a^2_f (v^2_e + a^2_e)}{(1-\hat{m}^2_Z)^2 + \left(\frac{\Gamma_Z}{m_Z}\right)^2}, \end{aligned} \tag{3.15}$$

and Γ_Z the width of the Z, which has to be included near the Z pole.

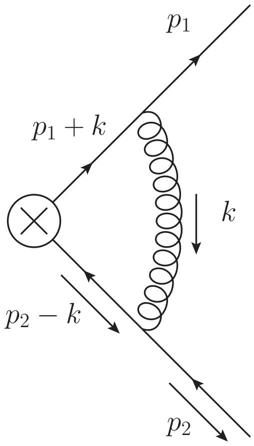

Figure 3.1: The virtual QCD diagram.

3.2 Born Cross Section

To get the Born cross section for $e^+e^- \to q\bar{q}$, we apply the QCD Feynman rules to calculate the hadronic tensor and compute the phase space integral in a straightforward way. When contracting with the leptonic tensor, we can use the Ward identity $q_\mu H^{v,\mu\nu} = 0$ to simplify the calculation.

In $d = 4 - 2\varepsilon$ dimensions the vector and axial Born cross sections read

$$\begin{aligned}
\sigma^{v,\varepsilon}_{\text{tot,Born}} &= \frac{N_c Q^2 \tilde{\mu}^{-2\varepsilon}}{2\pi} \frac{\Gamma(1-\varepsilon)}{\Gamma(2-2\varepsilon)} \left(\frac{4\pi}{Q^2}\right)^{\varepsilon} v^{1-2\varepsilon}(1 + 2\hat{m}^2 - \varepsilon) c^{v,\varepsilon}_{\text{lep}}, \\
\sigma^{a,\varepsilon}_{\text{tot,Born}} &= \frac{N_c Q^2 \tilde{\mu}^{-2\varepsilon}}{2\pi} \frac{\Gamma(1-\varepsilon)}{\Gamma(2-2\varepsilon)} \left(\frac{4\pi}{Q^2}\right)^{\varepsilon} v^{1-2\varepsilon}(1-\varepsilon)(1 - 4\hat{m}^2) c^{a,\varepsilon}_{\text{lep}},
\end{aligned} \tag{3.16}$$

with $v := \sqrt{1 - 4\hat{m}^2}$.

In the $d \to 4$ limit we get

$$\begin{aligned}
\sigma^{v}_{\text{tot,Born}} &= \frac{N_c Q^2}{2\pi} v(1 + 2\hat{m}^2) c^{v,0}_{\text{lep}}, \\
\sigma^{a}_{\text{tot,Born}} &= \frac{N_c Q^2}{2\pi} v(1 - 4\hat{m}^2) c^{a,0}_{\text{lep}},
\end{aligned} \tag{3.17}$$

and furthermore the massless $d \to 4$ Born cross section

$$\sigma^i_0 := \frac{N_c Q^2}{2\pi} c^{i,0}_{\text{lep}}, \tag{3.18}$$

with $i = v, a$ will be used as a normalization in the following calculations.

3.3 Virtual Contribution

The virtual contributions arise from the diagram in Fig. 3.1. The corresponding result will be used in two places: It is part of the $\mathcal{O}(\alpha_s)$ fixed order cross section, and it is needed for the SCET to QCD current matching calculation in section 6.1.

Since the virtual diagram has just two back-to-back final state particles, it is obvious that the virtual differential cross section is proportional to $\delta(\rho - \rho_{\text{min}})$. The factor of this delta function has to be equal to the integrated virtual cross section to give the right integral, hence, we just have to compute the total cross section from the beginning. For convenience we will use the variable $\bar{\rho} := \rho - \rho_{\rm min}$.

Using QCD Feynman rules in Feynman gauge, the virtual diagram reads

$$
\begin{aligned}
V_i^\mu = \bar{u}(p_1, s_1) \int \frac{\mathrm{d}^d k}{(2\pi)^d} & \left(i g_s \gamma^\alpha T^A \tilde{\mu}^\varepsilon\right) \frac{i\left(\not{p}_1 + \not{k} + m\right)}{(p_1 + k)^2 - m^2 + i0} \Gamma_i^\mu \\
& \times \frac{i(-\not{p}_2 + \not{k} + m)}{(p_2 - k)^2 - m^2 + i0} (i g_s \gamma_\alpha T^A \tilde{\mu}^\varepsilon) \frac{-i}{k^2 + i0} v(p_s, s_2) \\
= & - i 4\pi \alpha_s C_F \bar{u}(p_1, s_1) \\
& \times \left\{ \tilde{\mu}^{2\varepsilon} \int \frac{\mathrm{d}^d k}{(2\pi)^d} \frac{\gamma^\alpha (\not{p}_1 + \not{k} + m) \Gamma_i^\mu (-\not{p}_2 + \not{k} + m) \gamma_\alpha}{[(p_1 + k)^2 - m^2 + i0]\,[(p_2 - k)^2 - m^2 + i0]\,[k^2 + i0]} \right\} v(p_2, s_2). \quad (3.19)
\end{aligned}
$$

The calculation of this loop integral is performed in appendix A and the results read

$$
\begin{aligned}
V_v^\mu &= \frac{C_F \alpha_s}{4\pi} \bar{u}(p_1, s_1) \left[A \frac{(p_1 - p_2)^\mu}{2m} + B \gamma^\mu \right] v(p_2, s_2), \\
V_a^\mu &= \frac{C_F \alpha_s}{4\pi} \bar{u}(p_1, s_1) \left[C \gamma^\mu + D \frac{q^\mu}{2m} \right] \gamma_5 v(p_2, s_2),
\end{aligned} \tag{3.20}
$$

with

$$
\begin{aligned}
A &= \frac{v^2 - 1}{v} \log \frac{v - 1}{v + 1}, \\
B &= \frac{1}{\varepsilon} \left(1 - \frac{1 + v^2}{v} \log \frac{v - 1}{v + 1} \right) - \log \frac{m^2}{\mu^2} - 3v \log \frac{v - 1}{v + 1} \\
&\quad + \frac{1 + v^2}{v} \left(\frac{\pi^2}{6} - \frac{1}{2} \log^2 \frac{v - 1}{v + 1} + \log \frac{m^2}{\mu^2} \log \frac{v - 1}{v + 1} \right. \\
&\quad \left. + 2 \log \frac{2v}{1 + v} \log \frac{v - 1}{v + 1} + 2 \mathrm{Li}_2 \frac{1 - v}{1 + v} \right), \\
C &= B + 2 \frac{v^2 - 1}{v} \log \frac{v - 1}{v + 1}, \\
D &= \frac{1 - v^2}{v} \left(2v + (2 + v^2) \log \frac{v - 1}{v + 1} \right).
\end{aligned} \tag{3.21}
$$

Note that $v := \sqrt{1 - 4\hat{m}^2}$ and that the term proportional to q^μ in Eq. (3.20) vanishes when contracting with the leptonic tensor due to the Ward identity. The result coincides with the corresponding expressions in [26, 27].

Including LSZ and wave function renormalization factors, the physical current matrix element reads

$$
\langle q\bar{q} | \mathcal{J}_i^\mu | 0 \rangle_{\rm QCD} = Z_\psi^{\rm OS} \Big(\bar{u}(p_1, s_1) \Gamma_i^\mu v(p_2, s_2) + V_i^\mu \Big), \tag{3.22}
$$

where

$$
Z_\psi^{\rm OS} = 1 + \frac{C_F \alpha_s}{4\pi} \left[-\frac{3}{\varepsilon} + 3 \log \frac{m^2}{\mu^2} - 4 \right], \tag{3.23}
$$

is the $\mathcal{O}(\alpha_s)$ on-shell wave function renormalization factor [4]. Note that the vector and axial quark current operators are conserved in QCD, and therefore no further renormalization is needed [28].

For the virtual cross section contribution, we square the matrix element, sum over spins, and contract it with the leptonic structure $\tilde{l}_{\mu\nu}$ given in Eq. (3.10). Due to the Ward identity, the term proportional to $q_\mu q_\nu$ in the leptonic structure vanishes in the vector case, and only the $-g_{\mu\nu}$ contraction is relevant. We obtain

$$
\begin{aligned}
&-g_{\mu\nu}\,\langle q\bar{q}|\mathcal{J}_v^\mu|0\rangle_{\text{QCD}}\,\langle 0|\mathcal{J}_v^\nu|q\bar{q}\rangle_{\text{QCD}} = -\text{Tr}\left[\gamma^\mu(\not{p}_2 - m)\gamma_\mu(\not{p}_1 + m)\right]\\
&\quad - 2\frac{C_F\alpha_s}{4\pi}\left[\frac{\text{Re}(A)}{2m}\text{Tr}\left[\gamma^\mu(\not{p}_2 - m)(\not{p}_1 + m)\right](p_1 - p_2)^\mu + \text{Re}(B)\text{Tr}\left[\gamma^\mu(\not{p}_2 - m)\gamma_\mu(\not{p}_1 + m)\right]\right.\\
&\quad\left. + \left(-\frac{3}{\varepsilon} + 3\log\frac{m^2}{\mu^2} - 4\right)\text{Tr}\left[\gamma^\mu(\not{p}_2 - m)\gamma_\mu(\not{p}_1 + m)\right]\right]\\
&= 2Q^2(3 - v^2 - 2\varepsilon)\\
&\quad + \frac{C_F\alpha_s}{4\pi}\left\{-\text{Re}(A)\left[4Q^2v^2\right] + \left(\text{Re}(B) - \frac{3}{\varepsilon} + 3\log\frac{m^2}{\mu^2} - 4\right)\left[4Q^2(3 - v^2 - 2\varepsilon)\right]\right\}, \qquad (3.24)
\end{aligned}
$$

and

$$
\tilde{l}_{\mu\nu}\,\langle q\bar{q}|\mathcal{J}_a^\mu|0\rangle_{\text{QCD}}\,\langle 0|\mathcal{J}_a^\nu|q\bar{q}\rangle_{\text{QCD}} = 2Q^2\left[2v^2(1-\varepsilon)\right]\left\{1 + \frac{C_F\alpha_s}{4\pi}2\left(\text{Re}(C) - \frac{3}{\varepsilon} + 3\log\frac{m^2}{\mu^2} - 4\right)\right\}. \qquad (3.25)
$$

Since the expressions (3.24) and (3.25) are independent of the particle momenta, the phase space integral reduces to a factor

$$
\tilde{\mu}^{-2\varepsilon}\int\prod_{i=1}^{2}\left(\frac{\mathrm{d}^{d-1}p_i}{(2\pi)^{d-1}2p_i^0}\right)(2\pi)^d\delta^{(d)}(q - p_1 - p_2) = \frac{v\tilde{\mu}^{-2\varepsilon}}{16\pi^{\frac{1}{2}}\Gamma\left(\frac{3}{2} - \varepsilon\right)}\left(\frac{16\pi}{Q^2v^2}\right)^{\varepsilon}. \qquad (3.26)
$$

Finally, including this phase space factor, the normalization (3.18) and the squared matrix element (3.25), and after summing over colors, one can write the virtual part of the differential cross section as

$$
\frac{1}{\sigma_0^i}\left(\frac{\mathrm{d}\sigma^i_{\text{Born}}}{\mathrm{d}\rho} + \frac{\mathrm{d}\sigma^i_{\text{virt}}}{\mathrm{d}\rho}\right) = \delta(\bar{\rho})\frac{\pi^{\frac{1}{2}}v\tilde{\mu}^{-2\varepsilon}}{8\Gamma\left(\frac{3}{2} - \varepsilon\right)}\left(\frac{16\pi}{Q^2v^2}\right)^{\varepsilon}\frac{c^{i,\varepsilon}_{\text{lep}}}{c^{i,0}_{\text{lep}}}\frac{1}{Q^2}\tilde{l}_{\mu\nu}\,\langle q\bar{q}|\mathcal{J}_i^\mu|0\rangle_{\text{QCD}}\,\langle 0|\mathcal{J}_i^\nu|q\bar{q}\rangle_{\text{QCD}}\,, \qquad (3.27)
$$

with $i = v, a$. After simplifying the expressions, the final results for the $\mathcal{O}(\alpha_s)$ virtual cross sections read

$$
\begin{aligned}
\frac{1}{\sigma_0^v}\frac{\mathrm{d}\sigma^v_{\text{virt}}}{\mathrm{d}\rho} = \frac{C_F\alpha_s}{4\pi}\Bigg[&\frac{(v^2-3)\left((v^2+1)\log\frac{1-v}{v+1} + 2v\right)}{\varepsilon}\\
&- 2\left(v^2-3\right)\left(v^2+1\right)\text{Li}_2\left(\frac{1-v}{v+1}\right) - \frac{2\pi^2}{3}\left(v^2-3\right)\left(v^2+1\right)\\
&+ 4v\left(2v^2-5\right) - 2v\left(v^2-3\right)\log\left(-\frac{1}{4}v^2\left(v^2-1\right)\right) + 4v(3-v^2)\log\frac{Q^2}{\mu^2}\\
&+ \frac{1}{2}\log\frac{1-v}{v+1}\Bigg(8v^4 - 20v^2 - 4\left(v^2-3\right)\left(v^2+1\right)\log\frac{v^2Q^2}{\mu^2}\\
&+ \left(-v^4+2v^2+3\right)\log\frac{1-v}{v+1} - 8\Bigg) + \mathcal{O}(\varepsilon)\Bigg]\delta(\bar{\rho}),
\end{aligned}
$$

$$
\begin{aligned}
\frac{1}{\sigma_0^a}\frac{\mathrm{d}\sigma_{\text{virt}}^a}{\mathrm{d}\rho} = \frac{C_F\alpha_s}{4\pi}\Bigg[&-\frac{2v^2\left(2v+(v^2+1)\log\frac{1-v}{v+1}\right)}{\varepsilon}\\
&+\frac{4v^2}{3}\left(\pi^2\left(v^2+1\right)+3v\log\left(\frac{1}{4}v^2\left(1-v^2\right)\right)-9v+6v\log\frac{Q^2}{\mu^2}\right)\\
&+v^2\log\frac{1-v}{v+1}\left(-4v^2+4\left(v^2+1\right)\log\frac{v^2Q^2}{\mu^2}+\left(v^2+1\right)\log\frac{1-v}{v+1}-6\right)\\
&+4v^2\left(v^2+1\right)\mathrm{Li}_2\left(\frac{1-v}{v+1}\right)+\mathcal{O}\left(\varepsilon\right)\Bigg]\delta(\bar{\rho}).
\end{aligned}
\tag{3.28}
$$

Note that there are still divergences in terms of $1/\varepsilon$ present. These are of IR type and will be canceled by equivalent terms in the real radiation part.

3.4 Real Radiation Contribution

We will now consider the real radiation contribution to the $\mathcal{O}(\alpha_s)$ heavy jet mass distribution. In this setting it is quite useful to define the dimensionless variables

$$
x_i := \frac{2p_i^0}{Q}, \tag{3.29}
$$

where $i = 1, 2$ denotes the two quarks, and $i = 3$ the gluon. As an intermediate step to the real radiation contribution to the HJM cross section, we will compute the cross section with respect to x_1 and x_2, which contains the full kinematic information, and then project the result onto the heavy jet mass.

Using the x_i variables, energy and momentum conservation read

$$
x_1 + x_2 + x_3 = 2, \quad \text{and} \quad \vec{0} = \hat{n}_1\sqrt{x_1^2 - 4\hat{m}^2} + \hat{n}_2\sqrt{x_2^2 - 4\hat{m}^2} + \hat{n}_3 x_3, \tag{3.30}
$$

respectively, and the scalar products of the particle momenta can be written as

$$
\begin{aligned}
p_1\cdot p_2 &= \frac{Q^2}{2}\left(x_1 + x_2 - 1 - 2\hat{m}^2\right),\\
p_1\cdot p_3 &= \frac{Q^2}{2}\left(x_1 + x_3 - 1\right),\\
p_2\cdot p_3 &= \frac{Q^2}{2}\left(x_2 + x_3 - 1\right).
\end{aligned}
\tag{3.31}
$$

The contribution from real radiation can be calculated via the two diagrams shown in Fig. 3.2. Using Feynman rules, the sum of both diagrams gives

$$
\begin{aligned}
h^\mu_{i,R(1+2)} = \bar{u}(p_1, s_1)\Bigg[&\left(ig_s\tilde{\mu}^\varepsilon T^A\gamma^\alpha\right)\frac{i\left(\not{p}_1 + \not{p}_3 + m\right)}{(p_1+p_3)^2 - m^2 + i0}\Gamma_i^\mu\\
&+\Gamma_i^\mu\frac{-i(\not{p}_2 + \not{p}_3 - m)}{(p_2+p_3)^2 - m^2 + i0}\left(ig_s\tilde{\mu}^\varepsilon T^A\gamma^\alpha\right)\Bigg]v(p_2, s_2)\varepsilon_\alpha^{A\,*}(p_3),
\end{aligned}
\tag{3.32}
$$

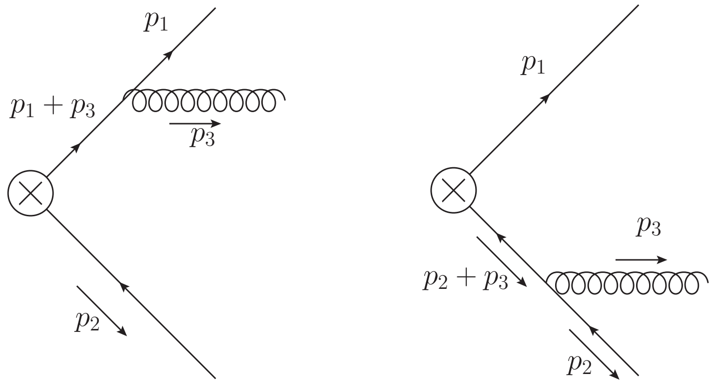

Figure 3.2: Real emission QCD diagrams.

and after squaring this expression and summing over final particle spins, polarizations, and colors, the hadronic tensor reads

$$\begin{aligned}H^{\mu\nu}_{R,i} &= g_s^2 \tilde{\mu}^{2\varepsilon} C_F N_C \\ &\times \mathrm{Tr}\Big[(\not{p}_1 + m)\left(\gamma^\alpha \frac{\not{p}_1 + \not{p}_3 + m}{(p_1+p_3)^2 - m^2 + i0}\Gamma^\mu_i - \Gamma^\mu_i \frac{\not{p}_2 + \not{p}_3 - m}{(p_2+p_3)^2 - m^2 + i0}\gamma^\alpha\right) \\ &\times (\not{p}_2 - m)\left(\gamma_\alpha \frac{\not{p}_2 + \not{p}_3 - m}{(p_2+p_3)^2 - m^2 + i0}\Gamma^\nu_i - \Gamma^\nu_i \frac{\not{p}_1 + \not{p}_3 + m}{(p_1+p_3)^2 - m^2 + i0}\gamma_\alpha\right)\Big]. \end{aligned} \tag{3.33}$$

To derive the x_1, x_2 cross section, we consider the contribution of real radiation to the total cross section

$$\sigma^i_{\mathrm{rad}} = \tilde{\mu}^{-2\varepsilon} \int \frac{\mathrm{d}^{d-1}p_1}{(2\pi)^{d-1}} \frac{\mathrm{d}^{d-1}p_2}{(2\pi)^{d-1}} \frac{\mathrm{d}^{d-1}p_3}{(2\pi)^{d-1}} \frac{1}{2p_1^0\, 2p_2^0\, 2p_3^0} (2\pi)^d \delta^{(d)}(q - p_1 - p_2 - p_3) c^{i,\varepsilon}_{\mathrm{lep}} \tilde{l}_{\mu\nu} H^{\mu\nu}_{R,i}, \tag{3.34}$$

and change the variables of the phase space integration to x_1 and x_2, so that the differential cross section can be read off.

Here, we use polar coordinates so that

$$\begin{aligned}\mathrm{d}^{d-1}p_1\, \mathrm{d}^{d-1}p_2 &= \Omega^{d-2}_{\mathrm{tot}} \Omega^{d-3}_{\mathrm{tot}} \left|\vec{p}_1\right|^{d-2} \left|\vec{p}_2\right|^{d-2} \mathrm{d}\theta\, \mathrm{d}\left|\vec{p}_1\right|\, \mathrm{d}\left|\vec{p}_2\right| \sin^{d-3}\theta \\ &= \Omega^{d-2}_{\mathrm{tot}} \Omega^{d-3}_{\mathrm{tot}} \left|\vec{p}_1\right|^{d-3} \left|\vec{p}_2\right|^{d-3} p_1^0 p_2^0 \mathrm{d}u\, \mathrm{d}p_1^0\, \mathrm{d}p_2^0\, (1-u^2)^{\frac{d-4}{2}}, \end{aligned} \tag{3.35}$$

with $u := \cos\theta = \frac{\vec{p}_1 \cdot \vec{p}_2}{|\vec{p}_1||\vec{p}_2|} \in [-1, 1]$, and $|\vec{p}_i| = \sqrt{(p_i^0)^2 - m^2}$. Moreover, we use the relation

$$\delta(x^2 - c^2) = \frac{\delta(x-c)}{|2c|} + \frac{\delta(x+c)}{|2c|}, \tag{3.36}$$

to rewrite the delta function in the form

$$\delta(Q - p_1^0 - p_2^0 - p_3^0) = 2p_3^0 \delta\left((Q - p_1^0 - p_2^0)^2 - (p_3^0)^2\right) - \delta(Q - p_1^0 - p_2^0 + p_3^0). \tag{3.37}$$

We will negelect the second term, since it does not correspond to the considered physical situation, and therefore vanishes within the considered phase space region.

After inserting Eqs. (3.35) and (3.37) into (3.34), and integrating over the p_3 components, we obtain

$$\sigma^i_{\rm rad} = \frac{\tilde{\mu}^{-2\varepsilon}}{4Q^2}\Omega^{d-2}_{\rm tot}\Omega^{d-3}_{\rm tot}\int\frac{\mathrm{d}p_1^0}{(2\pi)^{d-1}}\frac{\mathrm{d}p_2^0}{(2\pi)^{d-2}}\int\limits_{-1}^{1}\mathrm{d}u\,(1-u^2)^{\frac{d-4}{2}}\,|\vec{p}_1|^{d-3}\,|\vec{p}_2|^{d-3}$$
$$\times\,\delta\left(1-\frac{2p_1^0}{Q}-\frac{2p_2^0}{Q}+\frac{1}{2}\frac{2p_1^0 2p_2^0}{Q^2}+2\hat{m}^2-2\frac{|\vec{p}_1|\,|\vec{p}_2|}{Q^2}u\right)\left[c^{i,\varepsilon}_{\rm lep}\tilde{l}_{\mu\nu}H^{\mu\nu}_{R,i}\right]_{\vec{p}_3=-\vec{p}_1-\vec{p}_2}$$
$$=\frac{\tilde{\mu}^{-2\varepsilon}Q^2}{32}\Omega^{2-2\varepsilon}_{\rm tot}\Omega^{1-2\varepsilon}_{\rm tot}\int\frac{\mathrm{d}x_1}{(2\pi)^{3-2\varepsilon}}\frac{\mathrm{d}x_2}{(2\pi)^{2-2\varepsilon}}\int\limits_{-1}^{1}\mathrm{d}u\,(1-u^2)^{-\varepsilon}\,|\vec{p}_1|^{-2\varepsilon}\,|\vec{p}_2|^{-2\varepsilon}$$
$$\times\,\delta\left(u-\frac{Q^2}{2\,|\vec{p}_1|\,|\vec{p}_2|}\left(1-x_1-x_2+\frac{1}{2}x_1x_2+2\hat{m}^2\right)\right)\left[c^{i,\varepsilon}_{\rm lep}\tilde{l}_{\mu\nu}H^{\mu\nu}_{R,i}\right]_{\vec{p}_3=-\vec{p}_1-\vec{p}_2}, \qquad (3.38)$$

where we changed the variables p_1^0 and p_2^0 to x_1 and x_2.

We use the remaining delta distribution to perform the u-integration. Finally, one can read off the cross section with respect to x_1 and x_2 from the integrand. The vector and axial contributions are

$$\frac{1}{\sigma_0^v}\frac{\mathrm{d}^2\sigma^v_{\rm rad}}{\mathrm{d}x_1\,\mathrm{d}x_2} = \frac{C_F\alpha_s\tilde{\mu}^{4\varepsilon}}{2\pi}\left(\frac{Q^2}{8\pi}\right)^{-2\varepsilon}\frac{(x_1^2-4\hat{m}^2)^{-\varepsilon}(x_2^2-4\hat{m}^2)^{-\varepsilon}(1-u^2)^{-\varepsilon}}{(x_1-1)^2(x_2-1)^2\Gamma(2-2\varepsilon)}$$
$$\times\Bigg\{\varepsilon^2(x_1-1)(x_2-1)(x1+x2-2)^2$$
$$+2\varepsilon\left[-(x_1-1)(x_2-1)\left(x_1^2+x_1(x_2-2)+x_2(x_2-2)+2\right)+\hat{m}^2(x_1+x_2-2)^2\right]$$
$$+(x1-1)(x_2-1)\left(x_1^2+x_2^2\right)+2\hat{m}^2\left(x_1^2(2x_2-3)+2x_1(x_2-2)^2+x_2(8-3x_2)-6\right)$$
$$-4\hat{m}^4\,(x_1+x_2-2)^2\Bigg\},$$

$$\frac{1}{\sigma_0^a}\frac{\mathrm{d}^2\sigma^a_{\rm rad}}{\mathrm{d}x_1\,\mathrm{d}x_2} = \frac{C_F\alpha_s\tilde{\mu}^{4\varepsilon}}{2\pi}\left(\frac{Q^2}{8\pi}\right)^{-2\varepsilon}\frac{(x_1^2-4\hat{m}^2)^{-\varepsilon}(x_2^2-4\hat{m}^2)^{-\varepsilon}(1-u^2)^{-\varepsilon}}{(x_1-1)^2(x_2-1)^2\Gamma(2-2\varepsilon)}$$
$$\times\Bigg\{\varepsilon^2(x_1-1)(x_2-1)(x_1+x_2-2)^2$$
$$-2\varepsilon\Bigg[(x_1-1)(x_2-1)\left(x_1^2+x_1(x_2-2)+x_2(x_2-2)+2\right)$$
$$+\hat{m}^2\Bigg(x_1^3(x_2-1)+x_1^2\left(x_2\left(2x_2-11\right)+8\right)$$
$$+x_1(x_2-2)\left(x_2(x_2-9)+6\right)-(x_2-6)(x_2-2)x_2+4\Bigg)$$
$$+4\hat{m}^4(x_1+x_2-2)^2\Bigg]$$
$$+(x_1-1)(x_2-1)(x_1^2+x_2^2)+2\hat{m}^2\Bigg(x_1^3(x_2-1)+x_1^2\left(x_2(2x_2-11)+8\right)$$
$$+x_1(x_2-2)(x_2(x_2-9)+6)-x_2(x_2-6)(x_2-2)+4\Bigg)+8\hat{m}^4(x_1+x_2-2)^2\Bigg\}. \qquad (3.39)$$

3.4.1 Real Radiative Heavy Jet Mass Cross Section for $\rho > \rho_{\min}$

As mentioned at the beginning of this chapter, we will calculate the HJM distribution in two parts. In the first part we compute the cross section in $d = 4$ dimensions, which gives an expression which is adequate to calculate in the region $\bar{\rho} > 0$ where only real radiation contributes.

We obtain the 4-dimensional cross section with respect to x_1 and x_2 by taking the $\varepsilon \to 0$ limit of Eq. (3.39). They read

$$\begin{aligned}
\frac{1}{\sigma_0^v}\frac{\mathrm{d}^2\sigma_{\mathrm{rad}}^{v,d=4}}{\mathrm{d}x_1\,\mathrm{d}x_2} = {} & \frac{C_F\alpha_s}{2\pi(x_1-1)^2(x_2-1)^2} \\
& \times\Big\{(x_1-1)(x_2-1)\left(x_1^2+x_2^2\right) \\
& + 2\hat{m}^2\left(-6+2x_1(x_2-2)^2+x_1^2(2x_2-3)+x_2(8-3x_2)\right) \\
& - 4\hat{m}^4(x_1+x_2-2)^2\Big\}, \\
\frac{1}{\sigma_0^a}\frac{\mathrm{d}^2\sigma_{\mathrm{rad}}^{a,d=4}}{\mathrm{d}x_1\,\mathrm{d}x_2} = {} & \frac{C_F\alpha_s}{2\pi(x_1-1)^2(x_2-1)^2} \\
& \times\Big\{(x_1-1)(x_2-1)\left(x_1^2+x_2^2\right) \\
& + 2\hat{m}^2\Big(4+x_1^3(x_2-1)-x_2(x_2-6)(x_2-2) \\
& \quad + x_1(x_2-2)((x_2-9)x_2+6)+x_1^2(x_2(2x_2-11)+8)\Big) \\
& + 8\hat{m}^4(x_1+x_2-2)^2\Big\},
\end{aligned} \tag{3.40}$$

and agree with the corresponding expressions in the literature [29–31] (note that there is a known sign error in [29]).

Phase Space Considerations

To simplify the calculation, it is convenient to divide the phase space into three regions as shown in Fig. 3.3. Each region represents a specific kinematic situation for the heavy jet mass as follows:

- Region 1 (2): The heavy hemisphere consists of quark number 1 (number 2) and the gluon,
- Region 3: The heavy hemisphere consists of the two quarks.

The lines which separate these different regions are the lines where the hemisphere division, and therefore, per definition, the thrust axis changes. Note that for three final state particles the thrust axis is always aligned with the momentum of one of them.

Let's consider some characteristic points on the border of phase space depicted in Fig. 3.3 and 3.4:

Point A: Zero gluon energy and a symmetric quark configuration with $x_3 = 0$, $x_1 = x_2 = 1$.

Point B: Maximal gluon energy. For the x_i follows

$$\begin{aligned}
& x_3 = 4\hat{p} = 2 - x_1 - x_2 = 2 - 4\sqrt{\hat{m}^2+\hat{p}^2}, \\
\Rightarrow \quad & x_1 = x_2 = \frac{1}{2} + 2\hat{m}^2, \quad x_3 = 1 - 4\hat{m}^2,
\end{aligned} \tag{3.41}$$

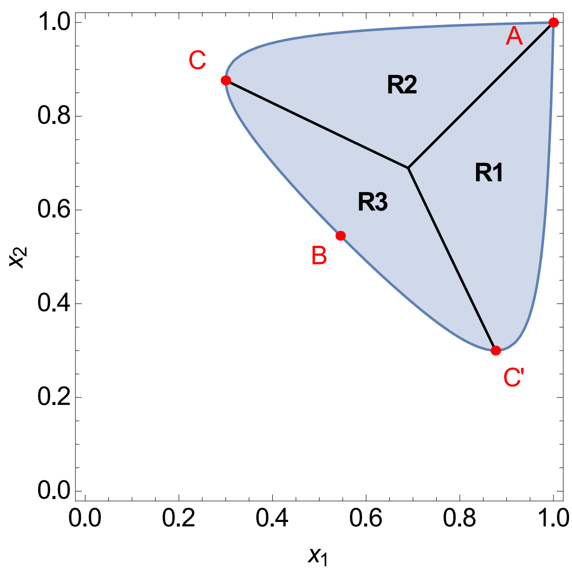

Figure 3.3: Three particle phase space showing characteristic points and regions with $\hat{m} = 0.15$.

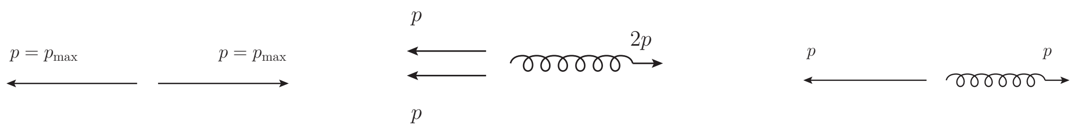

(A) (B) (C)

Figure 3.4: Kinematic situations at the characteristic points.

where $\hat{p} := |\vec{p}|/Q$, and $\vec{p}$ is the momentum of each quark as depicted in Fig. 3.4.

Point C: Zero quark energy. The x_i read

$$
\begin{aligned}
& x_1 = 2\hat{m}^2, \\
& x_2 = 2\sqrt{\hat{m}^2 + \hat{p}^2} : \\
\Rightarrow \quad & x_1 = 2\hat{m}, \quad x_2 = \frac{(1-\hat{m})^2 + \hat{m}^2}{1-\hat{m}}, \quad x_3 = \frac{1-2\hat{m}}{1-\hat{m}}.
\end{aligned}
\tag{3.42}
$$

Point C′: Zero antiquark energy. Same as point C with x_1 and x_2 interchanged.

The expression describing the boundary line CBC′ can be derived from the maximal gluon energy line, which corresponds to a kinematic situation shown in the left panel in Fig. 3.5. By using

Figure 3.5: Kinematic situation for the maximal and “minimal” gluon energy line.

energy conservation for the three particles, we find

$$
\begin{aligned}
& x_3 = 2\hat{p} = 2 - 2\sqrt{\hat{m}^2 + y^2\hat{p}^2} - 2\sqrt{\hat{m}^2 + (1-y)^2\hat{p}^2}, \\
& x_1^2 = 4\hat{m}^2 + 4y^2\hat{p}^2, \\
& x_2^2 = 4\hat{m}^2 + 4(1-y)^2\hat{p}^2 : \\
\Rightarrow \quad & x_2 = \frac{1}{2(1+\hat{m}^2 - x_1)}\left((1+2\hat{m}^2 - x_1)(2-x_1) - (1-x_1)\sqrt{x_1^2 - 4\hat{m}^2}\right). \qquad (3.43)
\end{aligned}
$$

Note that Eq. (3.43) is symmetric in x_1 and x_2.

For the boundary line CAC$'$ we consider the kinematic configuration in the right panel of Fig. 3.5. Again by using energy conservation we obtain

$$
\begin{aligned}
& x_3 = 2(1-y)\hat{p}, \quad x_1 = 2\sqrt{\hat{m}^2 + \hat{p}^2}, \quad x_2 = 2\sqrt{\hat{m}^2 + y^2\hat{p}^2} : \\
\Rightarrow \quad & 2 - x1 - x2 = \sqrt{x_1^2 - 4\hat{m}^2} - \sqrt{x_2^2 - 4\hat{m}^2}. \qquad (3.44)
\end{aligned}
$$

The solution of this equation is identical to Eq. (3.43), such that this expression describes the full boundary.

To separate the regions in the way mentioned at the beginning of this section and depicted in Fig. 3.3, we use the fact that for three particles thrust can be written as

$$
T = \max\left\{\sqrt{x_1^2 - 4\hat{m}^2}, \sqrt{x_2^2 - 4\hat{m}^2}, x_3\right\}, \qquad (3.45)
$$

which can be easily derived from the thrust definition in Eq. (2.1). The lines where the thrust axis changes are found by setting two of these arguments equal which gives

- $x_1 = x_2$,
- $\sqrt{x_2^2 - 4\hat{m}^2} = x_3 = 2 - x_1 - x_2 \quad \Rightarrow \quad x_2 = \frac{4\hat{m}^2 + (2-x_1)^2}{2(2-x_1)}$,
- $\sqrt{x_1^2 - 4\hat{m}^2} = x_3 \quad \Rightarrow \quad x_2 = 2 - x_1 - \sqrt{x_1^2 - 4\hat{m}^2}$,

and the intersection of all lines lies at $x_1 = x_2 = \frac{2}{3}(2 - \sqrt{1 - 3\hat{m}^2})$.

Projection onto the Heavy Jet Mass

We project the double differential cross section in $d = 4$ dimensions onto the heavy jet mass via

$$
\frac{\mathrm{d}\sigma^i}{\mathrm{d}\rho} = \int \mathrm{d}x_1\, \mathrm{d}x_2\, \frac{\mathrm{d}^2\sigma^i}{\mathrm{d}x_1\, \mathrm{d}x_2}\delta(\rho - \rho(x_1, x_2)). \qquad (3.46)
$$

A useful set of variables to obtain $\rho(x_1, x_2)$ in the different phase space regions are the invariant masses of two out of the three final state particles

$$
\begin{aligned}
t_1^2 &:= \frac{(p_1 + p_3)^2}{Q^2} = 1 + \hat{m}^2 - x_2, \\
t_2^2 &:= \frac{(p_2 + p_3)^2}{Q^2} = 1 + \hat{m}^2 - x_1, \\
\tau^2 &:= \frac{(p_1 + p_2)^2}{Q^2} = x_1 + x_2 - 1, \qquad (3.47)
\end{aligned}
$$

which correspond to $\rho(x_1, x_2)$ in the different regions: $\rho = t_2^2$ in region 1, $\rho = t_1^2$ in region 2 and $\rho = \tau^2$ in region 3.

Region 1 (2):

To obtain the contribution from region 1 (which is identical to the contribution of region 2 for symmetry reasons), we divide region 1 further into the parts 1A and 1B to simplify the integral, where the line of separation goes through point C′ with constant x_1. Consequently the projection looks like

$$\begin{aligned}\frac{1}{\sigma_0^i}\frac{\mathrm{d}\sigma_{\mathrm{rad,R1}}^{i,\bar{\rho}>0}}{\mathrm{d}\rho} &= \int\limits_{L_1}^{L_2}\mathrm{d}x_1\int\limits_{L_3}^{x_1}\mathrm{d}x_2\,\delta(\rho - t_2^2(x_1,x_2))\frac{1}{\sigma_0^i}\frac{\mathrm{d}^2\sigma_{\mathrm{rad}}^{i,d=4}}{\mathrm{d}x_1\,\mathrm{d}x_2}\\ &+\int\limits_{L_2}^{1}\mathrm{d}x_1\int\limits_{L_4}^{x_1}\mathrm{d}x_2\,\delta(\rho - t_2^2(x_1,x_2))\frac{1}{\sigma_0^i}\frac{\mathrm{d}^2\sigma_{\mathrm{rad}}^{i,d=4}}{\mathrm{d}x_1\,\mathrm{d}x_2},\end{aligned}\tag{3.48}$$

where the first integration corresponds to region 1A, and the second one corresponds to region 1B. The integration limits are

$$\begin{aligned}L_1 &= \frac{2}{3}\left(2-\sqrt{1-3\hat{m}^2}\right),\\ L_2 &= \frac{(1-\hat{m})^2+\hat{m}^2}{1-\hat{m}^2},\\ L_3 &= 2 - x_1 - \sqrt{x_1^2-4\hat{m}^2},\\ L_4 &= \frac{1}{2(1+\hat{m}^2-x_1)}\left((1+2\hat{m}^2-x_1)(2-x_1)-(1-x_1)\sqrt{x_1^2-4\hat{m}^2}\right).\end{aligned}\tag{3.49}$$

To carry out the integrations, we put $t_2(x_1, x_2)$ from Eq. (3.47) into the delta function which gives $\delta(\rho - t_2^2(x_1, x_2)) = \delta(x_1 - (1 + \hat{m}^2 - \rho))$.

The validity intervals for ρ in these regions are

$$\frac{\hat{m}^3+\hat{m}^2-\hat{m}}{\hat{m}-1} \le \rho \le \frac{1}{3}\left(-1+3\hat{m}^2+2\sqrt{1-3\hat{m}^2}\right),\tag{3.50}$$

for 1A and

$$\hat{m}^2 < \rho \le \frac{\hat{m}^3+\hat{m}^2-\hat{m}}{\hat{m}-1},\tag{3.51}$$

for 1B.

We use a similar approach for region 3 and divide it into region 3C and 3D, where the separating lineconnects point C and C′. Here we use the more convenient coordinates $x := \tau^2 = x_1 + x_2 - 1$ and $t := x_1 - x_2$. The contribution of region 3 is given by

$$\begin{aligned}\frac{1}{\sigma_0^i}\frac{\mathrm{d}\sigma_{\mathrm{rad,R3}}^{i,\bar{\rho}>0}}{\mathrm{d}\rho} &= \int\limits_{4\hat{m}^2}^{L_5}\mathrm{d}x\int\limits_{x-1}^{L_6}\mathrm{d}t\,\delta(\rho - x)\frac{1}{2}\frac{1}{\sigma_0^i}\frac{\mathrm{d}^2\sigma_{\mathrm{rad}}^{i,d=4}}{\mathrm{d}x_1\,\mathrm{d}x_2}\\ &+\int\limits_{L_5}^{L_7}\mathrm{d}x\int\limits_{-L_8}^{L_8}\mathrm{d}t\,\delta(\rho - x)\frac{1}{2}\frac{1}{\sigma_0^i}\frac{\mathrm{d}^2\sigma_{\mathrm{rad}}^{i,d=4}}{\mathrm{d}x_1\,\mathrm{d}x_2},\end{aligned}\tag{3.52}$$

with

$$
\begin{aligned}
L_5 &= \frac{\hat{m}}{1-\hat{m}}, \\
L_6 &= (1-x)\sqrt{\frac{x-4\hat{m}^2}{x}}, \\
L_7 &= \frac{1}{3}\left(5-4\sqrt{1-3\hat{m}^2}\right), \\
L_8 &= -1-x+2\sqrt{(1-x)^2+4\hat{m}^2}.
\end{aligned} \tag{3.53}
$$

The corresponding intervals of validity are

$$
\frac{\hat{m}}{1-\hat{m}} \leq \rho \leq \frac{1}{3}\left(5-4\sqrt{1-3\hat{m}^2}\right), \tag{3.54}
$$

for 3C and

$$
4\hat{m}^2 \leq \rho \leq \frac{\hat{m}}{1-\hat{m}}, \tag{3.55}
$$

for 3D.

The complete HJM cross section for $\bar{\rho} > 0$ results from adding the contributions of all regions, which gives

$$
\frac{1}{\sigma_0^i}\frac{\mathrm{d}\sigma^{i,\bar{\rho}>0}_{\text{rad}}}{\mathrm{d}\rho} = \frac{1}{\sigma_0^i}\left(2\left(\frac{\mathrm{d}\sigma^{i,\bar{\rho}>0}_{\text{rad,1A}}}{\mathrm{d}\rho} + \frac{\mathrm{d}\sigma^{i,\bar{\rho}>0}_{\text{rad,1B}}}{\mathrm{d}\rho}\right) + \left(\frac{\mathrm{d}\sigma^{i,\bar{\rho}>0}_{\text{rad,3C}}}{\mathrm{d}\rho} + \frac{\mathrm{d}\sigma^{i,\bar{\rho}>0}_{\text{rad,3D}}}{\mathrm{d}\rho}\right)\right). \tag{3.56}
$$

The full expressions of the different terms are collected in appendix B.

As mentioned above, this expression is not properly regularized (i.e. not integrable), and information about the distribution at $\bar{\rho} = 0$ is lost. The expression which describes the HJM distribution for all values of ρ has to be integrable and the left IR divergence in the virtual contribution has to be canceled, which is a clear indication that a delta function at $\bar{\rho} = 0$ is missing and the $\bar{\rho}^{-1}$ divergence at 0 is unphysical. It is known that the general structure of the distribution of a generic event-shape e with a corresponding minimal value e_{min} has the structure

$$
\frac{1}{\sigma_0^i}\frac{\mathrm{d}\sigma^i}{\mathrm{d}e} = f_0^i\delta(\bar{e}) + \frac{C_F\alpha_s}{4\pi}\left[f_\delta^i\delta(\bar{e}) + \sum_{j=0} f^i_{+,j}\mathcal{L}_j(\bar{e}) + \mathcal{O}\left(\bar{e}^0\right)\right], \tag{3.57}
$$

where $\bar{e} = e - e_{\text{min}}$. $\mathcal{L}_n(x)$ is a plus distribution, which is defined in appendix C, and behaves like $x^{-1}\log^n x$ for $x > 0$. Since the $\mathcal{O}(\bar{e})$ terms consist only of integrable regular functions, they are called "non-distributional". It turns out that at $\mathcal{O}(\alpha_s)$ only the $j = 0$ term arises in the heavy jet mass fixed order result with massive quarks, so

$$
\frac{1}{\sigma_0^i}\frac{\mathrm{d}\sigma^i}{\mathrm{d}\rho} = f_0^i\delta(\bar{\rho}) + \frac{C_F\alpha_s}{4\pi}\left[f_\delta^i\delta(\bar{\rho}) + f^i_{+}\mathcal{L}_0(\bar{\rho}) + \mathcal{O}\left(\bar{\rho}^0\right)\right], \tag{3.58}
$$

where $f^i_+ \equiv f^i_{+,0}$.

The plus distribution in the full result corresponds to a $\mathcal{O}(\bar{\rho}^{-1})$ term in our $d = 4$ result, valid in the region $\bar{\rho} > 0$. Thus we can extract the plus distribution coefficient via obtaining the coefficient of the term proportional to $\bar{\rho}^{-1}$ in the $d = 4$ result by applying an expansion around small $\bar{r}ho$. The only region in phase space contributing to this term is 1B (and the equivalent area in region 2), thus

$$
\frac{1}{\sigma_0^i}\frac{\mathrm{d}\sigma^{i,\bar{\rho}>0}_{\text{rad,1B}}}{\mathrm{d}\rho} = \frac{C_F\alpha_s}{4\pi}\left(\frac{1}{2}f^i_+\frac{1}{\bar{\rho}}\right) + \mathcal{O}\left(\bar{\rho}^0\right). \tag{3.59}
$$

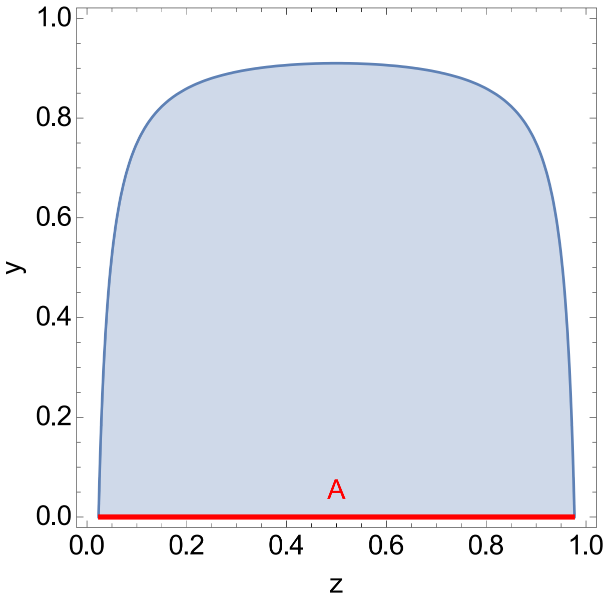

Figure 3.6: The three particle phase space parametrized by the new coordinates y and z.

We obtain

$$\begin{aligned} f_+^v &= -2(3-v^2)\left(2v + (1+v^2)\log\frac{1-v}{1+v}\right), \\ f_+^a &= -8\left(v^3 + \frac{v^2}{2}(1+v^2)\log\frac{1-v}{1+v}\right), \end{aligned} \tag{3.60}$$

with $v = \sqrt{1-4\hat{m}^2}$ for the plus distribution coefficients.

The remaining expressions to obtain are f_0^i, f_δ^i, and the non-distributional terms. f_0^i is given by the Born cross section, the non-distributional part can be obtained from the $d=4$ HJM cross section via subtracting the $\bar{\rho}^{-1}$ term, and f_δ^i is computed in the following section. Note that f_+^i and the non-distributional part do not contain any virtual contributions.

3.4.2 Derivation of the Real Radiative Delta Function Coefficient

In this section we compute the contribution of real radiation to the delta coefficient f_δ^i at $\mathcal{O}(\alpha_s)$. To this end we will introduce a method which can be applied for a general 2-jet event-shape e.

General method

At the beginning of this chapter we derived the general $d = 4-2\varepsilon$ dimensional double differential cross section with respect to x_1 and x_2, where the final expressions are given in Eq. (3.39). The contribution of real radiation to the delta coefficient, $f_{\delta,\mathrm{rad}}^i$, corresponds to the region where the gluon is very soft, or equivalently $x_1 + x_2 \approx 2$ and $\bar{e} \approx 0$. In the following calculation we take the soft limit of the double differential cross section and compute the real radiative cumulant

$$\Sigma_{\mathrm{rad}}^i(e_c) := \int_{e_{\min}}^{e_c} \mathrm{d}e\, \frac{\mathrm{d}\sigma_{\mathrm{rad}}^i}{\mathrm{d}e}, \tag{3.61}$$

with $e_c = e_{\min} + \Delta$ in the limit $\Delta \ll 1$. Afterwards, we expand the result for small Δ. The resulting constant term corresponds to $f_{\delta,\mathrm{rad}}^i$, while the next term is proportional to $\log\Delta$ and originates from the integrated plus distribution.

To take the soft limit we use the coordinates

$$\begin{aligned} x_1 &=: 1 - zy, \\ x_2 &=: 1 - (1-z)y, \end{aligned} \tag{3.62}$$

where $y \equiv x_3$ and the soft limit corresponds to $y \to 0$. In Fig. 3.6 we show the three particle phase space with respect to the new coordinates.

Let us start with the projection of the double differential cross section onto the generic 2-jet event-shape e by considering the expression

$$\frac{\mathrm{d}\sigma^i_{\mathrm{rad}}}{\mathrm{d}e} = \int \mathrm{d}x_1\,\mathrm{d}x_2\,\frac{\mathrm{d}^2\sigma^i_{\mathrm{rad}}}{\mathrm{d}x_1\,\mathrm{d}x_2}\delta(e - e(x_1, x_2)). \tag{3.63}$$

Using this equation we write the cumulant of the event-shape as

$$\begin{aligned} \Sigma^i_{\mathrm{rad}}(e_{\mathrm{min}} + \Delta) &= \int\limits_{e_{\mathrm{min}}}^{e_{\mathrm{min}}+\Delta} \mathrm{d}e \int \mathrm{d}x_1\,\mathrm{d}x_2\,\frac{\mathrm{d}^2\sigma^i_{\mathrm{rad}}}{\mathrm{d}x_1\,\mathrm{d}x_2}\delta(e - e(x_1, x_2)) \\ &= \int \mathrm{d}z\,\mathrm{d}y\,y\,\frac{\mathrm{d}^2\sigma^i_{\mathrm{rad}}}{\mathrm{d}x_1\,\mathrm{d}x_2}(y,z)\Theta\left(\Delta + e_{\mathrm{min}} - e(y,z)\right), \end{aligned} \tag{3.64}$$

where we took the integral over e to obtain the second line. Now we expand the expression in $y \ll 1$ up to the leading order. Since e is a 2-jet event-shape, the corresponding soft expansion reads $e(y,z) = e_{\mathrm{min}} + y\,\frac{\mathrm{d}e}{\mathrm{d}y}\Big|_{y=0} + \mathcal{O}(y^2)$, and therefore we can write

$$\Sigma^i_{\mathrm{rad,soft}}(e_{\mathrm{min}} + \Delta) = \int \mathrm{d}z\,\mathrm{d}y\,y\,\frac{\mathrm{d}^2\sigma^i_{\mathrm{rad,soft}}}{\mathrm{d}x_1\,\mathrm{d}x_2}(y,z)\Theta\left(\Delta - y\,\frac{\mathrm{d}e}{\mathrm{d}y}\Big|_{y=0}\right), \tag{3.65}$$

where the subscript "soft" denotes that only the leading order term in y is taken into account. Note that we assumed $\frac{\mathrm{d}e}{\mathrm{d}y}\Big|_{y=0} \neq 0$. The $\mathcal{O}(\alpha_s)$ soft x_1, x_2 cross sections read

$$\begin{aligned} \frac{1}{\sigma_0^v}\frac{\mathrm{d}^2\sigma^v_{\mathrm{rad,soft}}}{\mathrm{d}x_1\,\mathrm{d}x_2}(y,z) &= \left\{\frac{Q^{2-4\varepsilon}}{2^{7-6\varepsilon}\pi^{3-2\varepsilon}\Gamma(2-2\varepsilon)}y^{1-2\varepsilon}\left(4z(1-z) + v^2 - 1\right)^{-\varepsilon}\right\} \\ &\quad\times\left\{\alpha_s C_F \pi^2 \frac{16(3 - v^2 - 2\varepsilon)(v^2 - 1 + 4z(1-z))}{y^2 z^2(1-z^2)}\frac{\tilde{\mu}^{4\varepsilon}}{Q^2}\right\}, \\ \frac{1}{\sigma_0^a}\frac{\mathrm{d}^2\sigma^a_{\mathrm{rad,soft}}}{\mathrm{d}x_1\,\mathrm{d}x_2}(y,z) &= \left\{\frac{Q^{2-4\varepsilon}}{2^{7-6\varepsilon}\pi^{3-2\varepsilon}\Gamma(2-2\varepsilon)}y^{1-2\varepsilon}\left(4z(1-z) + v^2 - 1\right)^{-\varepsilon}\right\} \\ &\quad\times\left\{\alpha_s C_F \pi^2 \frac{32v^2(1-\varepsilon)(v^2 - 1 - 4z(z-1))}{y^2 z^2(1-z^2)}\frac{\tilde{\mu}^{4\varepsilon}}{Q^2}\right\}, \end{aligned} \tag{3.66}$$

where the first factor originates from phase space, and the second one from the amplitude.

The relevant phase space region for the delta term is 1B (and the equivalent area in region 2), so we apply the known integration limits corresponding to this region. Applying the Heaviside function we get

$$\begin{aligned}
\frac{1}{\sigma_0^v}\Sigma^v_{\text{rad,soft}}(e_{\min}+\Delta) &= \frac{Q^{-4\varepsilon}C_F\alpha_s\tilde{\mu}^{4\varepsilon}(3-v^2-2\varepsilon)}{4^{1-3\varepsilon}\pi^{1-2\varepsilon}\Gamma(2-2\varepsilon)} \\
&\quad\times\left(\int\limits_0^{\Delta/\frac{\mathrm{d}e}{\mathrm{d}y}\big|_{y=0}}\mathrm{d}y\,y^{-1-2\varepsilon}\right)\int\limits_{\frac{1}{2}(1-v)}^{\frac{1}{2}}\mathrm{d}z\,\frac{(v^2-1+4z(1-z))^{1-\varepsilon}}{z^2(1-z)^2} \\
&= \frac{C_F\alpha_s}{4\pi}\frac{-3+v^2+2\varepsilon}{2^{1-6\varepsilon}\pi^{-2\varepsilon}\Gamma(2-2\varepsilon)}\left(\frac{\tilde{\mu}^2}{Q^2}\right)^{2\varepsilon}\frac{\Delta^{-2\varepsilon}}{\varepsilon} \\
&\quad\times\int\limits_{\frac{1}{2}(1-v)}^{\frac{1}{2}}\mathrm{d}z\,\frac{(v^2-1+4z(1-z))^{1-\varepsilon}}{z^2(1-z)^2\left(\frac{\mathrm{d}e(y,z)}{\mathrm{d}y}\Big|_{y=0}\right)^{-2\varepsilon}},
\end{aligned}$$

$$\begin{aligned}
\frac{1}{\sigma_0^a}\Sigma^a_{\text{rad,soft}}(e_{\min}+\Delta) &= \frac{C_F\alpha_s}{4\pi}\frac{v^2(\varepsilon-1)}{2^{-6\varepsilon}\pi^{-2\varepsilon}\Gamma(2-2\varepsilon)}\left(\frac{\tilde{\mu}^2}{Q^2}\right)^{2\varepsilon}\frac{\Delta^{-2\varepsilon}}{\varepsilon} \\
&\quad\times\int\limits_{\frac{1}{2}(1-v)}^{\frac{1}{2}}\mathrm{d}z\,\frac{(v^2-1+4z(1-z))^{1-\varepsilon}}{z^2(1-z)^2\left(\frac{\mathrm{d}e(y,z)}{\mathrm{d}y}\Big|_{y=0}\right)^{-2\varepsilon}}.
\end{aligned} \tag{3.67}$$

Note that in the vector and axial case just the prefactors are different, while the integrals are identical. In order to get the y integral correct, it had to be properly regularized by dimensional regularization, however, it is save to expand the remaining z integrand in ε prior to the integration, since there are no divergences present. We obtain

$$\begin{aligned}
&\frac{(v^2-1+4z(1-z))^{1-\varepsilon}}{z^2(1-z)^2\left(\frac{\mathrm{d}e(y,z)}{\mathrm{d}y}\Big|_{y=0}\right)^{-2\varepsilon}} = \frac{v^2-1+4z(1-z)}{z^2(1-z)^2} \\
&+\varepsilon\frac{(v^2-1+4z(1-z))\left(2\log\frac{\mathrm{d}e(y,z)}{\mathrm{d}y}\Big|_{y=0}-\log\left(v^2-1+4z(1-z)\right)\right)}{z^2(1-z)^2}+\mathcal{O}(\varepsilon^2),
\end{aligned} \tag{3.68}$$

and moreover the corresponding integrals give

$$F_0 := \int\limits_{\frac{1}{2}(1-v)}^{\frac{1}{2}}\mathrm{d}z\,\frac{v^2-1+4z(1-z)}{z^2(1-z)^2} = 2v\left(-2-\frac{1+v^2}{v}\log\frac{1-v}{1+v}\right),$$

$$\begin{aligned}
F_1 &:= \int\limits_{\frac{1}{2}(1-v)}^{\frac{1}{2}}\mathrm{d}z\,\frac{v^2-1+4z(1-z)}{z^2(1-z)^2}\left(2\log\frac{\mathrm{d}e(y,z)}{\mathrm{d}y}\Big|_{y=0}-\log(v^2-1+4z(1-z))\right) \\
&= 2\int\limits_{\frac{1}{2}(1-v)}^{\frac{1}{2}}\mathrm{d}z\,\frac{v^2-1+4z(1-z)}{z^2(1-z)^2}\log\frac{\mathrm{d}e(y,z)}{\mathrm{d}y}\Big|_{y=0}+2\Bigg\{4v\log(2v)+2\log\frac{1-v}{1+v} \\
&\quad-(1+v^2)\left[-\frac{\pi^2}{6}-\log\frac{1-v}{1+v}\log(2v(1+v))+\mathrm{Li}_2\left(\frac{2v}{v-1}\right)+\mathrm{Li}_2\left(\frac{1-v}{1+v}\right)\right]\Bigg\}.
\end{aligned} \tag{3.69}$$

The only part which depends on the event-shape is the integral in the second line of Eq. (3.69). The last piece needed is the $\mathcal{O}(\varepsilon^0, \Delta^0)$ expansion of the non-integral factors in Eq. (3.67). For these we get

$$\begin{aligned}\frac{C_F\alpha_s}{4\pi}\frac{-3+v^2+2\varepsilon}{2^{1-6\varepsilon}\pi^{-2\varepsilon}\Gamma(2-2\varepsilon)}\left(\frac{\tilde{\mu}^2}{Q^2}\right)^{2\varepsilon}\frac{\Delta^{-2\varepsilon}}{\varepsilon} &= \frac{C_F\alpha_s}{4\pi}\left[\frac{1}{\varepsilon}\frac{v^2-3}{2}+\left(-2+v^2+(3-v^2)\log\frac{Q^2}{2\mu^2}\right)\right] \\ &\quad + \mathcal{O}(\varepsilon, \log\Delta) \\ &=: \frac{C_F\alpha_s}{4\pi}\left[\frac{1}{\varepsilon}G^v_{-1}+G^v_0\right]+\mathcal{O}(\varepsilon,\log\Delta),\end{aligned} \tag{3.70}$$

in the vector and

$$\begin{aligned}\frac{C_F\alpha_s}{4\pi}\frac{v^2(\varepsilon-1)}{2^{-6\varepsilon}\pi^{-2\varepsilon}\Gamma(2-2\varepsilon)}\left(\frac{\tilde{\mu}^2}{Q^2}\right)^{2\varepsilon}\frac{\Delta^{-2\varepsilon}}{\varepsilon} &= \frac{C_F\alpha_s}{4\pi}\left[-\frac{1}{\varepsilon}-1+2\log\frac{Q^2}{2\mu^2}\right]v^2+\mathcal{O}(\varepsilon,\log\Delta) \\ &=: \frac{C_F\alpha_s}{4\pi}\left[\frac{1}{\varepsilon}G^a_{-1}+G^a_0\right]+\mathcal{O}(\varepsilon,\log\Delta),\end{aligned} \tag{3.71}$$

in the axial case. The term proportional to $\log\Delta$ would correspond to the plus distribution coefficient. The final result for the cumulant in the soft limit is

$$\frac{1}{\sigma^0_i}\Sigma^i_{\text{rad,soft}}(e_{\min}+\Delta) = \frac{C_F\alpha_s}{4\pi}\left[\frac{1}{\varepsilon}G^i_{-1}F_0+G^i_{-1}F_1(e)+G^i_0F_0+\mathcal{O}(\log\Delta,\varepsilon)\right]. \tag{3.72}$$

Now we can easily read off the delta function coefficients which have the form

$$f^i_{\delta,\text{rad}} = \frac{1}{\varepsilon}G^i_{-1}F_0+G^i_{-1}F_1(e)+G^i_0F_0. \tag{3.73}$$

Application to the Heavy Jet Mass

Here we apply the general method to the heavy jet mass. Using $\left.\frac{\mathrm{d}\rho(y,z)}{\mathrm{d}y}\right|_{y=0} = z$, we can carry out the remaining integral in F_1, defined in Eq. (3.69). We obtain

$$\begin{aligned}\int\limits_{\frac{1}{2}(1-v)}^{\frac{1}{2}}\mathrm{d}z\,\frac{v^2-1+4z(1-z)}{z^2(1-z)^2}2\log z &= -4\left(v^2+1\right)\mathrm{Li}_2\left(\frac{v+1}{2}\right) \\ &\quad+\frac{1}{3}\left[\pi^2\left(v^2+1\right)-6\left(v\left(v\left(2+\log^2 2\right)+2-4\log 2\right)+\log^2 2\right)\right] \\ &\quad+2\log(1-v)\left(\left(v^2+1\right)\log\frac{4}{1-v}-4v\right)+2\left(v^2-1\right)\log\frac{1-v}{v+1},\end{aligned} \tag{3.74}$$

and after several manipulations we get

$$
\begin{aligned}
f^{v}_{\delta,\mathrm{rad}} =\; & \frac{(3-v^2)\left((v^2+1)\log\frac{1-v}{v+1}+2v\right)}{\varepsilon} + \left(v^2-3\right) \\
& \times\Bigg[\left(v^2+1\right)\left(-2\left(\mathrm{Li}_2\left(\frac{v+1}{2}\right)+\mathrm{Li}_2\left(\frac{1-v}{v+1}\right)\right)-\frac{3}{2}\log^2(v+1)+\log\frac{1-v}{v+1}\right. \\
& \quad \left.+\log(1-v)\left(\log(v+1)-\frac{1}{2}\log\frac{1-v}{16}\right)-\log^2 2\right) \\
& \quad +\frac{\pi^2}{2}\left(v^2+1\right)-2v(v+1)-4v\log\frac{1-v}{4v}\Bigg] \\
& -4\left(\frac{1}{2}\left(v^2+1\right)\log\frac{1-v}{v+1}+v\right)\left(\left(3-v^2\right)\log\frac{Q^2}{2\mu^2}+v^2-2\right),
\end{aligned}
$$

and

$$
\begin{aligned}
f^{a}_{\delta,\mathrm{rad}} = v^2\Bigg[& 2\frac{2v+(v^2+1)\log\frac{1-v}{v+1}}{\varepsilon}-\left(v^2+1\right) \\
& \times\left(4\left(\mathrm{Li}_2\left(\frac{v+1}{v-1}\right)-\mathrm{Li}_2\left(\frac{2v}{v-1}\right)\right)-4\log 2\,\log\left(1-v^2\right)-\log^2(v+1)\right. \\
& \quad \left.+\log(1-v)\left(2\log(v+1)-\log\frac{1-v}{256}\right)\right) \\
& -4\left(v^2+1\right)\log\frac{1-v}{v+1}\,\log\frac{Q^2 v}{2\mu^2}-8v\log\frac{Q^2}{\mu^2} \\
& +\frac{1}{3}\left(12v(v+2-\log 4)-\pi^2\left(v^2+1\right)\right)+8v\log\frac{1-v}{v}\Bigg].
\end{aligned}
\tag{3.75}
$$

Note that the $1/\varepsilon$ terms precisely cancel the IR divergences in the virtual contributions given in Eq. (3.28).

3.5 The Fixed Order Delta Function Coefficient

Adding the corresponding real and virtual contributions from Eqs. (3.28) and (3.75) we obtain the full fixed order delta coefficients

$$
\begin{aligned}
f^{v}_{\delta} =\; & \left(\frac{C_F\alpha_s}{4\pi}\right)^{-1}\frac{\sigma^{v}_{\mathrm{virt}}}{\sigma^{v}_{0}}+f^{v}_{\delta,\mathrm{rad}} = -(3+10v^2-3v^4)\log\frac{1-v}{1+v} \\
& +(v^2-3)\Bigg\{2v(1-v)-2v\log\frac{(1-v)^3(1+v)}{16} \\
& +(1+v^2)\left[-\frac{\pi^2}{6}-2\log\frac{1-v}{1+v}\,\log\frac{2v^2}{1+v}+2\mathrm{Li}_2\left(\frac{v+1}{v-1}\right)-4\mathrm{Li}_2\left(\frac{1-v}{1+v}\right)\right]\Bigg\},
\end{aligned}
\tag{3.76}
$$

and

$$
\begin{aligned}
f^{a}_{\delta} =\; & \left(\frac{C_F\alpha_s}{4\pi}\right)^{-1}\frac{\sigma^{a}_{\mathrm{virt}}}{\sigma^{a}_{0}}+f^{v}_{\delta,\mathrm{rad}} = v^2\Bigg\{-2(3+2v^2)\log\frac{1-v}{1+v}+4v\left(v-1+\log\frac{(1+v)(1-v)^3}{16}\right) \\
& +(1+v^2)\left[\frac{\pi^2}{3}+4\log\frac{2v^2}{1+v}\,\log\frac{1-v}{1+v}-4\mathrm{Li}_2\left(\frac{v+1}{v-1}\right)+8\mathrm{Li}_2\left(\frac{1-v}{1+v}\right)\right]\Bigg\}.
\end{aligned}
\tag{3.77}
$$

Note that our results are cross checked via integrating the differential distribution and comparing it with the total cross section, which can be found in [32] and reads

$$\sigma_{\text{tot}} = \sigma^v_{\text{tot}} + \sigma^a_{\text{tot}} = \sigma^v_{\text{tot,Born}} \left[1 + \frac{C_F \alpha_s}{\pi} K^v(v)\right] + \sigma^a_{\text{tot,Born}} \left[1 + \frac{C_F \alpha_s}{\pi} K^a(v)\right], \tag{3.78}$$

with the coefficients

$$\begin{aligned}
K^v(v) &:= \frac{1}{v}\left[A(v) + \frac{P^v(v)}{1-v^2/3}\log\frac{1+v}{1-v} + \frac{Q^v(v)}{1-v^2/3}\right],\\
K^a(v) &:= \frac{1}{v}\left[A(v) + \frac{P^a(v)}{v^2}\log\frac{1+v}{1-v} + \frac{Q^a(v)}{v^2}\right],\\
A(v) &:= (1+v^2)\left[\mathrm{Li}_2\left(\left[\frac{1-v}{1+v}\right]^2\right) + 2\mathrm{Li}_2\left(\frac{1-v}{1+v}\right) + \log\frac{1+v}{1-v}\log\frac{(1+v)^3}{8v^2}\right]\\
&\quad + 3v\log\frac{1-v^2}{4v} - v\log v,
\end{aligned}$$

$$\begin{aligned}
P^v(v) &:= \frac{33}{24} + \frac{22}{24}v^2 - \frac{7}{24}v^4, & Q^v(v) &:= \frac{5}{4}v - \frac{3}{4}v^3,\\
P^a(v) &:= \frac{21}{32} + \frac{59}{32}v^2 + \frac{19}{32}v^4 - \frac{3}{32}v^6, & Q^a(v) &:= -\frac{21}{16}v + \frac{30}{16}v^3 + \frac{3}{16}v^5.
\end{aligned} \tag{3.79}$$

3.6 Large Logarithms and the Need for Resummation

Although fixed order calculations properly describe the partonic contribution of event-shape cross sections in the far-tail region, in the dijet region one needs to address two relevant issues.

The first issue arises since perturbative cross sections are calculated with partons in the final states, what's measured in experiment, however, are hadronic final states. Therefore, to obtain the full prediction one has to account for non-perturbative contributions, which we implement by using a so called "model function" [10, 12, 33], explained in more detail in section 6.6.

The second issue is related to the problem of large logarithms that are appearing in the dijet limit [1, 2]. Looking at the $\mathcal{O}(\alpha_s)$ cumulant of the heavy jet mass distribution in the limit $\hat{m} \sim \bar{\rho} \ll 1$, one obtains

$$\frac{1}{\sigma_0^i}\Sigma^i_\rho(\rho) = 1 + \frac{C_F\alpha_s}{4\pi}\left[-6\log\bar{\rho} - 4\log^2\bar{\rho} + \mathcal{O}(\bar{\rho}^0, \hat{m}^0)\right]. \tag{3.80}$$

It is evident that for small $\bar{\rho}$ the logarithms are large and spoil the perturbative expansion.

The source of this problem lies in the presence of a strong scale hierarchy in the dijet limit. In fact, the enhancement of collinear and soft radiation leads to three distinct scales, namely the hard scale $\mu_H \sim Q$, related to the hard interaction, the jet scale $\mu_J \sim Q\sqrt{\bar{\rho}}$, related to the collinear particles in the jet, and the soft scale $\mu_S \sim Q\bar{\rho}$, related to soft radiation (of course in QCD we also have the non-perturbative scale Λ_{QCD}). The cross section contains logarithms of ratios of these characteristic scales, which leads to the logarithms of $\bar{\rho}$ we see above.

These logarithms have to be resummed to get a valid expansion in the region of small ρ, and it is necessary to introduce a new counting by considering $\alpha_s \log\bar{\rho} \sim \mathcal{O}(1)$. This counting can be best understood by considering the logarithm of the cumulant, which has the form [34]

$$\log\Sigma_\rho \sim \log\bar{\rho}\sum_{i=0}(\alpha_s\log\bar{\rho})^{i+1} + \sum_{i=0}(\alpha_s\log\bar{\rho})^{i+1} + \alpha_s\sum_{i=0}(\alpha_s\log\bar{\rho})^i + \dots\,. \tag{3.81}$$

These terms are called leading log (LL), next to leading log (NLL), next to next to leading log (N^2LL), and so on [10].

To resum these terms we will factorize the cross section in the dijet limit into parts which contain only one of the characteristic scales via using soft-collinear effective theory. In this framework we resum large logarithms by using the renormalization group evolution for each sector independently.

Chapter 4

Soft-Collinear Effective Theory with Masses

In this chapter we will give a short introduction to soft-collinear effective theory (SCET) [3–9], which is an effective field theory suitable for situations in which just soft radiation and jets of collinear particles are present. In the setup considered in this thesis, this corresponds to the 2-jet limit with two thin pencil-like jets and soft radiation where we found large logarithms in the fixed order result.

The SCET framework will be used in chapter 5 to prove the factorization formula where hard, collinear, and soft contributions to the cross section decouple, which consequently allows us to resum the large logarithms [10–12].

First we will introduce light-cone coordinates, which are very convenient when dealing with highly boosted particles. To obtain the SCET Lagrangian we will explore the scaling of collinear and soft particles, which we use to expand the QCD Lagrangian.

4.1 Basic Setup

Since collinear particles are boosted objects with velocities near the speed of light, we will use light-cone coordinates which are useful in calculations, and make lots of formulations very transparent. To introduce these coordinates we define two light-like vectors

$$n^\mu = (1,0,0,1), \quad \bar{n}^\mu = (1,0,0,-1), \tag{4.1}$$

where

$$n \cdot \bar{n} = 2, \quad n \cdot n = \bar{n} \cdot \bar{n} = 0. \tag{4.2}$$

n and $\bar{n}$ can be used to split any vector p into three components in the form

$$p^\mu = \frac{\bar{n}^\mu}{2} p \cdot n + \frac{n^\mu}{2} p \cdot \bar{n} + p_\perp^\mu = \frac{\bar{n}^\mu}{2} p^+ + \frac{n^\mu}{2} p^- + p_\perp^\mu. \tag{4.3}$$

One obtains a component parallel to n and $\bar{n}$ respectively, and a contribution perpendicular to both vectors, which can have two non-zero components. The scalar product of two vectors expressed in terms of these coordinates reads

$$p \cdot q = p^+ q^- + p^- q^+ + p_\perp \cdot q_\perp. \tag{4.4}$$

Light-cone coordinates are very handy when thinking about momentum scalings and therefore we will use the notation

$$p = (p^+, p^-, p_\perp), \tag{4.5}$$

for scaling considerations from now on.

Let's consider the mentioned 2-jet limit with collinear and soft particles. A collinear particle per definition moves in a specific direction with high momentum and is nearly on-shell. To learn how the scaling of boosted particles looks like, we consider a particle with small momentum and no preferred direction

$$p_s \sim Q(\lambda, \lambda, \lambda), \tag{4.6}$$

where λ is a small parameter, and Q is the center of mass energy. Boosting this momentum into the $-x_3$ direction by a large amount of $1/\lambda$ leads to a scaling

$$p_c \sim Q(\lambda^2, 1, \lambda), \quad p_c^2 \sim Q^2\lambda^2. \tag{4.7}$$

This is the momentum scaling of a boosted particle. We see that there is a strong hierarchy $p^- \ll p_\perp \ll p^+$ between the momentum components, where the large component scales with Q like we would expect.

We already mentioned that there is one more mode to consider in jet processes, which comes from homogeneously radiated soft gluons. Since the interaction of such a soft particle with collinear modes should not push the collinear particle too far off-shell, and soft radiation should be homogeneous, the scaling has to be

$$p_{us} \sim Q(\lambda^2, \lambda^2, \lambda^2), \quad p_{us}^2 \sim Q^2\lambda^4. \tag{4.8}$$

This can also be seen as the consequence of fixing the scaling of a jet mass m_J^2 to $m_J^2 \sim Q^2\lambda^2$ [9]. In the SCET literature this mode is mostly called the ultra-soft mode, however, in this context we will call them soft, since we don't have other types of soft modes.

It should be mentioned that additional "mass modes" with soft scaling have to be included in $\mathcal{O}(\alpha_s^2)$ calculations, originating from secondary massive quark corrections [35].

4.2 SCET Lagrangian

After considering the modes and scalings which are important in the 2-jet limit, let's construct the effective Lagrangian describing them. To do so we split the original QCD fields into the relevant modes of our problem. Both the quark and the gluon field, denoted with ψ and A^μ, are split into a n-collinear, $\bar{n}$-collinear, and a soft part in the form

$$\begin{aligned} \psi &\to \psi_n + \psi_{\bar{n}} + \psi_s, \\ A^\mu &\to A_n^\mu + A_{\bar{n}}^\mu + A_s^\mu. \end{aligned} \tag{4.9}$$

Using the projection operators

$$P_n = \frac{\not{n}\not{\bar{n}}}{4}, \quad P_{\bar{n}} = \frac{\not{\bar{n}}\not{n}}{4}, \tag{4.10}$$

we split the collinear quark field further, which we demonstrate on the n-collinear field (the $\bar{n}$-collinear one behaves in an analogous manner). We write

$$\psi_n = P_n\psi_n + P_{\bar{n}}\psi_n =: \xi_n + \eta_n, \tag{4.11}$$

and it follows that

$$
\begin{aligned}
P_n\xi_n &= \xi_n,\\
P_{\bar n}\xi_n &= 0,\\
\Rightarrow \not{n}\xi_n &= 0.
\end{aligned}
\tag{4.12}
$$

The scaling of these two fields can be checked by considering the related two point functions. It turns out that [4]

$$
\xi_n(x) \sim \lambda, \quad \eta_n(x) \sim \lambda^2, \tag{4.13}
$$

thus, the η_n field is suppressed relative to ξ_n.

The scaling of the remaining fields can also be checked quite easily. They read

$$
\psi_s \sim \lambda^3, \quad A_s^\mu \sim \lambda^2, \tag{4.14}
$$

and the collinear gluon components $A^\mu_{n,\bar n}$ scale just like the analog momentum components

$$
p_n \sim Q(\lambda^2, 1, \lambda), \quad p_{\bar n} \sim Q(1, \lambda^2, \lambda). \tag{4.15}
$$

To derive the SCET Lagrangian we consider the collinear quark contribution to the QCD Lagrangian. By writing the covariant derivative in light-cone coordinates and using Eqs. (4.11) and (4.12) we get

$$
\begin{aligned}
\mathcal{L}_{q,n} &= \bar\psi_n(i\not{D} - m)\psi_n\\
&= \bar\xi_n\frac{\not{\bar n}}{2}iD^+\xi_n + \bar\xi_n(i\not{D}_\perp - m)\eta_n + \bar\eta_n(i\not{D}_\perp - m)\xi_n + \bar\eta_n\frac{\not{n}}{2}iD^-\eta_n.
\end{aligned}
\tag{4.16}
$$

As mentioned above, η_n is suppressed in the SCET power counting parameter λ and therefore it can be integrated out. Since the Lagrangian is quadratic, this can be done exactly by using the classical equations of motion for η_n [4, 36]

$$
\eta_n = \frac{i\not{D}_\perp + m}{iD^-}\frac{\not{\bar n}}{2}\xi_n, \tag{4.17}
$$

which leads to

$$
\mathcal{L}_{q,n} = \bar\xi_n\frac{\not{\bar n}}{2}iD^+\xi_n + \bar\xi_n(i\not{D}_\perp - m)\frac{1}{iD^-}(i\not{D}_\perp + m)\frac{\not{\bar n}}{2}\xi_n. \tag{4.18}
$$

Here we applied SCET power counting to the covariant derivatives.

In contrast to this more complicated structure, the soft Lagrangian and the collinear gluon Lagrangian look just like in QCD with only soft or collinear particles (including covariant derivatives). Finally the full leading order SCET Lagrangian appropriate for a dijet problem reads

$$
\begin{aligned}
\mathcal{L}_{\text{SCET}} = \bar\psi_s(i\not{D}_s - m)\psi_s &- \frac{1}{4}\left(F_s^{\mu\nu\,A}\right)^2 - \frac{1}{4}\left(F_n^{\mu\nu\,A}\right)^2\\
&+ \bar\xi_n\frac{\not{\bar n}}{2}iD^+\xi_n + \bar\xi_n(i\not{D}^n_\perp - m)\frac{1}{iD^-_n}(i\not{D}^n_\perp + m)\frac{\not{\bar n}}{2}\xi_n + [\bar n\text{-terms}],
\end{aligned}
\tag{4.19}
$$

where the subscript s and n mean that only soft or n-collinear fields are involved. This Lagrangian can be used to derive the SCET Feynman rules given in appendix D.

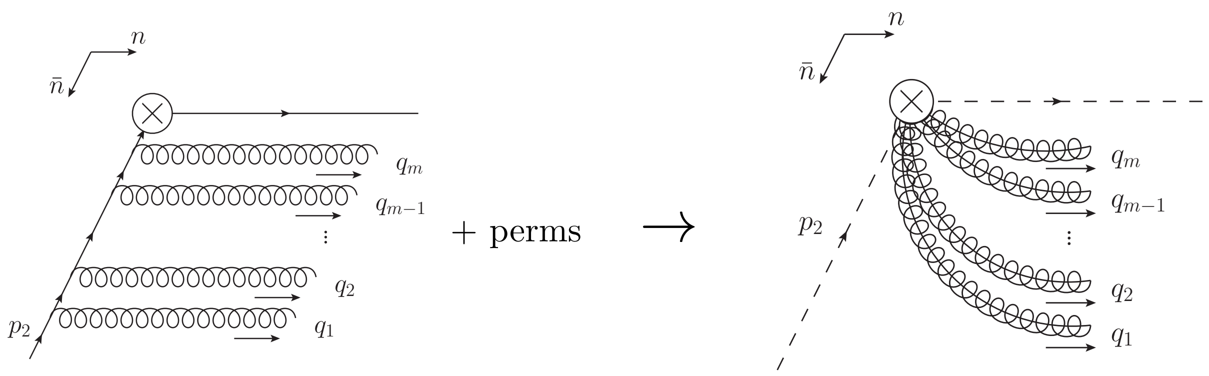

Figure 4.1: Graphical representation of the emergence of a collinear Wilson line.

4.3 Wilson Lines

4.3.1 Collinear Wilson Lines

In QCD, interactions between $\bar{n}$-collinear (anti)quarks and n-collinear gluons are possible, however, they produce (anti)quarks which are far off-shell. Such contributions have to be integrated out in SCET and reappear in the matching conditions to QCD. In the following section we will focus on collinear Wilson lines [4, 6], which account for these contributions and are needed to preserve collinear gauge invariance.

Let us consider a diagram containing a $\bar{n}$-collinear antiquark, a n-collinear quark, and several n-collinear gluons radiated off the $\bar{n}$-collinear quark, as shown in Fig. 4.1. The full theory amplitude with spinors and polarization vectors replaced by SCET fields is

$$\begin{aligned}\frac{1}{m!}\sum_{\text{perm}}\bar{\xi}_n\Gamma_i^{\mu}\frac{i(-\not{p}_2-\sum_i\not{q}_i+m)}{(p_2+\sum_i q_i)^2-m^2+i0}\left(ig_s\gamma_{\mu_m}A_n^{\mu_m}(q_m)\tilde{\mu}^{\varepsilon}\right)\times\ldots\\ \cdots\times\frac{i(-\not{p}_2-\not{q}_1+m)}{(p_2+q_1)^2-m^2+i0}\left(ig_s\gamma_{\mu_1}A_n^{\mu_1}(q_1)\tilde{\mu}^{\varepsilon}\right)\xi_{\bar{n}}.\end{aligned} \tag{4.20}$$

Since we have to consider diagrams with crossed gluon lines, we have to sum over all permutations of the gluon momenta q_i. Additionally, the symmetry factor $m!$ accounts for the fact that all the gluon fields are identical and can be contracted with any external gluon state.

After applying SCET power counting to Eq. (4.20) we obtain

$$\sum_{\text{perm}}\frac{(g_s\tilde{\mu}^{\varepsilon})^m}{m!}\frac{\bar{n}_{\mu_m}\cdots\bar{n}_{\mu_1}}{(q_1^-+i0)\cdots(\sum_i q_i^-+i0)}\bar{\xi}_n\Gamma_i^{\mu}\left(A_n^{\mu_m}(q_m)\cdots A_n^{\mu_1}(q_1)\right)\xi_{\bar{n}}+\mathcal{O}(\lambda). \tag{4.21}$$

Summing over all numbers of radiated gluons, we can read off the n-collinear Wilson line in momentum space

$$W_n=\sum_m\sum_{\text{perm}}\frac{(g_s\tilde{\mu}^{\varepsilon})^m}{m!}\frac{\bar{n}_{\mu_m}\cdots\bar{n}_{\mu_1}}{(q_1^-+i0)\cdots(\sum_i q_i^-+i0)}A_n^{\mu_m}(q_m)\cdots A_n^{\mu_1}(q_1), \tag{4.22}$$

and analogously the adjoint $\bar{n}$-collinear Wilson line

$$W_{\bar{n}}^{\dagger}=\sum_m\sum_{\text{perm}}\frac{(-g_s\tilde{\mu}^{\varepsilon})^m}{m!}\frac{n_{\mu_1}\cdots n_{\mu_m}}{(q_1^++i0)\cdots(\sum_i q_i^++i0)}A_{\bar{n}}^{\mu_1}(q_1)\cdots A_{\bar{n}}^{\mu_m}(q_m). \tag{4.23}$$

In position space they read

$$W_n = \bar{\mathrm{P}} \exp\left(-i g_s \tilde{\mu}^{\varepsilon} \int_0^{\infty} \mathrm{d}s\, \bar{n} \cdot A_n(s\bar{n} + x)\right),$$
$$W_{\bar{n}}^{\dagger} = \mathrm{P} \exp\left(i g_s \tilde{\mu}^{\varepsilon} \int_0^{\infty} \mathrm{d}s\, n \cdot A_{\bar{n}}(sn + x)\right), \tag{4.24}$$

where P is the path ordering, and $\bar{\mathrm{P}}$ the anti-path ordering operator.

After integrating out these modes the SCET current reads $\bar{\chi}_n \Gamma_i^{\mu} \chi_{\bar{n}}$, where $\chi_n := W_n^{\dagger} \xi_n$ is the jet field [7] which contains the n-collinear quark field, as well as the n-collinear Wilson line which encodes n-collinear gluon emissions off $\bar{n}$-collinear quarks.

4.3.2 Soft Wilson Lines

Let's look at a similar situation for soft gluons interacting with collinear quarks. In this case the resulting propagators do not become off-shell as in the situation before, however, it turns out that the soft radiation can be resummed anyways in terms of soft Wilson lines [6, 37]. Using these soft Wilson lines we can completely decouple interactions of soft and collinear degrees of freedom. This is the basis of the SCET factorization formula for the cross section.

Considering a diagram analogous to fig. 4.1 with soft gluons, we find the soft Wilson lines in n and $\bar{n}$ direction

$$Y_n = \sum_m \sum_{\text{perm}} \frac{(g_s \tilde{\mu}^{\varepsilon})^m}{m!} \frac{n_{\mu_m} \cdots n_{\mu_1}}{(q_1^+ + i0) \cdots (\sum_i q_i^+ + i0)} A_s^{\mu_m}(q_m) \cdots A_s^{\mu_1}(q_1),$$
$$Y_{\bar{n}}^{\dagger} = \sum_m \sum_{\text{perm}} \frac{(-g_s \tilde{\mu}^{\varepsilon})^m}{m!} \frac{\bar{n}_{\mu_1} \cdots \bar{n}_{\mu_m}}{(q_1^- + i0) \cdots (\sum_i q_i^- + i0)} A_s^{\mu_1}(q_1) \cdots A_s^{\mu_m}(q_m), \tag{4.25}$$

in momentum space and

$$Y_n = \bar{\mathrm{P}} \exp\left(-i g_s \tilde{\mu}^{\varepsilon} \int_0^{\infty} \mathrm{d}s\, n \cdot A_s(sn + x)\right),$$
$$Y_{\bar{n}}^{\dagger} = \mathrm{P} \exp\left(i g_s \tilde{\mu}^{\varepsilon} \int_0^{\infty} \mathrm{d}s\, \bar{n} \cdot A_s(s\bar{n} + x)\right), \tag{4.26}$$

in position space.

In chapter 5 we will also use barred Wilson lines, which are defined as

$$\bar{Y}_n = \bar{\mathrm{P}} \exp\left(-i g_s \tilde{\mu}^{\varepsilon} \int_0^{\infty} \mathrm{d}s\, n \cdot \bar{A}_s(sn + x)\right), \tag{4.27}$$

where $\bar{A} = A^A \bar{T}^A = -A^A \left(T^A\right)^T$ is the gluon field in the $\bar{3}$ representation of $SU(3)$.

To achieve the soft-collinear decoupling we perform the field redefinitions

$$\xi_n \to Y_n \xi_n^{(0)}, \quad A_n \to Y_n A_n^{(0)} Y_n^{\dagger}, \tag{4.28}$$

and analogously for the $\bar{n}$-collinear fields. The added (0) indicates that these fields are not interacting with soft fields any more. These interactions reappear in the SCET current in terms of soft Wilson lines (see Eq. (4.35)).

4.4 Label Formalism

Here we derived the SCET Lagrangian in pure position space. However, in chapter 5 and in most of the literature [4–7, 11, 36] the label formalism is used, which works with a mixture of momentum and position space [8].

When using the label formalism, one splits the collinear momentum p into a large label momentum $\tilde{p}$ and a small residual momentum k like

$$p^\mu = \tilde{p}^\mu + k^\mu, \tag{4.29}$$

with

$$\tilde{p}^\mu = p^- \frac{n^\mu}{2} + p_\perp^\mu, \tag{4.30}$$

where the residual momentum scales like a soft one.

One can now write the jet fields as

$$\chi_n(x) = \sum_{\tilde{p}} \mathrm{e}^{-i\tilde{p}x} \chi_{n,\tilde{p}}(x), \tag{4.31}$$

such that a derivative acting on $\chi_{n,\tilde{p}}(x)$ is of order λ^2. The analogous decomposition is also performed on the collinear gluon field.

The notation of the sum in Eq. (4.31) is of course symbolic and $\tilde{p}$ is still a continuous variable, nevertheless it is often useful to think of the label momentum as discrete, dividing momentum space into a certain number of bins. In this picture the small residual momentum specifies the position inside one bin.

Since collinear fields have large label momenta it is problematic to sum over the whole range of values of the labels (e.g. in collinear loop integrals), including the small ones (the "zero-bin"). This leads to double counting of soft contributions, that can be cured by the so called "zero-bin subtraction" [38], where one subtracts the contributions corresponding to collinear diagrams with soft scaling.

To extract the label momentum of a collinear field one can introduce the label operator $\mathcal{P}$, which acts in the form

$$\mathcal{P}^\mu \chi_{n,\tilde{p}}(x) = \tilde{p}^\mu \chi_{n,\tilde{p}}(x). \tag{4.32}$$

Using the label formalism the collinear quark Lagrangian (prior to the field redefinition) takes the form

$$\mathcal{L}_{n,q} = \mathrm{e}^{-ix\cdot\mathcal{P}} \bar{\xi}_{n,p'} \frac{\bar{\not{n}}}{2} iD^+ \xi_{n,p} + \mathrm{e}^{-ix\cdot\mathcal{P}} \bar{\xi}_{n,p'} (i\not{D}_\perp^n - m) \frac{1}{iD_n^-} (i\not{D}_\perp^n + m) \frac{\bar{\not{n}}}{2} \xi_{n,p}, \tag{4.33}$$

with an implicit sum over the appearing label momenta in the form $\xi_{n,p} \equiv \sum_p \xi_{n,p}$ and

$$\begin{aligned} iD_\perp^{n\,\mu} &= \mathcal{P}_\perp^\mu + g \sum_k A_{\perp,k}^{n\,\mu}, \\ iD_n^- &= \mathcal{P}^- + g \sum_k A_{n,k}^-. \end{aligned} \tag{4.34}$$

Integrating out off-shell propagators, redefining the collinear fields using soft Wilson lines, and using the label formalism leads to the current operator

$$J_i^{(0)\mu}(\omega, \bar{\omega}, \mu) = \left(\bar{\chi}_{n,\omega} Y_n^\dagger S_n^\dagger \Gamma_i^\mu S_{\bar{n}} Y_{\bar{n}} \chi_{\bar{n},\bar{\omega}} \right)(0), \tag{4.35}$$

which is used as a starting point for proving the factorization theorem in chapter 5. S_n is the mass mode Wilson line, which describes contributions of virtual secondary massive particles, which start contributing at the two-loop level (see [11]).

Chapter 5

Factorization Theorem for Jet Cross Sections

Here we will derive the factorized heavy jet mass (HJM) cross section in the dijet limit. We start by considering the QCD cross section in this limit and match the QCD to the SCET current operator. As the final result we will factorize the cross section into three sectors in the form

$$\sigma = H \cdot J \otimes S. \tag{5.1}$$

The resulting three functions describe the dynamics at different characteristic scales, which are used in the resummation procedure by choosing appropriate scales for each factor. H is called the hard function, which is the squared Wilson coefficient and describes the hard interaction, J is the jet function and describes the dynamics of the jets i.e. the collinear particles, and S is the soft function, which describes the soft radiation and soft crosstalk between the jets.

5.1 General Factorization Theorem in SCET

In this and the following section we will largely follow [11] and therefore we omit some of the intermediate steps. Starting from the expression for the leading order QED, full QCD cross section as written in Eq. (3.12), we restrict the final state particles to a situation with just back-to-back jets and soft radiation via writing

$$\sigma = \sum_X^{\text{res}} (2\pi)^4 \delta^{(4)}(q - P_X) \sum_{i=v,a} L^i_{\mu\nu} \left\langle 0 \middle| \mathcal{J}_i^{\dagger\,\mu}(0) \middle| X \right\rangle \left\langle X \middle| \mathcal{J}_i^{\nu}(0) \middle| 0 \right\rangle . \tag{5.2}$$

Here the first sum includes the phase space integration and accounts for all possible final states restricted to the dijet kinematics, which is denoted by "res". In this region of phase space SCET is applicable and we can make use of to the SCET current J_i^μ with the matching condition

$$\mathcal{J}_i^\mu(0) = \int \mathrm{d}\omega \, \mathrm{d}\bar{\omega} \, C(\omega, \bar{\omega}, \mu) J_i^{(0)\mu}(\omega, \bar{\omega}, \mu), \tag{5.3}$$

where $\mathcal{J}_i^\mu$ is the QCD current, and C is the matching coefficient. As derived in the last chapter the SCET current is given by

$$J_i^{(0)\mu}(\omega, \bar{\omega}, \mu) = \left(\bar{\chi}_{n,\omega} Y_n^\dagger S_n^\dagger \Gamma_i^\mu S_{\bar{n}} Y_{\bar{n}} \chi_{\bar{n},\bar{\omega}} \right)(0). \tag{5.4}$$

We impose factorization of the final state (and consequently the phase space) into collinear and soft degrees of freedom in the form

$$|X\rangle = |X_n\rangle\,|X_{\bar{n}}\rangle\,|X_s\rangle\,. \tag{5.5}$$

It is worth noting that when squaring the hadronic matrix element

$$\left\langle X\middle|\mathrm{T}\bar{\chi}_{n,\omega}Y_n^\dagger S_n^\dagger \Gamma_i^\mu S_{\bar{n}} Y_{\bar{n}} \chi_{\bar{n},\bar{\omega}}\middle|0\right\rangle^\dagger = \left\langle 0\middle|\bar{\mathrm{T}}\bar{\chi}_{\bar{n},\bar{\omega}}Y_{\bar{n}}^\dagger S_{\bar{n}}^\dagger \Gamma_i^\mu S_n Y_n \chi_{n,\omega}\middle|X\right\rangle, \tag{5.6}$$

where $\bar{\mathrm{T}}$ is the anti-time ordering operator. The (anti-) time ordering can be dropped when using the bared Wilson lines as defined in Eq. (4.27) because of the intrinsic path ordering structure.

Using some manipulations, SCET power counting, and a generalized Fierz identity (which can be derived from Eq. (33) in [39]), one can write the total cross section as

$$\begin{aligned}\sigma^i = {}& \frac{K_0^i}{16N_C^2}\mathcal{M}_m \sum_{\vec{n}} \sum_{X_{n,\bar{n},s}}^{\text{res}} (2\pi)^4 \delta^{(4)}(q - P_{X_n} - P_{X_{\bar{n}}} - P_{X_s}) \left\langle 0\middle|\bar{Y}_{\bar{n}} Y_n\middle|X_s\right\rangle \left\langle X_s\middle|Y_n^\dagger \bar{Y}_{\bar{n}}^\dagger\middle|0\right\rangle \\ &\times \int \mathrm{d}\omega\,\mathrm{d}\bar{\omega}\,|C(\omega,\bar{\omega},\mu)|^2 \langle 0|\bar{\not{n}}\chi_n|X_n\rangle \langle X_n|\bar{\chi}_{n,\omega}|0\rangle \langle 0|\bar{\chi}_{\bar{n}}|X_{\bar{n}}\rangle \langle X_{\bar{n}}|\not{n}\chi_{\bar{n},\bar{\omega}}|0\rangle\,, \end{aligned} \tag{5.7}$$

where color and spin traces are implied in every factor and $K_0^i = 2(d-2)c^i_{\text{lep}}$. $\mathcal{M}_m = \frac{1}{N_c^2}\left|\left\langle 0\middle|\bar{S}_{\bar{n}} S_n\middle|0\right\rangle\right|^2$ is the mass mode vacuum amplitude, which will be neglected for the rest of this presentation since it is, as mentioned, of order α_s^2.

In the next step we note that due to momentum conservation $C(\omega,\bar{\omega},\mu) = C(Q,-Q,\mu) =: C(Q,\mu)$. Furthermore we implement kinematic constraints by introducing delta functions and use label and residual momentum splitting. The remaining delta functions are turned into integrals over exponentials, which gives the general factorized SCET cross section formula

$$\begin{aligned}\sigma^i = {}& \frac{N_C Q^2 K_0^i}{8\pi}|C(Q,\mu)|^2 \mathcal{M}_m \int \mathrm{d}k_n^+\,\mathrm{d}k_{\bar{n}}^-\,\mathrm{d}k_s^+\,\mathrm{d}k_s^- \\ &\times \sum_{X_n}^{\text{res}} \frac{1}{2\pi}\int \mathrm{d}^4x\;\mathrm{e}^{\frac{i}{2}k_n^+ x^-} \left\langle 0\middle|\bar{\not{n}}\chi_n(x)\middle|X_n\right\rangle \left\langle X_n\middle|\bar{\chi}^{(0)}_{n,Q}\middle|0\right\rangle \\ &\times \sum_{X_{\bar{n}}}^{\text{res}} \frac{1}{2\pi}\int \mathrm{d}^4y\;\mathrm{e}^{\frac{i}{2}k_{\bar{n}}^+ y^+} \left\langle 0\middle|\bar{\chi}_{\bar{n}}(y)\middle|X_{\bar{n}}\right\rangle \left\langle X_{\bar{n}}\middle|\not{n}\chi^{(0)}_{\bar{n},-Q}\middle|0\right\rangle \\ &\times \sum_{X_s}^{\text{res}} \frac{1}{4N_C(2\pi)^2}\int \mathrm{d}z^+\,\mathrm{d}z^-\;\mathrm{e}^{\frac{i}{2}\left(k_s^+ z^- + k_s^- z^+\right)} \left\langle 0\middle|\bar{Y}_{\bar{n}} Y_n(z^+,z^-)\middle|X_s\right\rangle \left\langle X_s\middle|Y_n^\dagger \bar{Y}_{\bar{n}}^\dagger(0)\middle|0\right\rangle. \end{aligned} \tag{5.8}$$

Note that the momenta k are residual.

5.2 Factorization of the Double Hemisphere Mass Cross Section

In the following discussion we will use the general formula in Eq. (5.8) to derive the factorization theorem for the double hemisphere masses cross section. To achieve this we assign every particle in the final state (collinear as well as soft ones) to one of the two hemispheres, labeled by a and b. We define the invariant mass of the hemispheres as

$$\begin{aligned} M_a^2 &:= (p_n + k_s^a)^2, \\ M_b^2 &:= (p_{\bar{n}} + k_s^b)^2, \end{aligned} \tag{5.9}$$

where p_n ($p_{\bar{n}}$) is the sum of all n ($\bar{n}$)-collinear momenta, and k_s^a (k_s^b) the sum of soft momenta in hemisphere a (b). After integrating over k_s^+ and k_s^-, and consequently set the argument of the soft Wilson lines to zero, we implement the hemisphere masses via inserting the identity in the form

$$1 = \int \mathrm{d}M_a^2\, \mathrm{d}M_b^2\, \delta\left((p_n + k_s^a)^2 - M_a^2\right) \delta\left((p_{\bar{n}} + k_s^b)^2 - M_b^2\right), \tag{5.10}$$

under the sum over soft states in Eq. (5.8). Splitting the occurring momenta into label and residual ones, implementing kinematic constraints, and applying power counting one gets

$$(p_n + k_s^a)^2 \quad \to \quad Q(k_n^+ + k_s^{a+}). \tag{5.11}$$

Furthermore we rewrite the hemisphere mass as

$$M_i^2 = m^2 + s_i, \tag{5.12}$$

where m is the mass of the primary quark, produced in the hard interaction, and s_i is the corresponding off-shellness which is small in the two-jet limit.

To make the X_s dependence of $k_s^{a,b} \equiv k_s^{a,b}[X_s]$ explicit we insert the identity in the form

$$1 = \int \mathrm{d}\ell^+\, \mathrm{d}\ell^-\, \delta\left(\ell^+ - k_s^{a+}\right) \delta\left(\ell^- - k_s^{b-}\right). \tag{5.13}$$

Since now all kinematic constraints are implemented through the delta functions and the demanded smallness of the offshellness s_i, we can drop the "res" from the sums. Finally, after applying some more simplifications and taking the derivatives with respect to the hemisphere masses, we obtain the desired factorization formula for the double hemisphere mass cross section

$$\frac{\mathrm{d}^2\sigma^i}{\mathrm{d}M_a^2\, \mathrm{d}M_b^2} = \sigma_0^i H(Q,\mu) \int \mathrm{d}\ell^+\, \mathrm{d}\ell^-\; J_n(s_a - Q\ell^+, \mu) J_{\bar{n}}(s_b - Q\ell^-, \mu) S_{\mathrm{hemi}}(\ell^+, \ell^-, \mu). \tag{5.14}$$

The occurring ingredients are the hard function

$$H(Q,\mu) := |C(Q,\mu)|^2, \tag{5.15}$$

which encodes the hard interaction in the process, the jet functions

$$\begin{aligned} J_n(Qk_n^+ - m^2) &:= -\frac{1}{2\pi Q} \mathrm{Disc}\left[\int \mathrm{d}x^4\; \mathrm{e}^{ik_n x} \left\langle 0 \middle| \mathrm{T}\bar{\chi}_{n,Q}(0) \frac{\bar{\not{n}}}{4N_c} \chi_n(x) \middle| 0 \right\rangle\right], \\ J_{\bar{n}}(Qk_{\bar{n}}^- - m^2) &:= \frac{1}{2\pi Q} \mathrm{Disc}\left[\int \mathrm{d}x^4\; \mathrm{e}^{ik_{\bar{n}} x} \left\langle 0 \middle| \mathrm{T}\bar{\chi}_{\bar{n}}(x) \frac{\not{n}}{4N_c} \chi_{\bar{n},-Q}(0) \middle| 0 \right\rangle\right], \end{aligned} \tag{5.16}$$

which encode the dynamics of the jets, and the hemisphere soft function

$$S_{\mathrm{hemi}}(\ell^+, \ell^-) := \frac{1}{N_c} \sum_{X_s} \delta\left(\ell^+ - k_s^{a+}\right) \delta\left(\ell^- - k_s^{b-}\right) \left\langle 0 \middle| \bar{Y}_{\bar{n}} Y_n(0) \middle| X_s \right\rangle \left\langle X_s \middle| Y_n^\dagger \bar{Y}_{\bar{n}}^\dagger(0) \middle| 0 \right\rangle, \tag{5.17}$$

which describes the soft radiation and the communication of the two jets through soft crosstalk.

Since the soft function accounts for low energy radiation, it is partly governed by non-perturbative effects realized through power corrections to the partonic result [40]. In order to incorporate these effects, the soft function can be factorized further into a convolution of a perturbative partonic soft function and a non-perturbative shape or model function [12, 33] in the form

$$S_{\mathrm{hemi}}(\ell^+, \ell^-) = \int \mathrm{d}\ell'^+\, \mathrm{d}\ell'^-\; S_{\mathrm{hemi}}^{\mathrm{part}}(\ell^+ - \ell'^+, \ell^- - \ell'^-) S_{\mathrm{hemi}}^{\mathrm{mod}}(\ell'^+, \ell'^-), \tag{5.18}$$

where $S_{\mathrm{hemi}}^{\mathrm{part}}$ is the partonic soft function, and $S_{\mathrm{hemi}}^{\mathrm{mod}}$ is the soft model function, which will be described in more detail in section 6.6.

Note that the only function which depends on the primary quark mass is the jet function. However, at two loops additional mass dependencies associated with massive secondary particles come into play for all the corresponding functions.

5.3 Factorization of the Heavy Jet Mass Cross Section

To project the double differential cross section in Eq. (5.14) onto the heavy jet mass we use the HJM definition from Eq. (2.3) and insert the identity in the form

$$1 = \int \mathrm{d}\rho\, \delta\left(\rho - \frac{\max\{M_a^2, M_b^2\}}{Q^2}\right) = \int \mathrm{d}\rho\, \delta\left(\rho - \hat{m}^2 - \frac{\max\{s_a, s_b\}}{Q^2}\right), \tag{5.19}$$

into (5.14), such that the HJM cross section can be obtained by the formula

$$\begin{aligned}\frac{\mathrm{d}\sigma}{\mathrm{d}\rho} &= \int \mathrm{d}s_a\, \mathrm{d}s_b\, \frac{\mathrm{d}^2\sigma}{\mathrm{d}M_a^2\, \mathrm{d}M_b^2} \delta\left(\rho - \hat{m}^2 - \frac{\max\{s_a, s_b\}}{Q^2}\right) \\ &= 2Q^2 \int_0^{Q^2\bar{\rho}} \mathrm{d}s_a\ \frac{\mathrm{d}^2\sigma}{\mathrm{d}M_a^2\, \mathrm{d}M_b^2}\bigg|_{s_b = Q^2\bar{\rho}}.\end{aligned} \tag{5.20}$$

In the last line we used the basic structure of the double differential cross section as given in Eq. (5.14).

However, it should be stressed that the direct use of this formula can be problematic. The reason is that when deriving the partonic cross section, the double hemisphere mass cross section contains distributions such as delta functions or plus distributions, which make some of the transformations made in (5.20), and thus the final formula, not well defined. This can lead to ambiguous or wrong results. A convenient approach to deal with this problem is to calculate the cumulant

$$\Sigma_\rho(\rho_c) = \int_{\rho_{\min}}^{\rho_c} \mathrm{d}\rho\, \frac{\mathrm{d}\sigma}{\mathrm{d}\rho}, \tag{5.21}$$

and then differentiate $\Sigma_\rho(\rho_c)$ with respect to ρ_c to get the differential cross section. When first integrating over ρ in the first line of (5.20), the subsequent manipulations are well defined and the corresponding formula reads

$$\Sigma_\rho(\rho_c) = \int_0^{Q^2\bar{\rho}_c} \mathrm{d}s_a\, \mathrm{d}s_b\, \frac{\mathrm{d}^2\sigma}{\mathrm{d}M_a^2\, \mathrm{d}M_b^2}. \tag{5.22}$$

Chapter 6

Theoretical Ingredients for the Full Cross Section

In this chapter we present the differential cross section with respect to the heavy jet mass (HJM) and the corresponding ingredients including log resummation in the peak and tail region at N^2LL order, non-singular contributions, non-perturbative corrections, and renormalon subtractions.

First we determine the functions present in the SCET factorization formula given in Eq. (5.14) and discuss the corresponding renormalization group equations to resum the related logarithms of the hard, jet, and soft scales. To have accurate predictions in the far-tail region, where the fixed order result is valid, we include the non-singular contributions to the cross section, containing the unresummed contributions subleading in SCET.

Afterwards we will introduce the soft model function which accounts for non-perturbative power corrections. These are especially important in the peak region, whereas in the tail and far-tail region only the leading power corrections are dominant, resulting in a simple shift of the partonic soft function. Subsequently, we remove the $\mathcal{O}(\Lambda_{\mathrm{QCD}})$ renormalon ambiguity present in the pole mass and the soft function to improve convergence of the perturbative series.

6.1 Hard Function

The hard function is obtained from squaring the Wilson coefficient C, originating from matching the quark current operator in QCD and SCET as given in Eq. (5.3). To do so the corresponding matrix elements have to be computed and compared. The matching takes place at a certain scale named the hard scale, at which we impose the matrix elements to give the same results at all orders.

Since the mass is of order of the SCET expansion parameter λ, higher order mass effects are subleading and so in SCET only the leading IR structure of QCD is reproduced. Therefore, the matching has to be done by using the leading order λ expansion of the QCD result. It is easy to see that the tree level matrix elements are the same in QCD and SCET, thus only the loop contributions have to be considered in more detail.

The virtual $\mathcal{O}(\alpha_s)$ QCD diagram was calculated in section 3.3. Expanding Eq. (3.22) in $\hat{m}^2 \sim \lambda^2$

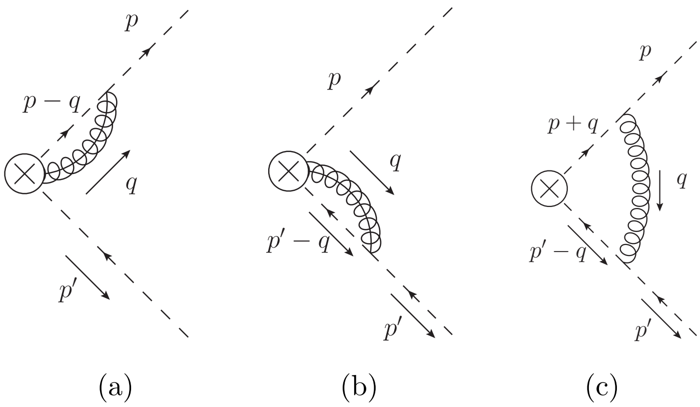

Figure 6.1: The Feynman diagrams which correspond to loop corrections to the SCET quark current, excluding obviously vanishing contributions.

we get

$$\langle q\bar{q}|\mathcal{J}_i^\mu|0\rangle_{\mathrm{QCD}} = \bar{u}(p_1,s_1)\Gamma_i^\mu v(p_2,s_2)\Big\{1+\frac{C_F\alpha_s}{4\pi}\Big[\frac{1}{\varepsilon}\left(-2-2\log\left(-\hat{m}^2\right)\right)+\frac{\pi^2}{3}-4-\log\left(-\hat{m}^2\right) + 2\log\frac{-Q^2}{\mu^2}+\log^2\left(-\hat{m}^2\right)+2\log\left(-\hat{m}^2\right)\log\frac{-Q^2}{\mu^2}\Big]+\mathcal{O}\left(\hat{m}^2\right)\Big\}, \tag{6.1}$$

where $\hat{m}^2 \equiv \hat{m}^2 - i0$, $Q^2 \equiv Q^2 + i0$.

To obtain the right expression for the $\mathcal{O}(\alpha_s)$ matrix elements in SCET we have to compute the diagrams shown in Fig. 6.1, which is done in appendix E.2. Note that diagrams with gluon loops including just Wilson line vertices are zero, since $n^2 = 0$.

Like in the fixed order QCD calculation we multiply the matrix element with the on-shell wave function renormalization $Z_\xi^{\mathrm{OS}} = Z_\psi^{\mathrm{OS}}$ and obtain the matrix element

$$\begin{aligned}\langle q\bar{q}|J_i^\mu|0\rangle_{\mathrm{SCET}} &= Z_\xi^{\mathrm{OS}}\bar{u}_n(p_1,s_1)\left(\Gamma_i^\mu+2H_a\right)v_{\bar{n}}(p_2,s_2)\\ &= \bar{u}_n(p_1,s_1)\Gamma_i^\mu v_{\bar{n}}(p_2,s_2)\left\{1+\frac{\alpha_s C_F}{4\pi}\left[\frac{2}{\varepsilon^2}+\frac{1}{\varepsilon}\left(1-2\log\frac{m^2}{\mu^2}\right)+4+\frac{\pi^2}{6}-\log\frac{m^2}{\mu^2}+\log^2\frac{m^2}{\mu^2}\right]\right\},\end{aligned} \tag{6.2}$$

where H_a corresponds to diagram (a) in Fig. 6.1 and is given in appendix E.2.

Using $C(\omega,\bar{\omega},\mu) = C(Q,\mu)$ (see chapter 5) the matching condition reads

$$\langle q\bar{q}|\mathcal{J}_i^\mu|0\rangle_{\mathrm{QCD}}\Big|_{\hat{m}\ll 1} = C^0(Q)\,\langle q\bar{q}|J_i^\mu|0\rangle_{\mathrm{SCET}}\,, \tag{6.3}$$

where C^0 is the bare Wilson coefficient

$$C^0(Q) = 1+\frac{\alpha_s C_F}{4\pi}\left[-\frac{2}{\varepsilon^2}-\frac{1}{\varepsilon}\left(3-2\log\frac{-Q^2}{\mu^2}\right)-8+\frac{\pi^2}{6}-\log^2\frac{-Q^2}{\mu^2}+3\log\frac{-Q^2}{\mu^2}\right]. \tag{6.4}$$

Note that all the remaining divergences are of UV type. The bare and renormalized coefficients are related by

$$C^0(Q) = Z_C(Q,\mu)C(Q,\mu), \tag{6.5}$$

which results in the renormalization factor

$$Z_C(Q,\mu) = 1-\frac{\alpha_s(\mu)C_F}{4\pi}\left[\frac{2}{\varepsilon^2}+\frac{1}{\varepsilon}\left(3-2\log\frac{-Q^2}{\mu^2}\right)\right], \tag{6.6}$$

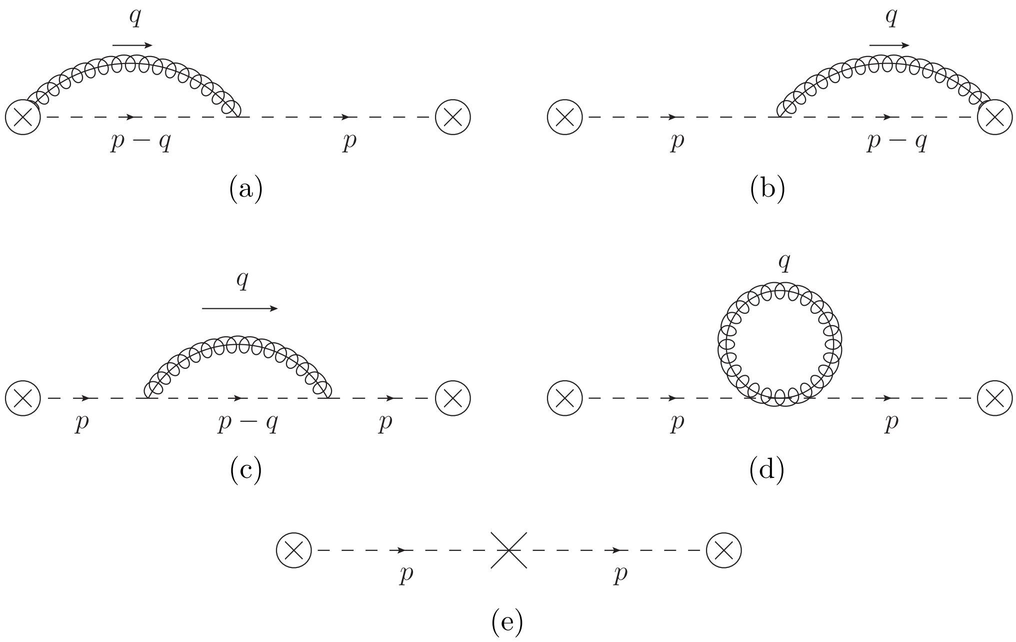

Figure 6.2: Feynman diagrams used for the jet function computation.

and the desired renormalized one-loop hard function

$$H(Q,\mu) = |C(Q,\mu)|^2 = 1 + \frac{\alpha_s(\mu) C_F}{4\pi}\left[-16 + \frac{7\pi^2}{3} + 6\log\frac{Q^2}{\mu^2} - 2\log^2\frac{Q^2}{\mu^2}\right]. \tag{6.7}$$

6.2 Jet Function

The jet function is defined in Eq. (5.16) and describes the dynamics of the collinear particles in the jets. Here we will calculate the jet function at $\mathcal{O}(\alpha_s)$ by taking the imaginary part of the diagrams in Fig. 6.2 and the tree level diagram (which is just the collinear propagator), multiplied with the appropriate factors [12]. The diagrams containing two gluon-Wilson line interactions are obviously zero, just as in the hard function.

The individual diagrams are computed in detail in appendix E.1. The sum of these diagrams, multiplied with the needed factors and traced, reads

$$\begin{aligned}\hat{J} &:= \hat{J}_{\text{tree}} + \hat{J}_a + \hat{J}_b + \hat{J}_c + \hat{J}_d + \hat{J}_e \\ &= -\frac{1}{\pi s}\Bigg\{1 + \frac{C_F\alpha_s}{4\pi}\Bigg[\frac{4}{\varepsilon^2} - \frac{4}{\varepsilon}\log\frac{-s}{\mu^2} + \frac{3}{\varepsilon} + 2\log^2\frac{-s}{\mu^2} - 2\log^2\frac{-s}{m^2} - 4\mathrm{Li}_2\left(\frac{-s}{m^2}\right) - 3\log\frac{-s}{\mu^2} \\ &\quad + 4\log\frac{-s}{m^2}\log\frac{-s}{m^2+s} - \frac{m^2(m^2+2s)}{(s+m^2)^2}\log\frac{-s}{m^2} - \frac{s}{m^2+s} + 8 + \pi^2\Bigg]\Bigg\},\end{aligned} \tag{6.8}$$

where $s = p^2 - m^2 + i0$. Using the imaginary part relations described in appendix C.3, we obtain the unrenormalized one-loop jet function

$$\begin{aligned}J_n^0(s) &= \delta(s) + \frac{C_F\alpha_s}{4\pi}\Bigg\{\left[\frac{4}{\varepsilon^2} + \frac{3}{\varepsilon} + 8 - \frac{\pi^2}{3} + \log\frac{m^2}{\mu^2} + 2\log^2\frac{m^2}{\mu^2}\right]\delta(s) \\ &\quad + \left[-\frac{4}{\varepsilon} - 4 - 4\log\frac{m^2}{\mu^2}\right]\mathcal{L}_0^{\mu^2}(s) + 8\mathcal{L}_1^{\mu^2}(s) + \Theta(s)\left[\frac{s}{(m^2+s)^2} - \frac{4}{s}\log\left(1+\frac{s}{m^2}\right)\right]\Bigg\}.\end{aligned} \tag{6.9}$$

Since the jet function depends on the dynamical quantity s and the renormalization procedure has to be local i.e. an ordinary multiplication in position space, the bare and renormalized momentum space jet functions are related via a convolution, so [12]

$$J^0_{n,\bar{n}}(s) = \int \mathrm{d}s'\, Z_{J_{n,\bar{n}}}(s-s',\mu) J_{n,\bar{n}}(s',\mu). \tag{6.10}$$

Subsequently, the jet function renormalization factor reads

$$Z_{J_{n,\bar{n}}}(s,\mu) = \delta(s) + \frac{C_F\alpha_s(\mu)}{4\pi}\left\{\left[\frac{4}{\varepsilon^2}+\frac{3}{\varepsilon}\right]\delta(s) - \frac{4}{\varepsilon}\mathcal{L}_0^{\mu^2}(s)\right\}, \tag{6.11}$$

and the one-loop renormalized jet function

$$\begin{aligned} J_n(s,\mu) = \delta(s) + \frac{C_F\alpha_s(\mu)}{4\pi}\Bigg\{ &\left[8 - \frac{\pi^2}{3} + \log\frac{m^2}{\mu^2} + 2\log^2\frac{m^2}{\mu^2}\right]\delta(s) \\ &+ \left[-4 - 4\log\frac{m^2}{\mu^2}\right]\mathcal{L}_0^{\mu^2}(s) + 8\mathcal{L}_1^{\mu^2}(s) + \Theta(s)\left[\frac{s}{(m^2+s)^2} - \frac{4}{s}\log\left(1+\frac{s}{m^2}\right)\right]\Bigg\}. \end{aligned} \tag{6.12}$$

Note that the jet function is mass dependent, while the renormalization constant is not, since the UV divergences are universal. Thus the jet function evolution, which will be derived in section 6.4, is identical to the massless one. Note also that at this point we use the pole mass scheme for convenience. We describe the procedure to change to a short distance mass scheme in section 6.7.2.

6.3 Soft Function

The hemisphere soft function is defined in Eq. (5.17). As already explained, the soft function has contributions from perturbative i.e. partonic, and non-perturbative regimes, where the partonic contribution at $\mathcal{O}(\alpha_s)$ is determined by the diagrams in Fig. 6.3 and the appropriate tree level diagram. Note that again some diagrams obviously vanish, namely the ones where the gluon connects two n or two $\bar{n}$ soft Wilson lines. At tree level the soft function can be computed in a straightforward way, since no soft gluons are emitted ($|X_s\rangle = |0\rangle$) and so

$$S^{\text{part,tree}}_{\text{hemi}} = \delta(\ell^+)\delta(\ell^-). \tag{6.13}$$

The $\mathcal{O}(\alpha_s)$ diagrams are calculated in appendix E.3 and the final result of the soft function reads

$$\begin{aligned} S^{\text{part},0}_{\text{hemi}}(\ell^+,\ell^-) &= \delta(\ell^+)\delta(\ell^-) + \frac{C_F\alpha_s\mu^{2\varepsilon}\,\mathrm{e}^{\gamma_E\varepsilon}}{\pi\varepsilon\Gamma(1-\varepsilon)}\left(\delta(\ell^-)\Theta(\ell^+)\left(\ell^+\right)^{-1-2\varepsilon} + \delta(\ell^+)\Theta(\ell^-)\left(\ell^-\right)^{-1-2\varepsilon}\right) \\ &= \delta(\ell^+)\delta(\ell^-) - \frac{C_F\alpha_s}{\pi}\left[\frac{1}{\varepsilon^2}\delta(\ell^-)\delta(\ell^+) - \frac{1}{\varepsilon}\delta(\ell^-)\mathcal{L}_0^{\mu}(\ell^+) - \frac{1}{\varepsilon}\delta(\ell^+)\mathcal{L}_0^{\mu}(\ell^-) - G_S(\ell^+,\ell^-) + \mathcal{O}(\varepsilon)\right], \end{aligned} \tag{6.14}$$

with

$$G_S(\ell^+,\ell^-) = \frac{\pi^2}{12}\delta(\ell^-)\delta(\ell^+) - 2\delta(\ell^-)\mathcal{L}_1^{\mu}(\ell^+) - 2\delta(\ell^+)\mathcal{L}_1^{\mu}(\ell^-). \tag{6.15}$$

To perform the ε expansion of Eq. (6.14) we used relation (C.4) to get the right distributional structure. Note that since in (C.4) the variable x is a dimensionless quantity, we had to introduce

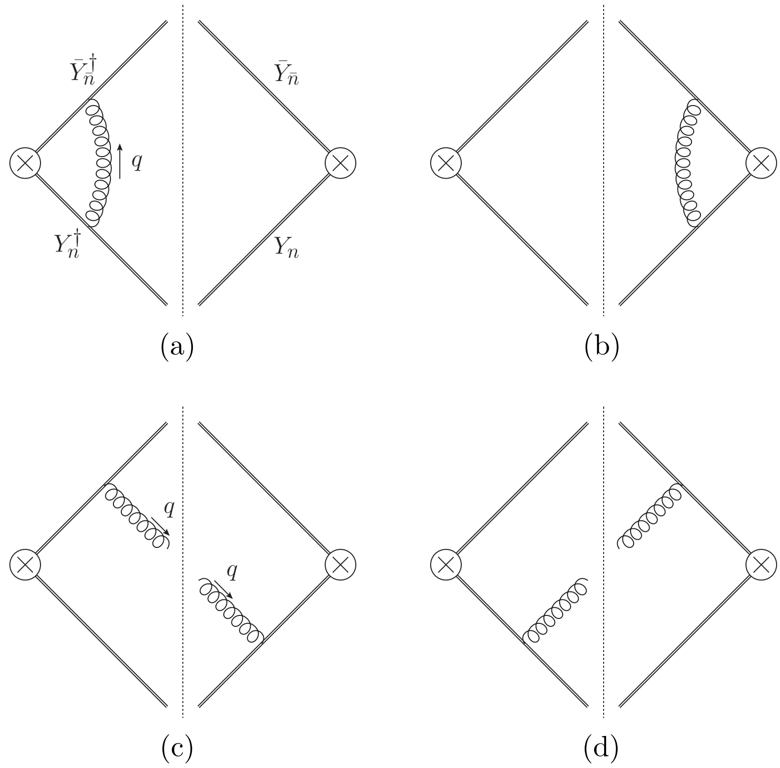

Figure 6.3: Diagrams determining the soft function.

an arbitrary dummy variable κ with energy dimension one, and set $l^i = \kappa x^i$. At the end we specified $\kappa = \mu$ to simplify the result.

Similar to the jet function the renormalized soft function is determined by

$$S_{\text{hemi}}^{\text{part},0}(\ell^+, \ell^-) = \int \mathrm{d}\ell'^+ \, \mathrm{d}\ell'^- \, Z_S(\ell^+ - \ell'^+, \ell^- - \ell'^-, \mu) S_{\text{hemi}}^{\text{part}}(\ell'^+, \ell'^-, \mu), \tag{6.16}$$

which leads to the renormalization factor

$$Z_S(\ell^+, \ell^-, \mu) = \delta(\ell^+)\delta(\ell^-) + \frac{C_F \alpha_s(\mu)}{\pi} \left[-\frac{1}{\varepsilon^2}\delta(\ell^-)\delta(\ell^+) + \frac{1}{\varepsilon}\delta(\ell^-)\mathcal{L}_0^{\mu}(\ell^+) + \frac{1}{\varepsilon}\delta(\ell^+)\mathcal{L}_0^{\mu}(\ell^-) \right], \tag{6.17}$$

and the renormalized one-loop hemisphere soft function

$$S_{\text{hemi}}^{\text{part}}(\ell^+, \ell^-, \mu) = \delta(\ell^+)\delta(\ell^-) + \frac{C_F \alpha_s(\mu)}{\pi} G_S(\ell^+, \ell^-, \mu). \tag{6.18}$$

Note that all our results coincide with [12].

6.4 Renormalization Group Equations and Solutions

To resum the large logarithms as explained in section 3.6, we have to solve the renormalization group equations (RGEs) for the hard, jet, and soft functions given in Eqs. (6.7), (6.12), and (6.18) respectively.

For the hard function, the RGE reads

$$\mu \frac{\mathrm{d}}{\mathrm{d}\mu} H(Q, \mu) = \gamma_H(Q, \mu) H(Q, \mu), \tag{6.19}$$

and the general form of the anomalous dimension of the hard function is [12]

$$\gamma_H(Q,\mu) = -\Gamma_H[\alpha_s]\log\frac{Q^2}{\mu^2} + \gamma_H[\alpha_s], \tag{6.20}$$

where $\Gamma_H[\alpha_s]$ and $\gamma_H[\alpha_s]$ are perturbative coefficients given by

$$\Gamma_H[\alpha_s] =: \sum_{i=0}\Gamma_{H,i}\left(\frac{\alpha_s(\mu)}{4\pi}\right)^{i+1}, \qquad \gamma_H[\alpha_s] =: \sum_{i=0}\gamma_{H,i}\left(\frac{\alpha_s(\mu)}{4\pi}\right)^{i+1}. \tag{6.21}$$

Solving the RGE leads to

$$\begin{aligned} H(Q,\mu) &= H(Q,\mu_H)\exp\left(-\omega_H(\mu,\mu_H,\Gamma_H,2)\log\frac{Q^2}{\mu_H^2} + K_H(\mu,\mu_H,\Gamma_H,\gamma_H)\right) \\ &=: H(Q,\mu_H)U_H(Q,\mu_H,\mu), \end{aligned} \tag{6.22}$$

where U_H is the "evolution kernel" of the hard function, and the occuring functions are

$$\begin{aligned} \omega_F(\mu,\mu_F,\Gamma_F,j) &:= \frac{2}{j}\int_{\alpha_s(\mu_F)}^{\alpha_s(\mu)} \mathrm{d}\alpha\,\frac{\Gamma_F[\alpha]}{\beta[\alpha]}, \\ K_F(\mu,\mu_F,\Gamma_F,\gamma_F) &:= 2\int_{\alpha_s(\mu_F)}^{\alpha_s(\mu)} \mathrm{d}\alpha\,\frac{\Gamma_F[\alpha]}{\beta[\alpha]}\int_{\alpha_s(\mu_H)}^{\alpha}\mathrm{d}\alpha'\,\frac{1}{\beta[\alpha']} + \int_{\alpha_s(\mu_i)}^{\alpha_s(\mu)}\mathrm{d}\alpha\,\frac{\gamma_F[\alpha]}{\beta[\alpha]}, \end{aligned} \tag{6.23}$$

with the QCD beta function

$$\beta[\alpha_s] = -\frac{\alpha_s^2(\mu)}{2\pi}\sum_{i=0}\beta_i\left(\frac{\alpha_s(\mu)}{4\pi}\right)^i, \tag{6.24}$$

which is described in more detail in appendix F.1.

The renormalization of the jet and soft functions in Eqs. (6.10) and (6.16) is given by a convolution, thus the running has a convoluted structure as well, so [12, 34]

$$\begin{aligned} \mu\frac{\mathrm{d}}{\mathrm{d}\mu}J(s,\mu) &= \int \mathrm{d}s'\,\gamma_J(s-s',\mu)J(s',\mu), \\ \mu\frac{\mathrm{d}}{\mathrm{d}\mu}S(\ell^+,\ell^-,\mu) &= \int \mathrm{d}\ell'^+\,\mathrm{d}\ell'^-\,\gamma_S(\ell^+-\ell'^+,\ell^--\ell'^-,\mu)S(\ell'^+,\ell'^-,\mu), \end{aligned} \tag{6.25}$$

with $S \equiv S_{\text{hemi}}$ and

$$\begin{aligned} \gamma_S(\ell^+,\ell^-,\mu) &= \delta(\ell^+)\gamma_s(\ell^-,\mu) + \delta(\ell^-)\gamma_s(\ell^+,\mu), \\ \gamma_F(t,\mu) &= -\frac{2}{j}\Gamma_F[\alpha_s]\mathcal{L}_0^{\mu^j}(t) + \gamma_F[\alpha_s]\delta(t), \quad F = J, s. \end{aligned} \tag{6.26}$$

j is the energy dimension of the argument t, and $\Gamma_F[\alpha_s]$ and $\gamma_F[\alpha_s]$ are defined perturbatively analogous to Eq. (6.21). The splitting of the soft anomalous dimension into two parts as given in (6.26) follows from the consistency relation given by Eq. (6.39).

To solve the RGEs in (6.25) it is convenient to Fourier transform these equations so that

$$\begin{aligned} \mu\frac{\mathrm{d}}{\mathrm{d}\mu}\tilde{J}(y,\mu) &= \tilde{\gamma}_J(y,\mu)\tilde{J}(y,\mu), \\ \mu\frac{\mathrm{d}}{\mathrm{d}\mu}\tilde{S}(Qy^+,Qy^-,\mu) &= \left(\tilde{\gamma}_s(Qy^+,\mu) + \tilde{\gamma}_s(Qy^-,\mu)\right)\tilde{S}(Qy^+,Qy^-,\mu), \end{aligned} \tag{6.27}$$

where y and $y^{+,-}$ are the Fourier space variables with energy dimension -2. These equations can be solved analogously to the hard function, giving the solutions

$$\begin{aligned}
\tilde{J}(y,\mu) &= \tilde{J}(y,\mu_J)\exp\Big(\omega_J(\mu,\mu_J,\Gamma_J,j)\log(iy\,\mathrm{e}^{\gamma_E}\mu_J^j) + K_J(\mu,\mu_J,\Gamma_J,\gamma_J)\Big)\\
&=: \tilde{J}(y,\mu_J)\tilde{U}_J(y,\mu_J,\mu),\\
\tilde{S}(y^+,y^-,\mu) &= \tilde{S}(y^+,y^-,\mu_S)\tilde{U}_S(y^+,y^-,\mu_S,\mu) =: \tilde{S}(y^+,y^-,\mu_S)\tilde{U}_s(y^+,\mu_S,\mu)\tilde{U}_s(y^-,\mu_S,\mu).
\end{aligned} \tag{6.28}$$

To Fourier transform the plus distribution present in the anomalous dimensions, we used the corresponding relation given in the second line of Eq. (C.9). The soft evolution kernel $\tilde{U}_s$ has the same structure as U_J, with the functions ω_F and K_F defined by the Eq. (6.23).

Taking the inverse Fourier transform, the final form of the evolution kernels read

$$U_F(t,\mu_F,\mu) = \frac{\mathrm{e}^{K_F}\,\mathrm{e}^{\gamma_E\omega_F}}{\Gamma(-\omega_F)}\mathcal{L}^{\mu^j}_{0,\omega_F}(t), \tag{6.29}$$

containing the fractional plus distribution, which is defined and explained in appendix C.1.

The calculation of the perturbative coefficients contained in the anomalous dimensions of the hard, jet, and soft functions is straightforward. Since the bare functions are independent of the renormalization scale μ, it holds that

$$\begin{aligned}
\mu\frac{\mathrm{d}}{\mathrm{d}\mu}H^0(Q) &= \mu\frac{\mathrm{d}}{\mathrm{d}\mu}\left(Z_H(Q,\mu)H(Q,\mu)\right) = 0,\\
\mu\frac{\mathrm{d}}{\mathrm{d}\mu}\tilde{J}^0(y) &= \mu\frac{\mathrm{d}}{\mathrm{d}\mu}\Big(\tilde{Z}_J(y,\mu)\tilde{J}(y,\mu)\Big) = 0,\\
\mu\frac{\mathrm{d}}{\mathrm{d}\mu}\tilde{S}^0(Qy^+,Qy^-) &= \mu\frac{\mathrm{d}}{\mathrm{d}\mu}\Big(\tilde{Z}_S(Qy^+,Qy^-,\mu)\tilde{S}(Qy^+,Qy^-,\mu)\Big)\\
&= \mu\frac{\mathrm{d}}{\mathrm{d}\mu}\Big(\tilde{Z}_s(Qy^+,\mu)\tilde{Z}_s(Qy^-,\mu)\tilde{S}(Qy^+,Qy^-,\mu)\Big) = 0,
\end{aligned} \tag{6.30}$$

where we used $Z_H = Z_C^2$ and $Z_S(Qy^+,Qy^-,\mu) = Z_s(Qy^+,\mu)Z_s(Qy^-,\mu)$, following from the first line in Eq. (6.26). The corresponding solutions read

$$\begin{aligned}
\gamma_H &= -\mu\frac{\frac{\mathrm{d}}{\mathrm{d}\mu}Z_H}{Z_H},\\
\tilde{\gamma}_F &= -\mu\frac{\frac{\mathrm{d}}{\mathrm{d}\mu}\tilde{Z}_F}{\tilde{Z}_F}, \quad F = J, s,
\end{aligned} \tag{6.31}$$

thus the results for the leading terms of the anomalous dimensions in Eq. (6.21) (and analogously for the jet and soft functions) are

$$\begin{aligned}
\gamma_{H,0} &= -12C_F,\\
\Gamma_{H,0} &= -8C_F,\\
\gamma_{J,0} &= 6C_F,\\
\Gamma_{J,0} &= 8C_F,\\
\gamma_{s,0} &= 0,\\
\Gamma_{s,0} &= -4C_F.
\end{aligned} \tag{6.32}$$

Since in this thesis we aim to carry out the analysis at N^{2}LL order, we need higher order coefficients, namely Γ_F up to three, and γ_F up to two-loop order. The relevant coefficients for

	Γ_F	γ_F	FO
LL	1	0	0
NLL	2	1	0
N^{2}LL	3	2	1
NLL$'$	2	1	1
N^{2}LL$'$	3	2	2

Table 6.1: This table shows to which order the various ingredients for the resummed cross section are needed to achieve a certain accuracy. The fixed order result is needed in the matching as well as for the non-singular contribution, and corresponds also to the needed order of the jet and soft functions. The numbers specify the order in α_s.

the hard and jet function can be found in [41–43], and the coefficients for the soft function running can be computed via the consistency relation (6.39). Table 6.1 shows to which order in perturbation theory the matrix elements and the anomalous dimensions are needed in the resummation procedure for specific orders of log resummation. The naming corresponds to reference [10].

In the following we give a summery of all perturbative coefficients regarding the anomalous dimensions needed for N^{2}LL resummation:

Hard Function ($j = 2$):

$$\begin{aligned}\Gamma_H[\alpha_s] &= -2\Gamma_{\text{cusp}}[\alpha_s],\\ \gamma_{H,0} &= -12C_F,\\ \gamma_{H,1} &= -\frac{7976}{27} - \frac{136}{9}\pi^2 + \frac{736}{3}\zeta_3 + \left(\frac{1040}{81} + \frac{16}{9}\pi^2\right) n_f.\end{aligned} \tag{6.33}$$

Jet Function ($j = 2$):

$$\begin{aligned}\Gamma_J[\alpha_s] &= 2\Gamma_{\text{cusp}}[\alpha_s],\\ \gamma_{J,0} &= 6C_F,\\ \gamma_{J,1} &= \frac{7220}{27} + \frac{8}{3}\pi^2 - \frac{704}{3}\zeta_3 - \left(\frac{968}{81} + \frac{16}{27}\pi^2\right) n_f.\end{aligned} \tag{6.34}$$

Soft Function ($j = 1$):

$$\begin{aligned}\Gamma_s[\alpha_s] &= -\Gamma_{\text{cusp}}[\alpha_s],\\ \gamma_{s,0} &= 0,\\ \gamma_{s,1} &= -\gamma_{J,1} - \frac{1}{2}\gamma_{H,1},\end{aligned} \tag{6.35}$$

where the cusp anomalous dimension Γ_{cusp} is defined as

$$\Gamma_{\text{cusp}}[\alpha_s] = \sum_{i=0} \Gamma_i^{\text{cusp}} \left(\frac{\alpha_s(\mu)}{4\pi}\right)^{i+1}, \tag{6.36}$$

with the perturbative coefficients

$$\begin{aligned}\Gamma_0^{\text{cusp}} &= \frac{16}{3},\\ \Gamma_1^{\text{cusp}} &= \frac{1072}{9} - \frac{16}{3}\pi^2 - \frac{160}{27}n_f,\\ \Gamma_2^{\text{cusp}} &= 1960 - \frac{2144}{9}\pi^2 + \frac{176}{15}\pi^4 + 352\zeta_3 + \left(-\frac{5104}{27} + \frac{320}{27}\pi^2 - \frac{832}{9}\zeta_3\right) n_f - \frac{64}{81}n_f^2.\end{aligned} \tag{6.37}$$

Now we derive the consistency relation used several times in this section. This relation corresponds to the fact that the double hemisphere mass cross section has to be independent of the renormalization scale, which leads to certain relations between the anomalous dimensions. Let's consider the Fourier transformed double hemisphere mass cross section. From the μ independence follows that

$$\begin{aligned}
\mathcal{F}\left(\frac{\mathrm{d}^2\sigma^i}{\mathrm{d}s_a\,\mathrm{d}s_b}\right)(x_a,x_b) &= \sigma_0^i H(Q,\mu)\tilde{J}_n(x_a,\mu)\tilde{J}_{\bar{n}}(x_b,\mu)\tilde{S}(Qx_a,Qx_b,\mu) \\
\Rightarrow \quad 0 &= \mu\frac{\mathrm{d}}{\mathrm{d}\mu}\left(\mathcal{F}\left(\frac{\mathrm{d}^2\sigma^i}{\mathrm{d}s_a\,\mathrm{d}s_b}\right)(x_a,x_b)\right) \\
&= \left(\gamma_H(Q,\mu)+\tilde{\gamma}_J(x_a,\mu)+\tilde{\gamma}_J(x_b,\mu)+\tilde{\gamma}_S(Qx_a,Qx_b,\mu)\right) \\
&\quad \times \mathcal{F}\left(\frac{\mathrm{d}^2\sigma^i}{\mathrm{d}s_a\,\mathrm{d}s_b}\right)(x_a,x_b), \qquad (6.38)
\end{aligned}$$

and therefore

$$\gamma_H(Q,\mu)+\tilde{\gamma}_J(x_a,\mu)+\tilde{\gamma}_J(x_b,\mu)+\tilde{\gamma}_S(Qx_a,Qx_b,\mu)=0. \qquad (6.39)$$

This equation justifies the splitting of $\tilde{\gamma}_S$ in the form $\tilde{\gamma}_S(Qx_a,Qx_b,\mu)=\tilde{\gamma}_s(Qx_a,\mu)+\tilde{\gamma}_s(Qx_b,\mu)$, as used in (6.26), and subsequently in the solution of the soft RGE. Considering the relations between the anomalous dimension $\tilde{\gamma}_S$, the renormalization factor $\tilde{Z}_S$, and the evolution kernel $\tilde{U}_S$, the respective splittings used in (6.28) and (6.30) are obvious.

Writing Eq. (6.39) in terms of cusp and non-cusp anomalous dimensions leads to the equations which give the relations between the respective coefficients

$$\begin{aligned}
&\gamma_H[\alpha_s]+2\gamma_J[\alpha_s]+2\gamma_s[\alpha_s]=0, \\
&\Gamma_H[\alpha_s]=-\Gamma_J[\alpha_s]=2\Gamma_s[\alpha_s]. \qquad (6.40)
\end{aligned}$$

Note that these relations are valid to all orders in perturbation theory.

6.5 Non-Singular Contribution

In this section we will calculate the non-singular contribution to the cross section, i.e. the subleading contributions in the SCET power counting parameter λ. As explained in chapter 4, SCET is an effective theory suitable for the dijet region, where large logs appear. Away from this region, especially in the far-tail, terms which are subleading in the SCET power counting are getting more and more important and have to be taken into account in a full description. In order to calculate these contributions we first derive the unresummed SCET cross section. For reasons explained in section 5.3, this will be done via the HJM cumulant (5.22), which is then differentiated. Then we subtract the result from our fixed order expression, derived in chapter 3. In the full description this non-singular contribution is added to the resummed singular terms of the factorized SCET cross section.

We start by computing the double hemisphere mass cross section in SCET using the factorization formula in Eq. (5.14), and the appearing functions derived in the sections 6.1, 6.2, and 6.3. In terms of off-shellness s_i, as defined in (5.12), the cross section gives

$$\begin{aligned}
\frac{1}{\sigma_0^i}\frac{\mathrm{d}^2\sigma^i_{\mathrm{SCET}}}{\mathrm{d}s_a\,\mathrm{d}s_b} = \Bigg\{\delta(s_a)+\frac{C_F\alpha_s}{4\pi}\Bigg[&\left(\pi^2+\log\hat{m}^2+2\log^2\hat{m}^2\right)\delta(s_a)+\left(-4-4\log\hat{m}^2\right)\mathcal{L}_0^{Q^2}(s_a) \\
&+\left(\frac{s_a}{(m^2+s_a)^2}-\frac{4}{s_a}\log\left(1+\frac{s_a}{m^2}\right)\right)\Theta(s_a)\Bigg]\Bigg\}\times\Big\{s_a\to s_b\Big\}+\mathcal{O}(\alpha_s^2), \qquad (6.41)
\end{aligned}$$

where the expression in the second pair of curly brackets is obtained by replacing $s_b \to s_a$ in the first one.

After applying the formula for the HJM cumulant, given in (5.22), the $\mathcal{O}(\alpha_s)$ expression reads

$$\frac{1}{\sigma_0^i}\Sigma^i_{\rho,\mathrm{SCET}}(\rho) = \Theta(\bar\rho) + \frac{C_F\alpha_s}{4\pi}\Bigg[(2\pi^2 + 2\log\hat m^2 + 4\log^2\hat m^2)\Theta(\bar\rho) - 8(1+\log\hat m^2)\Theta(\bar\rho)\log\bar\rho$$
$$+ 2\int_0^{Q^2\bar\rho} \mathrm{d}s\left(\frac{s}{(m^2+s)^2} - \frac{4}{s}\log\left(1+\frac{s}{m^2}\right)\right)\Bigg], \tag{6.42}$$

from which we can deduce the HJM differential cross section

$$\frac{1}{\sigma_0^i}\frac{\mathrm{d}\sigma^i_{\mathrm{SCET}}}{\mathrm{d}\rho} = \delta(\bar\rho) + \frac{C_F\alpha_s}{4\pi}\Bigg[\left(2\pi^2 + 2\log\hat m^2 + 4\log^2\hat m^2\right)\delta(\bar\rho) - 8\left(1+\log\hat m^2\right)\mathcal{L}_0(\bar\rho)$$
$$+ 2\left(\frac{\bar\rho}{\rho^2} - \frac{4}{\bar\rho}\log\left(1+\frac{\bar\rho}{\hat m^2}\right)\right)\Theta(\bar\rho)\Bigg]. \tag{6.43}$$

The non-singular cross section can now be obtained easily and is given by

$$\begin{aligned}\frac{1}{\sigma_0^i}\frac{\mathrm{d}\sigma^i_{\mathrm{ns}}}{\mathrm{d}\rho} &= \frac{1}{\sigma_0^i}\frac{\mathrm{d}\sigma^i_{\mathrm{QCD}}}{\mathrm{d}\rho} - \frac{1}{\sigma_0^i}\frac{\mathrm{d}\sigma^i_{\mathrm{SCET}}}{\mathrm{d}\rho}\\ &= f^{0,i}_{\mathrm{ns}}\delta(\bar\rho) + \frac{C_F\alpha_s}{4\pi}\left[f^{\delta,i}_{\mathrm{ns}}\delta(\bar\rho) + f^{+,i}_{\mathrm{ns}}\mathcal{L}_0(\bar\rho) + f^{\mathrm{nd},i}_{\mathrm{ns}}(\rho)\Theta(\bar\rho)\right] + \mathcal{O}(\alpha_s^2),\end{aligned} \tag{6.44}$$

where $f^{j,i}_{\mathrm{ns}} = f^{j,i}_{\mathrm{QCD}} - f^{j,i}_{\mathrm{SCET}}$, with the coefficients for SCET and QCD defined analogously to the non-singular ones. These coefficients can be found in Eq. (6.43) and chapter 3. Some of the non-singular coefficients are rather lengthy expressions but they can be computed in a straightforward way. It should be noted that the coefficients of the non-singular distributional parts vanish for $\hat m \to 0$, as expected.

6.6 Non-Perturbative Corrections

As explained in section 5.2 the soft function is partly governed by non-perturbative effects, appearing in the form of power corrections of the form $(\Lambda_{\mathrm{QCD}}/(Q\rho))^k$ [10, 40]. The structure of the power corrections makes clear that in the tail and far-tail, where $\rho \ll \Lambda_{\mathrm{QCD}}/Q$, only the leading terms, related to the lowest moments of the soft function, have to be considered, which leads to a simple shift of the distribution. However, in the peak region infinitely many terms are needed to fully account for non-perturbative corrections. In this context non-perturbative contributions in the form of power corrections were investigated in [44], using the so called "dispersive method".

We already mentioned the popular strategy to include these corrections via convoluting the partonic soft function with a model function. This approach incorporates the non-perturbative corrections in a continuous way and allows to smoothly connect the peak and tail region [10,12,33]. For such a model function it is useful to choose a series of linearly independent functions in a way that already the first orders give a qualitatively good choice for the peak region. The series of functions is then implemented to a specific order and the coefficients are fit to data.

Due to the structure of thrust with respect to the hemisphere masses for $\tau \ll 1$, it can be shown that for the singular distribution it does not matter if a model function is incorporated at the level of the double hemisphere mass cross section, or after a projection onto thrust. Of course in the first case a two-dimensional model is needed, where in the second case the model is just one-dimensional, which simplifies the situation. For example, a one-dimensional model function was implemented in the thrust analysis in [10]. However, in the case of heavy jet mass, one is forced to incorporate a two-dimensional model function at the hemisphere mass level and to do the projection afterwards.

Note that the structure of the factorized cross section (5.2) allows to rewrite the convolution with the partonic soft function into a convolution with the whole singular cross section.

A common set of functions for a one-dimensional model function is given in [45] and reads

$$\begin{aligned} F(k,\lambda,\{c_i\}) &:= \frac{1}{\lambda}\left[\sum_{n=0}^{N} c_n f_n\left(\frac{k}{\lambda}\right)\right]^2, \\ f_n(z) &:= 8\sqrt{\frac{2z^3(2n+1)}{3}}\,\mathrm{e}^{-2z} P_n[g(z)], \\ g(z) &:= \frac{2}{3}\left[3-\mathrm{e}^{-4z}\left(3+12z+24z^2+32z^3\right)\right]-1, \end{aligned} \tag{6.45}$$

where P_n are Legendre polynomials and $\sum_i c_i^2 = 1$ for normalization. A straightforward generalization to the two-dimensional case is given by

$$F(\ell_1,\ell_2,\lambda,\{c_{ij}\}) := \frac{1}{\lambda^2}\left[\sum_{m,n=0}^{N} c_{mn} f_m\left(\frac{\ell_1}{\lambda}\right) f_n\left(\frac{\ell_2}{\lambda}\right)\right]^2, \tag{6.46}$$

with $\mathrm{Tr}(c^2) = 1$. This function will be used in our analysis where we set $c_{00} = 1$ (and therefore all other coefficients to zero) for simplicity, denoted by $S^{\mathrm{mod}}(\ell^+,\ell^-,\lambda) \equiv F(\ell^+,\ell^-,\lambda,c_{00}=1)$. This has the advantage that a splitting of the model function, such that $S^{\mathrm{mod}}(\ell^+,\ell^-,\lambda) = S^{\mathrm{mod}}(\ell^+,\lambda)S^{\mathrm{mod}}(\ell^-,\lambda)$, is possible.

For HJM values $\rho \gg \Lambda_{\mathrm{QCD}}/Q$, an operator product expansion of the full cross section can be performed, which gives [46]

$$\frac{\mathrm{d}\sigma}{\mathrm{d}\rho} = \frac{\mathrm{d}\sigma^{\mathrm{part}}}{\mathrm{d}\rho} - \frac{\bar{\Omega}_{[1,0]}}{Q}\frac{\mathrm{d}^2\sigma^{\mathrm{part}}}{\mathrm{d}\rho^2} + \ldots, \tag{6.47}$$

with the $[m,n]$-moment of the soft model function

$$\bar{\Omega}_{[m,n]} := \int \mathrm{d}\ell_1\,\mathrm{d}\ell_2\,\ell_1^m \ell_2^n S^{\mathrm{mod}}(\ell_1,\ell_2,\lambda). \tag{6.48}$$

Eq. (6.47) shows that in this region the effect of convoluting with a model function is a shift of the distribution. This demonstrates that away from the peak the full form of the model function is not relevant, and therefore one only needs the first model moment for hadronic predictions in this region. Note also that the leading power correction can in principle be achieved by using a one-dimensional model with first moment $\bar{\Omega}_1 = \bar{\Omega}_{[1,0]}$. This agrees with the two-dimensional approach to a very high extent in the tail and far-tail region as expected.

Interestingly this shift is a universal quantity, which can relate several event-shape power corrections by multiplying an event-shape specific factor, which is easy to compute [47–49]. The HJM shift is related to the thrust (or 2-jettiness) one by a factor of 1/2 [49].

However, the first moment of the HJM distribution

$$M_1^\rho := \frac{1}{\sigma}\int \mathrm{d}\rho\,\rho\frac{\mathrm{d}\sigma}{\mathrm{d}\rho}, \tag{6.49}$$

which encodes information about the peak position, differs from the leading tail correction $\bar{\Omega}_{[1,0]}$, in contrast to the thrust case [46]:

$$M^{\rho}_{1,\text{tree}} = \rho_{\min} + \frac{1}{Q}\left(\bar{\Omega}_{[1,0]} + \Upsilon_{[0,0]}\right), \tag{6.50}$$

with

$$\Upsilon_{[m,n]} := \int \mathrm{d}\ell_1\,\mathrm{d}\ell_2\,\Theta(\ell_1-\ell_2)\,(\ell_1-\ell_2)\,\ell_1^m\ell_2^n S^{\text{mod}}(\ell_1,\ell_2,\lambda). \tag{6.51}$$

This is induced by the more complicated structure due to the two-dimensional model.

Note that the corrections realized through the model function convolution have to be applied to the non-singular contribution as well, such that the cancellations between singular and non-singular contributions, especially in the far-tail where the pure fixed order result is valid, remain intact.

For practical calculations there are essentially two ways to implement the model convolution: To perform a direct convolution in momentum space, and to do a multiplication in Fourier space. Both procedures are carried out numerically. Since the computation of the distributional singular part is numerically more stable in Fourier space, we chose this approach, while we use the momentum space computation as a cross check. The Fourier transformed non-distrubutional part of the jet function as well as the non-singular part are not known analytically, hence for them the calculation is done in momentum space only. The needed Fourier transformed one-variable model function with $c_0 = 1$ is

$$\mathcal{F}(S^{\text{mod}})(Qy) = \frac{256}{(Qy\lambda - 4i)^4}. \tag{6.52}$$

6.7 Renormalon Subtraction

In this section we will discuss another problem connected to non-perturbative effects, namely renormalons.

It is well known that perturbative expansions in a quantum field theory are in general divergent asymptotic series [50]. Renormalons are certain sources of divergence, which are related to large and small momentum behavior. Since QCD is an asymptotic free theory, especially renormalons originating from small momentum, infrared renormalons, are arising and have to be considered. Renormalons can be studied best when using the Borel transform of the perturbative series. The renormalons then manifest themselves as divergences in the Borel plane, which turn into ambiguities of order $(\Lambda_{\text{QCD}}/Q)^k$ when doing the inverse Borel transform. These ambiguities have to be removed to get good perturbative convergence and accurate predictions.

Basically these IR renormalons emerge when doing loop integrals, which always include small loop momenta and consequently include corrections from the non-perturbative region [51]. In the presented HJM cross section two quantities emerge which contain renormalons, which will be treated in the next two sections.

The first one is the soft renormalon, related to the soft function splitting into a perturbative and non-perturbative part, and to the problem that the partonic threshold at $l^{+,-} = 0$ is obviously unphysical [10]. To correct this issue we introduce a gap parameter [10, 33] in the soft model function, which shifts this threshold and can be interpreted as the minimal hadronic energy deposit in one hemisphere. This gap parameter is then split into a perturbative and non-perturbative part, where we use a scheme such that the non-perturbative one is free of the leading renormalon ambiguity and can be extracted from experimental data. The perturbative part on the other hand cancels the renormalon in the partonic soft function order by order. Note that the soft renormalon is just an artifact of the partonic soft function containing low energy contributions e.g. from loop integrals, so that the splitting into a partonic and non-perturbative part is problematic. The arising renormalon is then present in the partonic as well as in the non-perturbative part of the soft function, which finally cancel order by order by using the explained method.

The second renormalon is related to the mass scheme used for the heavy quark mass. So far we used the pole mass scheme in our calculations, which is known to be very sensitive to small energy dynamics and therefore introduces a renormalon ambiguity [51]. Mass schemes for which this is not the case are called “short distance masses” [52, 53], since the low energy effects are related to long distance fluctuations. From a physical point of view it is intuitive that the pole mass is a problematic quantity, since the quark propagator which is used to define it is an object assuming asymptotic quark states which do not exist.

6.7.1 Gap Formalism

As explained above, we switch to a new scheme for the non-perturbative soft function. We consider a class of non-perturbative functions with a gap parameter Δ with support for $k \geq \Delta$. This can be implemented in our usual model function, writing $S^{\text{mod}}(k,k') \to S^{\text{mod}}(k-\Delta, k'-\Delta)$ (we will suppress λ dependencies in this section and $S \equiv S_{\text{hemi}}$).

Hence the relation for the first moment becomes

$$\int \mathrm{d}k\,\mathrm{d}k'\, kS^{\text{mod}}(k,k') = \bar{\Omega}_{[1,0]} \quad \to \quad \Delta + \int \mathrm{d}k\,\mathrm{d}k'\, kS^{\text{mod}}(k,k') = \bar{\Omega}_{[1,0]}. \tag{6.53}$$

where Δ should contain the same renormalon as the power correction $\bar{\Omega}_{[1,0]}$.

Based on this, one can obtain a renormalon free definition of $\bar{\Omega}_{[1,0]}$, which we call $\Omega_{[1,0]}$, by splitting Δ into a non-perturbative component $\bar{\Delta}(R,\mu_S)$, free of the $\mathcal{O}(\Lambda_{\text{QCD}})$ ambiguity, and a perturbative series $\delta(R,\mu_S)$ with the same ambiguity as $\bar{\Omega}_{[1,0]}$. Note that in contrast to Δ, the new objects $\bar{\Delta}$ and δ depend on a subtraction scale R and the soft scale μ_S, and that $\Upsilon_{[0,0]}$ is not changed by the introduction of a gap. $\Omega_{[1,0]}$, the renormalon free definition of $\bar{\Omega}_{[1,0]}$, is consequently

$$\Omega_{[1,0]}(R,\mu_S) = \bar{\Omega}_{[1,0]} - \delta(R,\mu_S) = \bar{\Delta}(R,\mu_S) + \int \mathrm{d}k\,\mathrm{d}k'\, kS^{\text{mod}}(k,k'). \tag{6.54}$$

By applying this method to the full hemisphere soft function we can write

$$\begin{aligned} S(k^+,k^-) &= \int \mathrm{d}k'^+\,\mathrm{d}k'^-\; S^{\text{mod}}(k'^+ - \Delta, k'^- - \Delta) S^{\text{part}}(k^+ - k'^+, k^- - k'^-) \\ &= \int \mathrm{d}k'^+\,\mathrm{d}k'^-\; S^{\text{mod}}(k'^+ - \bar{\Delta}, k'^- - \bar{\Delta}) S^{\text{part}}(k^+ - k'^+ - \delta, k^- - k'^- - \delta) \\ &= \int \mathrm{d}k'^+\,\mathrm{d}k'^-\; S^{\text{mod}}(k'^+ - \bar{\Delta}, k'^- - \bar{\Delta})\, \mathrm{e}^{-\delta\frac{\partial}{\partial k^+}}\, \mathrm{e}^{-\delta\frac{\partial}{\partial k^-}} S^{\text{part}}(k^+ - k'^+, k^- - k'^-), \end{aligned} \tag{6.55}$$

where we omitted the dependence on R and μ_S. The last line induces a perturbative subtraction which must be done strictly order by order.

A convenient scheme for $\delta(R,\mu_S)$ is given and explained in [54, 55], which reads

$$\delta(R,\mu) = R\,\mathrm{e}^{\gamma_E} \left[\frac{\mathrm{d}}{\mathrm{d}(ix_1)} \log \tilde{S}^{\text{part}}(x_1,x_2,\mu)\right]_{x_1=x_2=(iR\,\mathrm{e}^{\gamma_E})^{-1}}, \tag{6.56}$$

where $\tilde{S}$ is the soft function in Fourier space and the scale R, already introduced above, is associated with the scale where the renormalon is subtracted.

Since the renormalon must be subtracted order by order, we define a perturbative expansion of δ in the form

$$\delta(R,\mu_S) = R\,\mathrm{e}^{\gamma_E} \sum_{i=1} \left(\frac{\alpha_s(\mu_S)}{4\pi}\right)^i \delta_i(R,\mu_S) =: \sum_{i=1} \hat{\delta}_i(R,\mu_S), \tag{6.57}$$

such that the $\mathcal{O}(\alpha_s)$ subtraction for the one-argument soft function reads

$$S(k-k'-\delta) = S(k-k') - S'(k-k')\delta + ... = S(k-k') - \delta'(k-k')\hat{\delta}_1 + \mathcal{O}(\alpha_s^2). \tag{6.58}$$

The first two coefficients of the perturbative series in (6.57) can be computed by using the log structure and exponentiation property of the soft function [54]. They read

$$\begin{aligned}
\hat{\delta}_1(R,\mu) &= R\,\mathrm{e}^{\gamma_E} \frac{\alpha_s(\mu)}{4\pi} \left(-8C_F \log\frac{\mu}{R}\right), \\
\hat{\delta}_2(R,\mu) &= R\,\mathrm{e}^{\gamma_E} \left(\frac{\alpha_s(\mu)}{4\pi}\right)^2 C_F \Bigg[\left(-\frac{808}{9} - \frac{22\pi^2}{3} + 84\zeta_3 + \left(-\frac{539}{3} + 8\pi^2\right)\log\frac{\mu}{R} - 88\log^2\frac{\mu}{R}\right) \\
&\quad + n_f \left(\frac{112}{27} + \frac{4}{9}\pi^2 + \frac{80}{9}\log\frac{\mu}{R} + \frac{16}{3}\log^2\frac{\mu}{R}\right)\Bigg].
\end{aligned} \tag{6.59}$$

Since $\bar{\Omega}_{[1,0]} \sim \Lambda_{\mathrm{QCD}}$, the natural choice to set R seems to be $R \sim 1\,\mathrm{GeV}$, such that $\Omega_{[1,0]} \sim \Lambda_{\mathrm{QCD}}$ and $\alpha_s(R)$ is still perturbative [10]. However, this leads to large logs in the tail region and is therefore not a wise choice. The solution to this problem is to parametrize $\bar{\Delta}$ at the reference scales $R_\Delta \sim \mu_\Delta \sim 1\,\mathrm{GeV}$, and then evolve them to the appropriate scale, namely the soft scale. The evolution of $\bar{\Delta}$ is explained in appendix F.3 and in [56, 57].

6.7.2 $\overline{\mathrm{MS}}$ Mass

At the beginning of this chapter we noted that we should change the mass scheme from the pole mass, which contains an IR renormalon ambiguity, to a short distance mass. A short distance mass suitable for our problem is the $\overline{\mathrm{MS}}$ mass. To change the mass scheme from pole to $\overline{\mathrm{MS}}$ we use the relation between these scemes at one-loop order, which reads [58]

$$\hat{m} \equiv \hat{m}^{\mathrm{pole}} = \hat{\overline{m}}(\mu) + \delta\hat{\overline{m}}(\mu), \tag{6.60}$$

with

$$\delta\hat{\overline{m}}(\mu) = \frac{\alpha_s(\mu)C_F}{\pi}\hat{\overline{m}}(\mu)\left[1 - \frac{3}{2}\log\frac{\overline{m}(\mu)}{\mu}\right] + \mathcal{O}(\alpha_s^2), \tag{6.61}$$

where $\hat{\overline{m}}(\mu)$ is the $\overline{\mathrm{MS}}$ mass in units of center of mass energy.

The $\overline{\mathrm{MS}}$ mass depends on a renormalization scale μ, which should be chosen at the characteristic scale where the mass dependence appears, namely the jet scale. On the other hand, it can be seen from the form of $\delta\hat{\overline{m}}(\mu)$ that it is best to choose $\mu \sim \hat{\overline{m}}$ to avoid large logarithms, which arise at scales far from the mass scale. Again we solve this issue by choosing $\overline{m}(\overline{m})$ as an input parameter, which we then evolve to the appropriate scale by using the renormalization group evolution, described in more detail in appendix F.4.

6.8 Final Result

In the past sections we introduced the most important corrections to the differential fixed order cross section. We introduced resummation of large logarithms, arising from strong scale hierarchies in the tail and peak region, non-perturbative corrections, and renormalon subtractions in the soft function and the heavy quark mass. As already mentioned, we computed the distributional singular cross section in Fourier space as well as in momentum space as a cross check. Here we present the final formula in Fourier space, since all the involved convolutions become multiplications, which makes the equation more overseeable. Including all the mentioned pieces the singular differential cross section reads

$$
\begin{aligned}
\frac{1}{\sigma_0^i}\frac{\mathrm{d}\sigma_{\mathrm{s}}^i}{\mathrm{d}\rho} &= 2Q^2 H(Q,\mu_H) U_H(Q,\mu_H,\mu)\frac{1}{(2\pi)^2} \\
&\times \int \mathrm{d}x_a\,\mathrm{d}x_b\,\frac{\exp\Big(i(x_a+x_b)Q\Big(Q\tilde{\rho}-\bar{\Delta}(R_\Delta,\mu_\Delta)-U_{\bar{\Delta}}(R_\Delta,R,\mu_\Delta,\mu_S)\Big)\Big)}{ix_a} \\
&\times \Big[\tilde{J}_n(x_a,\overline{m},\mu_J)\tilde{U}_J(x_a,\mu_J,\mu)\tilde{S}^{\mathrm{mod}}(Qx_a,\lambda)\tilde{U}_s(Qx_a,\mu_S,\mu) \\
&\times \Big(\tilde{S}^{\mathrm{part}}(Qx_a,\mu_S)-ix_aQ\Big(\hat{\delta}_1(R,\mu_S)+2Q\,\hat{\overline{m}}\,\delta\hat{\overline{m}}(\mu_J)\Big)\Big)\Big]\times\Big[a\to b\Big]+\mathcal{O}(\alpha_s^2),
\end{aligned}
\tag{6.62}
$$

where the tilde denotes the Fourier transformed expressions, which are easy to obtain by using the formulas given in appendix C.2, and the remaining expressions are defined as $\tilde{\rho}=\rho-\hat{\overline{m}}^2$ and $\overline{m}\equiv\overline{m}(\overline{m})U_m(\overline{m},\mu_J)$. The last factor in square brackets is the same as the first one with $x_a\to x_b$. When multiplying these brackets, one has to take care of the strict α_s expansion of the perturbative corrections.

A note to the numerical evaluation of the integral above: Taking the formula in (6.62) as it is, the evaluation contains numerical instabilities due to the presence of a pole and a branch cut at $x_{a,b}=0$. To solve this issue we considered the integrand on the complex plane, and used Cauchy's integral theorem to transform the integration path away from the pole such that an effective substitution $x\to x(1+i)-i$ is made in the integrand.

To convolute the non-singular contribution with the two-dimensional model we have to obtain the non-singular double hemisphere mass cross section. Knowing the expressions of the HJM cross section in the different phase space regions, introduced in section 3.4.1, and the associated kinematic situations for the three final state particles, we can obtain the double differential cross section by multiplying the HJM cross section, associated with the different regions, with the related delta functions, arising from the single particle in the light hemisphere. In phase space region 1, the light hemisphere consists of one heavy quark, where in region 3 the light hemisphere contains the massless gluon. These considerations lead to the expression

$$
\begin{aligned}
\frac{\mathrm{d}^2\sigma_{\mathrm{ns}}^i}{\mathrm{d}s_a\,\mathrm{d}s_b}(Q^2\bar{\rho}_a,Q^2\bar{\rho}_b) = \frac{1}{2Q^4}\Bigg[&2\frac{\mathrm{d}\sigma_{\mathrm{ns}}^{i,(1)}}{\mathrm{d}\rho}(\rho_a)\delta(\bar{\rho}_b)+2\frac{\mathrm{d}\sigma_{\mathrm{ns}}^{i,(1)}}{\mathrm{d}\rho}(\rho_b)\delta(\bar{\rho}_a) \\
&+\frac{\mathrm{d}\sigma_{\mathrm{ns}}^{i,(3)}}{\mathrm{d}\rho}(\rho_a)\delta(\rho_b)+\frac{\mathrm{d}\sigma_{\mathrm{ns}}^{i,(3)}}{\mathrm{d}\rho}(\rho_b)\delta(\rho_a)\Bigg],
\end{aligned}
\tag{6.63}
$$

where (1) and (3) denote the different phase space regions. The Born and virtual contributions are included in the expressions denoted with (1). Using the projection formula (5.20), including the gapped model function, and the $\overline{\text{MS}}$ mass scheme, the non-singular cross section reads

$$
\begin{aligned}
&\frac{1}{\sigma_0^i}\frac{\mathrm{d}\sigma_{\text{ns}}^i}{\mathrm{d}\rho} = \frac{1}{\sigma_0^i} Q \int \mathrm{d}\ell \\
&\times\Bigg\{ 2S^{\text{mod}}\left(Q\tilde{\rho}-\bar{\Delta}\right) S^{\text{mod}}(\ell) \int\limits_{\hat{\overline{m}}^2}^{\rho-\frac{\bar{\Delta}}{Q}} \mathrm{d}\rho' \, \frac{\mathrm{d}\sigma_{\text{ns}}^{i,(1)}}{\mathrm{d}\rho}\left(\rho'-\frac{\ell}{Q}\right) + 2\frac{\mathrm{d}\sigma_{\text{ns}}^{i,(1)}}{\mathrm{d}\rho}\left(\rho-\frac{\bar{\Delta}}{Q}-\frac{\ell}{Q}\right) S^{\text{mod}}(\ell) \int\limits_0^{\tilde{\rho}-\frac{\bar{\Delta}}{Q}} \mathrm{d}\rho' \, S^{\text{mod}}(Q\rho') \\
&+ S^{\text{mod}}\left(Q\rho-\bar{\Delta}\right) S^{\text{mod}}(\ell) \int\limits_{4\hat{\overline{m}}^2}^{\rho-\frac{\bar{\Delta}}{Q}} \mathrm{d}\rho' \, \frac{\mathrm{d}\sigma_{\text{ns}}^{i,(3)}}{\mathrm{d}\rho}\left(\rho'-\frac{\ell}{Q}\right) + \frac{\mathrm{d}\sigma_{\text{ns}}^{i,(3)}}{\mathrm{d}\rho}\left(\rho-\frac{\bar{\Delta}}{Q}-\frac{\ell}{Q}\right) S^{\text{mod}}(\ell) \int\limits_0^{\rho-\frac{\bar{\Delta}}{Q}} \mathrm{d}\rho' \, S^{\text{mod}}(Q\rho') \\
&-2\hat{\delta}_1 f_{\text{ns}}^{0,i}\Bigg[\left.\frac{\mathrm{d}S^{\text{mod}}(k)}{\mathrm{d}k}\right|_{k=Q\tilde{\rho}-\bar{\Delta}} S^{\text{mod}}(\ell) + \frac{\mathrm{d}S^{\text{mod}}(\ell)}{\mathrm{d}\ell} S^{\text{mod}}\left(Q\tilde{\rho}-\bar{\Delta}\right) \\
&\quad + \frac{\mathrm{d}S^{\text{mod}}(\ell)}{\mathrm{d}\ell}\delta\left(\tilde{\rho}-\frac{\bar{\Delta}}{Q}-\frac{\ell}{Q}\right) \int\limits_0^{\tilde{\rho}-\frac{\bar{\Delta}}{\ell}} \mathrm{d}\rho' \, S^{\text{mod}}(Q\rho') + \frac{1}{Q} S^{\text{mod}}\left(Q\tilde{\rho}-\bar{\Delta}\right) S^{\text{mod}}(\ell)\,\delta\left(\tilde{\rho}-\frac{\bar{\Delta}}{Q}-\frac{\ell}{Q}\right)\Bigg] \\
&-4\hat{\overline{m}}\,\delta\hat{\overline{m}}\Bigg[f_{\text{ns}}^{0,i} Q \left.\frac{\mathrm{d}S^{\text{mod}}(k)}{\mathrm{d}k}\right|_{k=Q\tilde{\rho}-\bar{\Delta}} S^{\text{mod}}(\ell) + S^{\text{mod}}\left(Q\tilde{\rho}-\bar{\Delta}\right) S^{\text{mod}}(\ell) \frac{\mathrm{d}f_{\text{ns}}^{0,i}\left(\hat{\overline{m}}\right)}{\mathrm{d}\hat{\overline{m}}} \\
&\quad + f_{\text{ns}}^{0,i}\delta\left(\tilde{\rho}-\frac{\bar{\Delta}}{Q}-\frac{\ell}{Q}\right) S^{\text{mod}}(\ell) S^{\text{mod}}\left(Q\tilde{\rho}-\bar{\Delta}\right) + \frac{\mathrm{d}f_{\text{ns}}^{0,i}\left(\hat{\overline{m}}\right)}{\mathrm{d}\hat{\overline{m}}}\delta\left(\tilde{\rho}-\frac{\bar{\Delta}}{Q}-\frac{\ell}{Q}\right) S^{\text{mod}}(\ell) \int\limits_0^{\tilde{\rho}-\frac{\bar{\Delta}}{Q}} \mathrm{d}\rho' \, S^{\text{mod}}(Q\rho') \\
&\quad - Q f_{\text{ns}}^{0,i}\delta\left(\tilde{\rho}-\frac{\bar{\Delta}}{Q}-\frac{\ell}{Q}\right) \frac{\mathrm{d}S^{\text{mod}}(\ell)}{\mathrm{d}\ell} \int\limits_0^{\tilde{\rho}-\frac{\bar{\Delta}}{Q}} \mathrm{d}\rho' \, S^{\text{mod}}(Q\rho') \Bigg]\Bigg\},
\end{aligned}
\tag{6.64}
$$

with omitted λ and μ dependencies. As in the singular contribution, $\bar{\Delta}$ and $\overline{m}$ are evolved from the log-minimizing to the appropriate characteristic scales.

Chapter 7

Analysis

In this chapter we will analyze our final results for the heavy jet mass (HJM) cross section regarding perturbative convergence and mass effects. While showing some plots we will draw first conclusions.

Prior to this we will introduce profile functions, which determine the renormalization scales such that logarithms are resummed correctly in all regions of the distribution.

7.1 Profile Functions

In chapter 5 we proved factorization for the heavy jet mass cross section in the 2-jet region, which led finally to the factorization formula (5.14). In this factorized form the cross section is built out of several functions, where each contains a distinct logarithm containing fractions of the renormalization scale and one of the characteristic scales, as explained in section 3.6. To ensure small logs we choose the renormalization scale in each function to be of the order of the contained characteristic scale, and evolve them to a common scale via the evolution kernels obtained in section 6.4, which resumms the large logs. Since the characteristic scales depend on the event-shape value, the renormalization scales should as well, which leads to certain theoretic constraints for different regions of the cross section [10]:

In the non-perturbative region: $\mu_H \sim Q, \quad \mu_J \sim \sqrt{\Lambda_{\mathrm{QCD}} Q}, \quad \mu_S \sim R \sim \Lambda_{\mathrm{QCD}}.$

In the resummation region: $\mu_H \sim Q, \quad \mu_J \sim Q\sqrt{\rho}, \quad \mu_S \sim R \sim Q\rho.$

In the fixed order region: $\mu_H = \mu_J = \mu_S = R \sim Q.$

The basic character of these regions can be understood rather easily. In the non-perturbative region, which is associated with the peak, the cross section is governed by non-perturbative effects (modeled by the model function in section 6.6), and the appearing scales are characterized by a distinct hierarchy where the soft scale is of order of Λ_{QCD} (note that resummation is nevertheless important in this region). The resummation region, associated with the tail, is the area where we want to apply our techniques to resum the large logarithms. Consequently, the scales are chosen to be similar to the scales appearing in the logarithms. In the fixed order region, associated with the far-tail, the scales are of the same order, and the cross section is well described by the fixed order result. To meet all these constraints we use profile functions [10, 59], which assign smooth functions of ρ to every renormalization scale. Note that the points of transition between these regions are in general process dependent.

The scale dependence of the cross section is a useful measure of the remaining theoretical uncertainty, arising from the truncation of the perturbation series [60], since this accounts for missing higher order effects. We use this feature by varying several parameters contained in the profile functions, to account for uncertainties and test the perturbative convergence of the cross section via comparing the resulting error bands at different orders.

For our analysis we use the same form and parameters as for massless thrust given in [59]. As noted in chapter 2, thrust and heavy jet mass are equivalent for three massless final state particles. Therefore, it is expected that for $\hat{m} \ll 1/2$ (which is necessary anyways in our analysis as we will explain in section 7.2), corrections for the profile parameters are negligible. Nevertheless, heavy jet mass specific massive profile functions will be constructed in future works to predict distributions for arbitrary $\hat{m}$.

According to the profile functions in [59], we set the hard scale to $\mu_H = e_H Q$, where e_H is a parameter which is varied between 0.5 and 2.

The soft profile function is more complicated and reads

$$\mu_S = \begin{cases} \mu_0 & (0 \leq \rho < t_0) \\ \zeta(\mu_0, 0, 0, r_s\mu_H, t_0, t_1, \rho) & (t_0 \leq \rho < t_1) \\ r_s \mu_H \rho & (t_1 \leq \rho < t_2) \\ \zeta(0, r_s\mu_H, \mu_H, 0, t_2, t_s, \rho) & (t_2 \leq \rho < t_s) \\ \mu_H & (t_s \leq \rho) \end{cases}, \tag{7.1}$$

where μ_0 controls the starting point of the soft scale at $\rho = \rho_{\min}$, r_0 determines the slope in the resummation region, and the t_i specify the transition points of the different regions as described above. Since t_0 and t_1 depend on the center of mass energy Q, we use the variable $n_i = \frac{t_i}{Q/1\,\mathrm{GeV}}$ when fixing central values and performing variations. The function $\zeta(a_1, b_1, a_2, b_2, t_1, t_2, t)$ connects the different profile regions so that the profile itself and its first derivative are continuous. ζ is a smooth piecewise function out of two quadratic equations, which meet at $t_m = \frac{t_1+t_2}{2}$. It reads

$$\zeta(a_1, b_1, a_2, b_2, t_1, t_2, t) := \begin{cases} \hat{a}_1 + b_1(t - t_1) + e_1(t - t_1)^2 & (t_1 \leq t \leq t_m) \\ \hat{a}_2 + b_2(t - t_2) + e_2(t - t_2)^2 & (t_m \leq t \leq t_2) \end{cases}, \tag{7.2}$$

with

$$\begin{aligned} &\hat{a}_1 = a_1 + b_1 t_1, \quad \hat{a}_2 = a_2 + b_2 t_2, \\ &e_1 = \frac{4(\hat{a}_2 - \hat{a}_1) - (3b_1 + b_2)(t_2 - t_1)}{2(t_2 - t_1)^2}, \quad e_2 = \frac{4(\hat{a}_1 - \hat{a}_2) + (3b_2 + b_1)(t_2 - t_1)}{2(t_2 - t_1)^2}. \end{aligned} \tag{7.3}$$

The jet scale profile function is motivated by the natural relations between the hard, jet and soft scales ($\mu_H \mu_S \sim \mu_J^2$) and reads

$$\mu_J(\rho) = \begin{cases} \left[1 + e_J(\rho - t_s)^2\right] \sqrt{\mu_H \mu_S(\rho)} & (\rho \leq t_s) \\ \mu_H & (t_s < \rho) \end{cases}, \tag{7.4}$$

where e_J allows to vary the jet scale with respect to this natural relation.

The scale R, used in the gap formalism, should have the same value as the soft scale in the resummation and fixed order region to avoid large logs. However, it has been shown in [10] that in the non-perturbative region a non-vanishing $\mathcal{O}(\alpha_s)$ subtraction piece has positive effects on

Parameter name	Central value	Variation interval
μ_0	1.1 GeV	-
R_0	0.7 GeV	-
n_0	2	1.5 to 2.5
n_1	10	8.5 to 11.5
t_2	0.25	0.225 to 0.275
t_s	0.4	0.375 to 0.425
r_s	2	1.77 to 2.26
e_J	0	-1.5 to 1.5
e_H	1	0.5 to 2
n_s	0	-1, 0, 1

Table 7.1: Central values and intervals of variation for the profile function parameters as given in [59].

perturbative convergence. Thus the R profile function is chosen to be

$$R(\rho) = \begin{cases} R_0 & (0 \leq \rho < t_0) \\ \zeta(R_0, 0, 0, r_s\mu_H, t_0, t_1, \rho) & (t_0 \leq \rho < t_1) \\ \mu_S(\rho) & (t_1 \leq \rho) \end{cases} , \tag{7.5}$$

where R_0 is the parameter which specifies R at $\rho = \rho_{\mathrm{min}}$.

For the renormalization scale of the non-singular distribution we use the three prescriptions [59]

$$\mu_{\mathrm{ns}}(\rho) = \begin{cases} \frac{1}{2}\left(\mu_H + \mu_J(\rho)\right) & (n_s = 1) \\ \mu_H & (n_s = 0) \\ \frac{1}{2}\left(3\mu_H - \mu_J(\rho)\right) & (n_s = -1) \end{cases} . \tag{7.6}$$

The standard values and variation ranges of all occurring parameters are summarized in Table 7.1. Note that the parameter r_s, which controls the slope, has the standard value 2. In contrast to the expected natural choice $r_s = 1$, it turns out that the factors of $\log r_s$, which get shifted between different orders, are small and the perturbative convergence is better due to increased smoothness of the profiles [59].

A plot showing the profile functions of the hard, jet, and soft scales, including the variation bands, are shown in Fig. 7.1 for a center of mass energy of $Q = 91.2\,\mathrm{GeV}$.

7.2 Initial Bottom Quark Pair Production

Let's start analyzing our results by looking at initial $b\bar{b}$ pair production. We will test perturbative convergence via varying the profile parameters as explained in the last section, and compare $b\bar{b}$ results with the massless distribution.

For a complete description, vector as well as axial contributions have to be included, so

$$\frac{1}{\sigma_0}\frac{\mathrm{d}\sigma}{\mathrm{d}\rho} = \frac{1}{\sigma_0}\sum_{i=v,a}\sigma_0^i\left(\frac{1}{\sigma_0^i}\frac{\mathrm{d}\sigma_{\mathrm{s}}^i}{\mathrm{d}\rho} + \frac{1}{\sigma_0^i}\frac{\mathrm{d}\sigma_{\mathrm{ns}}^i}{\mathrm{d}\rho}\right), \tag{7.7}$$

has to be considered. To see the tail region more clearly we multiply the distributions with ρ, which flattens the peak region.

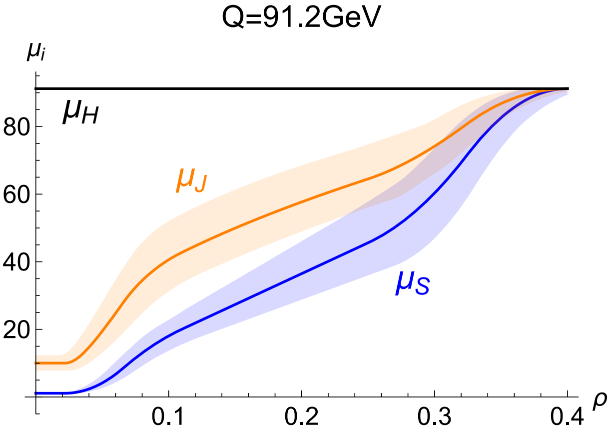

Figure 7.1: Profile functions for μ_H, μ_J, and μ_S, using the parameters given in Table 7.1 and including variation bands. Note that the hard scale variation is not shown.

The values for the appearing physical constants are taken to be [10]

$$m_Z = 91.187\,\text{GeV}, \qquad \Gamma_Z = 2.4952\,\text{GeV}, \qquad \theta_w = \sin^{-1}(\sqrt{0.23119}),$$
$$\alpha_s(m_Z) = 0.118, \qquad \alpha(m_Z) = (127.925)^{-1}, \tag{7.8}$$

and for the soft model parameter λ and the gap parameter $\bar{\Delta}$ we choose

$$\lambda = 0.5\,\text{GeV}, \qquad \bar{\Delta}(R_\Delta, \mu_\Delta) = \bar{\Delta}(2\,\text{GeV}, 2\,\text{GeV}) = 0.05\,\text{GeV}, \tag{7.9}$$

which are realistic values to check our results qualitatively.

It is important to note that our results are only valid in the region where the mass is smaller than the soft scale, i.e. $\mu_H > \mu_J > \mu_S > m \gg \Lambda_{\text{QCD}}$, which is called "scenario IV". At a certain point, which in our case lies near the peak, the mass gets larger than the soft scale (named scenario III). Here one has to account for threshold corrections in the evolution of the soft function, which is not included in our results. Thus our results are only designed for the tail and far-tail region.

A top quark analysis is beyond the scope of this thesis. Apart from finite lifetime effects, for masses of the order of the top a more general analysis, involving other scenarios, is necessary. When examining the jet function a bit more closely, it gets apparent that it contains the scale $Q\sqrt{\bar{\rho} + \hat{m}^2}$ as well as $Q\sqrt{\bar{\rho}}$. For small $\hat{m}$ these two scales are similar, and it's OK to choose $\mu_J \sim Q\sqrt{\bar{\rho}}$ in the resummation region, since no large logs are introduced. However, for large $\hat{m}$, including most situations containing top quarks, additional large logs emerge, which have to be resummed by an additional effective field theory called "boosted heavy quark effective theory" (bHQET).

To initiate the discussion let's consider the massless case. In Fig. 7.2 plots of the HJM distributions at N^{2}LL and NLL accuracy with the corresponding error bands at center of mass energies of 91.2 GeV and 35 GeV are depicted. We observe that the results converge very well in the tail region for both energies.

The massive results show a similar behavior. In Fig. 7.3 the same parameter setup as for the massless case is depicted, but for initial quark pair production with a finite quark mass of $\overline{m}(\overline{m}) = 4.2\,\text{GeV}$, corresponding to bottom quarks. In the same figure the profile functions, including the mass scale, for the considered center of mass energies can be seen. The intersection point of the soft and mass scale, and therefore the beginning of the region of scenario IV, where our results are valid, is clearly visible. For a center of mass energy of $Q = 91.2\,\text{GeV}$ the intersection point lies at $\rho \approx 0.05$, where for $Q = 35\,\text{GeV}$ we find $\rho \approx 0.12$.

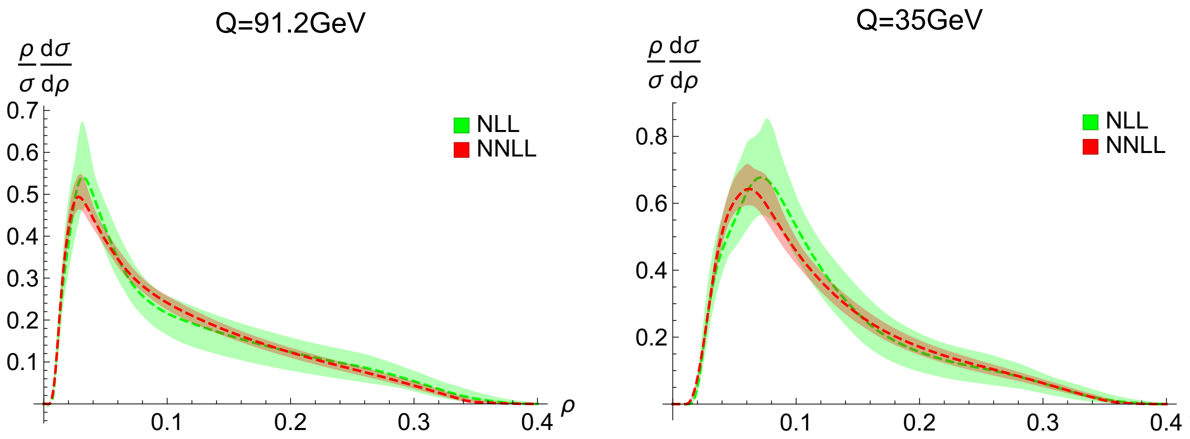

Figure 7.2: Massless heavy jet mass cross sections at different center of mass energies and orders of log resummation.

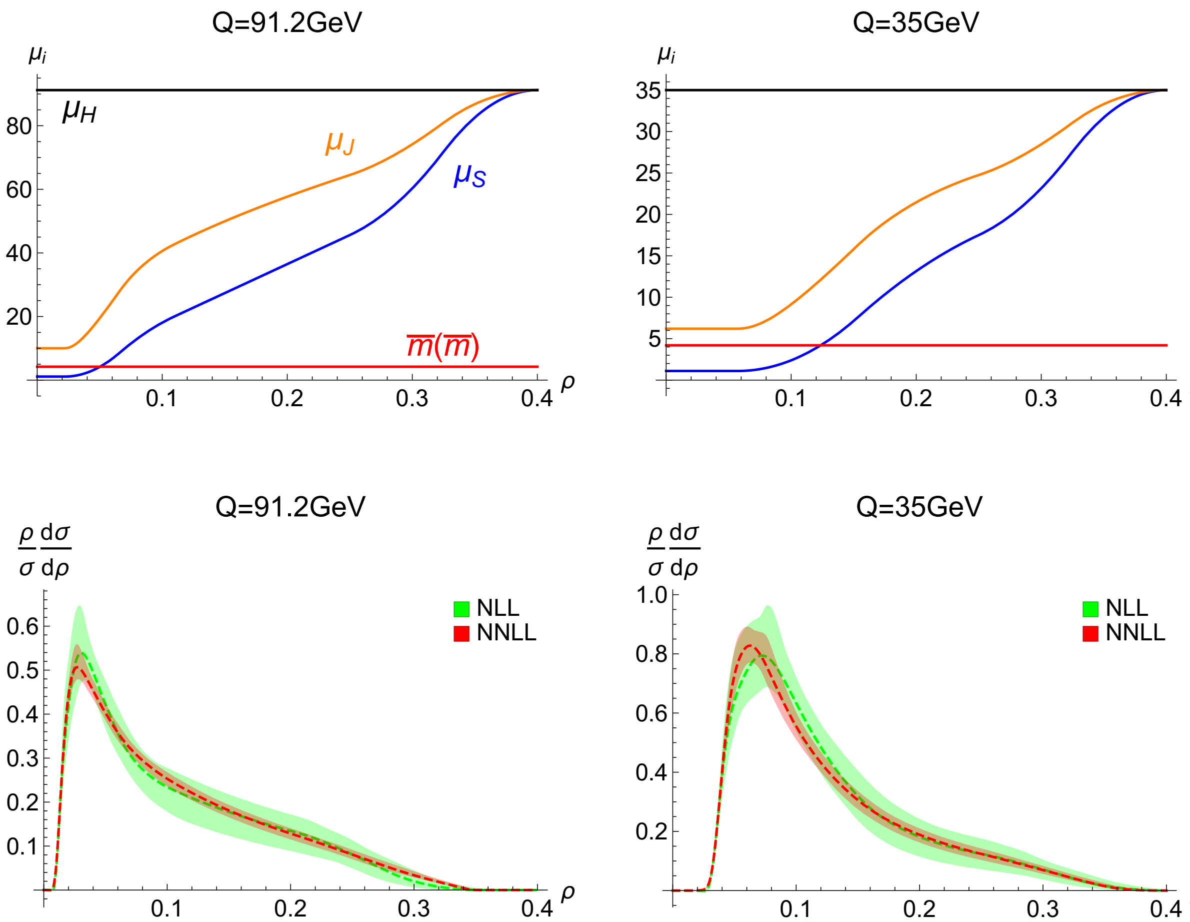

Figure 7.3: Massive heavy jet mass cross sections at different center of mass energies and orders of log resummation with $\overline{m}(\overline{m}) = 4.2\,\mathrm{GeV}$. In the upper row the related profiles including the mass scale are depicted.

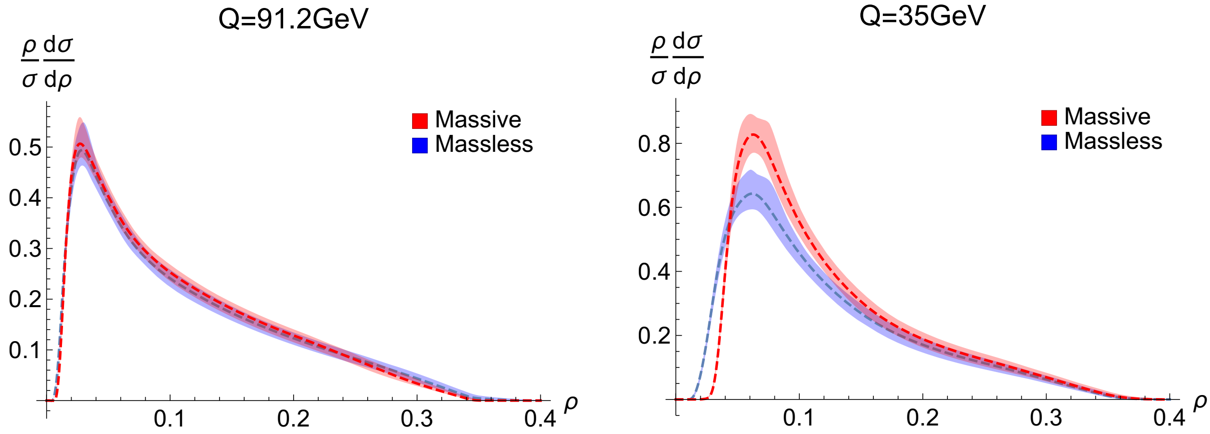

Figure 7.4: Comparison of the massless and massive heavy jet mass cross section at different center of mass energies and N^{2}LL accuracy.

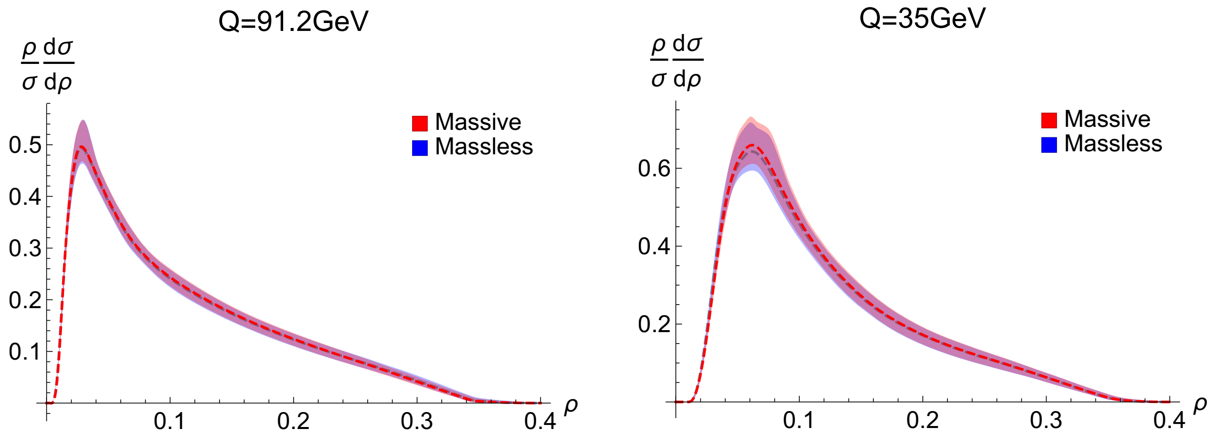

Figure 7.5: Comparison of the all-flavor heavy jet mass cross section with massless and massive b-quark.

In Fig. 7.4 a comparison between the massive and massless distribution at 91.2 GeV and 35 GeV is depicted. The difference at 91.2 GeV is very small, where the difference at 35 GeV is noticeable.

Note that tagged bottom quark cross sections are hard to measure experimentally, such that the given pure massive results may not be of practical use e.g. to determine the bottom mass. Hence in the next section we discuss the cross section for all-flavor production.

7.3 All-Flavor Production

In this section we investigate the all-flavor heavy jet mass distribution, which can actually be measured in experiments. For the massive case we include four massless and one massive quark flavors, such that the correct sum of up and down type quarks in the all-flavor cross section reads

$$\frac{d\sigma_{\mathrm{AF}}}{d\rho} = 2\left(\sigma_0^u + \sigma_0^d\right)\left(\frac{1}{\sigma_0}\frac{d\sigma_{\mathrm{s}}}{d\rho} + \frac{1}{\sigma_0}\frac{d\sigma_{\mathrm{ns}}}{d\rho}\right)_{m=0} + \sigma_0^d\left(\frac{1}{\sigma_0}\frac{d\sigma_{\mathrm{s}}}{d\rho} + \frac{1}{\sigma_0}\frac{d\sigma_{\mathrm{ns}}}{d\rho}\right)_{m\neq 0}. \tag{7.10}$$

Since the difference between the $b\bar{b}$ cross section and the massless one is small at a center of mass energy of 91.2 GeV, as seen in the last section, it is expected that the massive quark impacts the all-flavor production only slightly. This is confirmed by Fig. 7.5.

For a center of mass energy of 35 GeV the effect is also quite small (see Fig. 7.5). Apart from the quite low mass sensitivity we already saw in pure $b\bar{b}$ production, bottom mass effects are additionally suppressed, since at the considered energies the down type Born cross section is nearly four times smaller than the up type one. It can be seen that the two cross sections with massless and massive bottom quarks are compatible to a very high extend, such that at this stage mass effects on α_s determinations are negligible.

It should be noted that for top quarks, much larger effects are expected, and that tagging is much less problematic.

Chapter 8

Outlook

In this thesis we investigated effects of massive primary quarks in heavy jet mass (HJM) distributions, considering the process $e^+e^- \to$ hadrons. Heavy jet mass distributions were studied in several works including [17, 23–25], where quark mass effects were ignored since they provide only very small corrections at energies similar to LEP, and make the calculations considerably more complicated. In [13] the leading quark mass contribution was included by a Monte Carlo based approach, but it was pointed out that a full inclusion of bottom quark mass corrections should be considered to investigate the exact form of these contributions.

We contributed to this proposition by computing the full massive fixed order cross section at $\mathcal{O}(\alpha_s)$. This result was not known analytically before. Additionally we resummed large logarithms, which appear in the dijet region, up to N^{2}LL by using factorization in soft-collinear effective theory (SCET). To obtain a full description of the HJM distribution we included the non-singular contributions, which are absent in leading SCET, and due to the m/Q suppression of mass effects we had to implement non-perturbative effects and renormalon subtractions to get a stable and reliable analysis.

The non-perturbative effects were included by convoluting the partonic distribution with a soft model function, which encodes the non-perturbative power corrections. The leading renormalon ambiguities were prevented by using a short distance mass scheme, specifically the $\overline{\mathrm{MS}}$ mass, and by introducing a gap, which accounts for the minimal hadronic energy deposit in the final state, in a renormalon free scheme. Finally we used ρ dependent profile functions for the renormalization scales to resum the logarithms correctly over the full range of the distribution.

We analyzed tagged bottom pair production and all-flavor production with sufficiently low m/Q and showed that the effects of primary massive quarks are negligible (e.g. for α_s determinations). Nevertheless mass effects are important in cases which are very interesting for phenomenological studies with larger m/Q, e.g. top quark mass effects.

The study of such effects is beyond the scope of this thesis, since additional effects, like the instability of the top quark, have to be taken into account. Additionally, our analysis is valid only in a specific kinematic situation called "scenario IV", i.e. where the scale hierarchy is $m < \mu_S < \mu_J < \mu_H$. In the kinematic region where the soft scale gets smaller then the mass scale ("scenario III"), threshold corrections have to be implemented in the evolution kernels, and with even higher m/Q such that $\mu_S < \mu_J < m < \mu_H$ ("scenario II"), additional large logarithms appear in the jet function which can not be resummed by using the SCET approach. To do so, another effective field theory named "boosted heavy quark effective theory" (bHQET) has to be applied, which is the reason why scenario II is also called the "bHQET region".

All these generalizations of the results obtained in this thesis will be considered in future works.

Additionally, specific massive HJM profile functions have to be constructed for arbitrary m/Q.

The generalized results can be used to study the connection between the so called “Monte Carlo Top Mass” m_t^{MC} and theoretically well defined mass schemes, like the $\overline{\mathrm{MS}}$ or MSR mass. This application is very important, since top mass determinations are usually done by comparing the output of Monte Carlo event generators and experimental results, which leads to (presumably) small errors. Although one would naively expect the output to be the pole mass, due to the used parton shower structure and hadronization models this is not true [61]. The relation between the Monte Carlo mass and short distance masses is currently explored by comparing 2-jettiness in Monte Carlo event generators and N^2LL calculations [62]. Based on the initiated work in this thesis we can test the consistency of these results.

Appendix A

Virtual Integral

To solve the loop integral in Eq. (3.19) we first modify the Dirac structure with the symbolic manipulation program `FORM` [63]. Using

$$
\begin{aligned}
\bar{u}(p)\not{p} &= \bar{u}(p)m, \\
\not{p}v(p) &= -mv(p),
\end{aligned}
\tag{A.1}
$$

and anti-commutation relations we get

$$
\begin{aligned}
&\bar{u}(p_1)\gamma^\alpha \left(\not{p}_1 + \not{k} + m\right)\Gamma_v^\mu \left(-\not{p}_2 + \not{k} + m\right)\gamma_\alpha v(p_2) \\
&\qquad = 1\left[2\gamma^\mu\left(2m^2 - Q^2\right)\right] \\
&\qquad\quad + k^\alpha\left[4m\delta_\alpha^\mu - 4\gamma_\alpha\left(p_1 - p_2\right)^\mu + 4\gamma^\mu\left(p_1 - p_2\right)_\alpha\right] \\
&\qquad\quad + k^\alpha k^\beta\left[2\gamma_\alpha\delta_\beta^\mu\left(2 - d\right) + \gamma^\mu g_{\alpha\beta}\left(d - 2\right)\right], \\
&\bar{u}(p_1)\gamma^\alpha \left(\not{p}_1 + \not{k} + m\right)\Gamma_a^\mu \left(-\not{p}_2 + \not{k} + m\right)\gamma_\alpha v(p_2) \\
&\qquad = 1\left[2\gamma^\mu\left(2m^2 - Q^2\right)\right]\gamma^5 \\
&\qquad\quad + k^\alpha\left[4m\left(\delta_\alpha^\mu - \gamma_\alpha\gamma^\mu\right) - 4\gamma_\alpha\left(p_1 - p_2\right)^\mu + 4\gamma^\mu\left(p_1 - p_2\right)_\alpha\right]\gamma^5 \\
&\qquad\quad + k^\alpha k^\beta\left[2\gamma_\alpha\delta_\beta^\mu\left(2 - d\right) + \gamma^\mu g_{\alpha\beta}(d - 2)\right]\gamma^5.
\end{aligned}
\tag{A.2}
$$

So basically we obtain the integrals

$$
\mathcal{I}_3^{[0,\mu,\mu\nu]} := \mu^{2\varepsilon}\int \frac{\mathrm{d}^d k}{(2\pi)^d} \frac{\left[1, k^\mu, k^\mu k^\nu\right]}{\left[k^2 + i0\right]\left[(k + p_1)^2 - m^2 + i0\right]\left[(k - p_2)^2 - m^2 + i0\right]},
\tag{A.3}
$$

which will be solved by reducing the tensor integrals to known standard scalar loop integrals as defined in [64]. The solutions for the specific scalar integrals appearing in this calculation are given at the end of this appendix in Eq. (A.20).

By comparing $\mathcal{I}_3^0$ and the integrals in [64] we find the relation

$$
\mathcal{I}_3^0 = \frac{i\pi^{d/2} r_\Gamma}{(2\pi)^d} I_3^d(m^2, Q^2, m^2; 0, m^2, m^2),
\tag{A.4}
$$

with

$$
r_\Gamma := \frac{\Gamma^2(1-\varepsilon)\Gamma(1+\varepsilon)}{\Gamma(1-2\varepsilon)}.
\tag{A.5}
$$

Next, let us consider I_3^μ. Due to the symmetry $\mathcal{I}_3^\mu(p_1,p_2) = \mathcal{I}_3^\mu(-p_2,-p_1)$ and the fact that the only available vector-like quantities in the expression are p_1 and p_2, the solution has to be of the form

$$\mathcal{I}_3^\mu(p_1,p_2) = \mathcal{A}(p_1-p_2)^\mu, \tag{A.6}$$

with a yet unknown coefficient $\mathcal{A}$. Contracting both sides with $p_{1\mu}$ we obtain

$$\begin{aligned}\mu^{2\varepsilon}\int\frac{\mathrm{d}^dk}{(2\pi)^d}&\left[\frac{1}{[k^2+i0]\,[(k-p_2)^2-m^2+i0]}-\frac{1}{[(k+p_1+p_2)^2-m^2+i0]\,[k^2-m^2+i0]}\right]\\ &=\mathcal{A}\left(4m^2-Q^2\right),\end{aligned} \tag{A.7}$$

and therefore, comparing with the standard integrals in [64], the desired coefficient reads

$$\mathcal{A} = \frac{i\pi^{\frac{d}{2}}r_\Gamma}{(Q^2-4m^2)(2\pi)^d}\left[I_2^d(Q^2;m^2,m^2) - I_2^d(m^2;0,m^2)\right]. \tag{A.8}$$

Finally, the integral $\mathcal{I}_3^{\mu\nu}$ fulfills $\mathcal{I}_3^{\mu\nu}(p_1,p_2) = \mathcal{I}_3^{\nu\mu}(p_1,p_2) = \mathcal{I}_3^{\mu\nu}(-p_2,-p_1)$ and has therefore the form

$$\mathcal{I}_3^{\mu\nu} = \mathcal{B}\,(p_1^\mu p_1^\nu + p_2^\mu p_2^\nu) + \mathcal{C}\,(p_1^\mu p_2^\nu + p_1^\nu p_2^\mu) + \mathcal{D}g^{\mu\nu}, \tag{A.9}$$

where $\mathcal{B}$, $\mathcal{C}$, and $\mathcal{D}$ are again coefficients which have to be determined in terms of known standard integrals.

Contracting both sides of (A.9) with $g_{\mu\nu}$, the ansatz gives

$$2m^2\mathcal{B} + 2\left(\frac{Q^2}{2}-m^2\right)\mathcal{C} + d\mathcal{D} = \frac{i\pi^{\frac{d}{2}}r_\Gamma}{(2\pi)^d}I_2^d(Q^2;m^2,m^2). \tag{A.10}$$

Two more equations are needed to solve for the coefficients. We contract both sides of Eq. (A.9) with $p_{1\nu}$ and get

$$\begin{aligned}&\left[m^2p_1^\mu + \left(\frac{Q^2}{2}-m^2\right)p_2^\mu\right]\mathcal{B} + \left[m^2p_2^\mu + \left(\frac{Q^2}{2}-m^2\right)p_1^\mu\right]\mathcal{C} + p_1^\mu\mathcal{D}\\ &=\frac{1}{2}\left[\mathcal{I}_2^\mu(0,-p_2;0,m) - \mathcal{I}_2^\mu(0,q;m,m) - p_2^\mu\frac{i\pi^{\frac{d}{2}}r_\Gamma}{(2\pi)^d}I_2^d(Q^2;m^2,m^2)\right],\end{aligned} \tag{A.11}$$

with $q = p_1 + p_2$ and

$$\mathcal{I}_2^\mu(p_1,p_2;m_1,m_2) := \mu^{2\varepsilon}\int\frac{\mathrm{d}^dk}{(2\pi)^d}\frac{k^\mu}{[(k+p_1)^2-m_1^2+i0]\,[(k+p_2)^2-m_2^2+i0]}, \tag{A.12}$$

which has to be reduced to known scalar integrals as well. To do this reduction we set

$$\mathcal{I}_2^\mu(0,p;m_1,m_2) = \mathcal{E}(p;m_1,m_2)p^\mu, \tag{A.13}$$

and contract with p_μ to obtain

$$\mathcal{E}(p;m_1,m_2) = \frac{1}{2p^2}\frac{i\pi^{\frac{d}{2}}r_\Gamma}{(d\pi)^d}\left[I_1^d(m_1^2) - I_1^d(m_2^2) + (m_2^2-m_1^2-p^2)I_2^d(p^2;m_1^2,m_2^2)\right]. \tag{A.14}$$

For the special cases of $\mathcal{I}_2^\mu$, appearing in Eq. (A.11), the result simplifies to

$$\begin{aligned}\mathcal{I}_2^\mu(0,-p_2;0,m) &= -\mathcal{E}(0,-p_2;0,m)p_2^\mu,\\ \mathcal{E}(0,-p_2;0,m) &= -\frac{1}{2m^2}\frac{i\pi^{\frac{d}{2}}r_\Gamma}{(2\pi)^d}I_1^d(m^2),\end{aligned} \tag{A.15}$$

and

$$
\begin{aligned}
\mathcal{I}_2^\mu(0,q;m,m) &= \mathcal{E}(0,q;m,m)q^\mu, \\
\mathcal{E}(0,q;m,m) &= -\frac{1}{2}\frac{i\pi^{\frac{d}{2}}r_\Gamma}{(2\pi)^d} I_2^d(Q^2;m^2,m^2).
\end{aligned} \tag{A.16}
$$

Putting (A.15) and (A.16) back into (A.11), the equation reads

$$
\begin{aligned}
&\left[m^2 p_1^\mu + \left(\frac{Q^2}{2} - m^2\right) p_2^\mu\right] \mathcal{B} + \left[m^2 p_2^\mu + \left(\frac{Q^2}{2} - m^2\right) p_1^\mu\right] \mathcal{C} + p_1^\mu \mathcal{D} \\
&= \frac{1}{2}\frac{i\pi^{\frac{d}{2}}r_\Gamma}{(2\pi)^d}\left[\frac{p_2^\mu}{2m^2} I_1^d(m^2) + \frac{1}{2}(p_1-p_2)^\mu I_2^d(Q^2;m^2,m^2)\right].
\end{aligned} \tag{A.17}
$$

We again contract with p_1 and p_2, which results in two equations additional to (A.10), determining $\mathcal{B}$, $\mathcal{C}$, and $\mathcal{D}$. The equations read

$$
\begin{aligned}
m^2\mathcal{B} + \left(\frac{Q^2}{2} - m^2\right)\mathcal{C} + \mathcal{D} &= \frac{1}{4}\frac{i\pi^{\frac{d}{2}}r_\Gamma}{(2\pi)^d} I_2^d(Q^2;m^2,m^2), \\
\left(\frac{Q^2}{2} - m^2\right)\mathcal{B} + m^2\mathcal{C} &= \frac{1}{4}\frac{i\pi^{\frac{d}{2}}r_\Gamma}{(2\pi)^d}\left[\frac{1}{m^2} I_1^d(m^2) - I_2^d(Q^2;m^2,m^2)\right],
\end{aligned} \tag{A.18}
$$

and the resulting coefficients are

$$
\begin{aligned}
\mathcal{B} &= \frac{1}{2(d-2)Q^2(4m^2-Q^2)}\frac{i\pi^{\frac{d}{2}}r_\Gamma}{(2\pi)^d} \\
&\quad \times \left[(d-2)\frac{2m^2-Q^2}{m^2} I_1^d(m^2) + \left((d-2)Q^2 - 4m^2\right) I_2^d(Q^2;m^2,m^2)\right], \\
\mathcal{C} &= \frac{1}{2(d-2)Q^2(4m^2-Q^2)}\frac{i\pi^{\frac{d}{2}}r_\Gamma}{(2\pi)^d} \\
&\quad \times \left[2(d-2) I_1^d(m^2) - \left((d-4)Q^2 + 4m^2\right) I_2^d(Q^2;m^2,m^2)\right], \\
\mathcal{D} &= \frac{1}{2(d-2)}\frac{i\pi^{\frac{d}{2}}r_\Gamma}{(2\pi)^d} I_2^d(Q^2;m^2,m^2).
\end{aligned} \tag{A.19}
$$

The solutions to the scalar integrals needed in this calculation and given in [64] read

$$
\begin{aligned}
I_1^d(m^2) &= -\mu^{2\varepsilon}\Gamma(-1+\varepsilon)(m^2 - i0)^{1-\varepsilon}, \\
I_2^d(m^2;0,m^2) &= \left(\frac{\mu^2}{m^2}\right)^\varepsilon \left(\frac{1}{\varepsilon} + 2\right) + \mathcal{O}(\varepsilon),
\end{aligned}
$$

$$
\begin{aligned}
I_2^d(Q^2;m^2,m^2) &= \mu^{2\varepsilon}\Bigg\{\frac{1}{\varepsilon} + 2 - \log(Q^2 - i0) \\
&\quad + \sum_{i=1}^{2}\left[\gamma_i \log\frac{\gamma_i - 1}{\gamma_i} - \log(\gamma_i - 1)\right]\Bigg\} + \mathcal{O}(\varepsilon), \\
I_3^d(m^2,Q^2,m^2;0,m^2,m^2) &= \frac{\tilde{x}_s}{m^2(1-\tilde{x}_s^2)}\Bigg\{\log\tilde{x}_s\left[-\frac{1}{\varepsilon} - \frac{1}{2}\log\tilde{x}_s + 2\log(1-\tilde{x}_s^2) + \log\frac{m^2}{\mu^2}\right] \\
&\quad - \frac{\pi^2}{6} + \mathrm{Li}_2\left(\tilde{x}_s^2\right) + 2\mathrm{Li}_2(1-\tilde{x}_s)\Bigg\} + \mathcal{O}(\varepsilon),
\end{aligned} \tag{A.20}
$$

with

$$
\begin{aligned}
\gamma_{1,2} &= \frac{1}{2Q}\left(Q \pm \sqrt{Q^2 - 4(m^2 - i0)}\right), \\
\tilde{x}_s &= -\frac{1-\sqrt{1-\frac{4m^2}{Q^2+i0}}}{1+\sqrt{1-\frac{4m^2}{Q^2+i0}}}.
\end{aligned}
\tag{A.21}
$$

Inserting the obtained results into (A.2), working out all contractions, and performing an expansion in ε, the expression can be simplified to the final form in Eq. (3.20).

Appendix B

Expressions of the Real Radiative Cross Sections for $\rho > \rho_{\text{min}}$

In section 3.4.1 the $\mathcal{O}(\alpha_s)$ real radiative cross section for different regions in phase space with $\bar{\rho} > 0$ was calculated. In this appendix the full expressions are given. Remember the intervals of validity for the different regions as given in Eqs. (3.50), (3.51), (3.54), and (3.55).

With $\rho_1 := \sqrt{(\hat{m}^2 - \rho + 1)^2 - 4\hat{m}^2}$, $\rho_2 := \sqrt{\hat{m}^4 - 2\hat{m}^2(\rho + 1) + (\rho - 1)^2}$, $\rho_3 := \sqrt{4\hat{m}^2 + (\rho - 1)^2}$ and $\rho_4 := \sqrt{1 - \frac{4\hat{m}^2}{\rho}}$ the results are

$$\begin{aligned}\frac{1}{\sigma_0^v}\frac{\mathrm{d}\sigma^{v,\bar{\rho}>0}_{\text{rad,1A}}}{\mathrm{d}\rho} = \frac{\alpha_s C_F}{4\pi\bar{\rho}^2}\Bigg[&2\bar{\rho}\left(-3\hat{m}^4 + \hat{m}^2(2-6\rho) + \rho^2 - 2\rho + 2\right)\log\left(\frac{\rho_1}{\bar{\rho}} - 1\right) \\ &- 4\left(2\hat{m}^2+1\right)\rho(\rho_1 - 2\bar{\rho}) + \rho_1\bar{\rho}(\rho_1 - 2\bar{\rho}) + 4\hat{m}^2\bar{\rho}\frac{\rho_2 - 2\bar{\rho}}{\bar{\rho} - \rho_2}\left(2\hat{m}^2+1\right)\Bigg],\end{aligned}$$

$$\begin{aligned}\frac{1}{\sigma_0^v}\frac{\mathrm{d}\sigma^{v,\bar{\rho}>0}_{\text{rad,1B}}}{\mathrm{d}\rho} = \frac{\alpha_s C_F}{4\pi\bar{\rho}^2}\Bigg[&\frac{\bar{\rho}^3\left(\hat{m}^2 + \rho - \rho_2 - 1\right)^2}{4\rho^2} + 2\left(2\hat{m}^2+1\right)\bar{\rho}\left(-\hat{m}^2 + 3\rho - \rho_1 - 1\right) \\ &- \frac{8\hat{m}^2\left(2\hat{m}^2+1\right)\rho\bar{\rho}}{\hat{m}^2 + \rho - \rho_2 - 1} + 2\Big(3\hat{m}^6 + \hat{m}^4(3\rho - 2) + \hat{m}^2\left(-7\rho^2 + 4\rho - 2\right) \\ &+ \rho\left(\rho^2 - 2\rho + 2\right)\Big)\log\left(\frac{-\hat{m}^2 - \rho + \rho_1 + 1}{2\rho}\right) - \bar{\rho}^3\Bigg],\end{aligned}$$

$$\begin{aligned}\frac{1}{\sigma_0^v}\frac{\mathrm{d}\sigma^{v,\bar{\rho}>0}_{\text{rad,3C}}}{\mathrm{d}\rho} = &\frac{\alpha_s C_F}{\pi(\rho-1)(\rho_3-1)(\rho_3-\rho)} \\ &\times\Bigg[\left(8\hat{m}^4 - 4\hat{m}^2(\rho-1) - \rho^2 - 1\right)\left(-4\hat{m}^2 - \rho^2 + \rho\rho_3 + \rho + \rho_3 - 1\right)\log\left(\frac{\rho_3 - 1}{\rho - \rho_3}\right) \\ &+ (\rho - 1)\Big(-4\hat{m}^4(\rho - 2\rho_3 + 1) + 2\hat{m}^2(5\rho - 2\rho_3 + 5) \\ &+ \rho^2(3\rho - 3\rho_3 - 2) - 2\rho + 3(1 - \rho_3)\Big)\Bigg],\end{aligned}$$

$$\frac{1}{\sigma_0^v}\frac{\mathrm{d}\sigma^{v,\bar\rho>0}_{\mathrm{rad,3D}}}{\mathrm{d}\rho} = \frac{\alpha_s C_F}{2\pi(\rho-1)}\Big[2\rho_4\left(4\hat m^2\rho+\rho^2+1\right) + 2\left(8\hat m^4-4\hat m^2(\rho-1)-\rho^2-1\right)\log\left(\frac{1+\rho_4}{1-\rho_4}\right)\Big],$$

$$\frac{1}{\sigma_0^a}\frac{\mathrm{d}\sigma^{a,\bar\rho>0}_{\mathrm{rad,1A}}}{\mathrm{d}\rho} = \frac{\alpha_s C_F}{2\pi\bar\rho^2}\Big[2(\rho_2-2\bar\rho)\left(2\hat m^2\left(2\rho+\bar\rho^2\right)-\rho\right)+\frac{1}{2}\left(2\hat m^2+1\right)\bar\rho(\rho_1-\bar\rho)^2 - \frac{1}{2}\left(2\hat m^2+1\right)\bar\rho^3+2\hat m^2\left(4\hat m^2-1\right)\bar\rho - \frac{2\left(4\hat m^2-1\right)\left(\hat m^3-\hat m\rho\right)^2}{\rho_2-\bar\rho} + \bar\rho\left(2\hat m^6+\hat m^4(9-4\rho)+2\hat m^2(\rho(\rho+3)-5)+(\rho-2)\rho+2\right)\log\left(\frac{\rho_1}{\bar\rho}-1\right)\Big],$$

$$\frac{1}{\sigma_0^a}\frac{\mathrm{d}\sigma^{a,\bar\rho>0}_{\mathrm{rad,1B}}}{\mathrm{d}\rho} = \frac{\alpha_s C_F}{2\pi\bar\rho^2}\Big[\frac{\left(2\hat m^2+1\right)\bar\rho^3\left(\hat m^2+\rho-\rho_2-1\right)^2}{8\rho^2}+\frac{4\hat m^2\left(4\hat m^2-1\right)\rho\bar\rho}{\hat m^2+\rho-\rho_1-1} - \frac{1}{2}\left(2\hat m^2+1\right)\bar\rho^3+2\hat m^2\left(4\hat m^2-1\right)\bar\rho + \frac{\bar\rho\left(2\hat m^6-4\hat m^4\rho+2\hat m^2\rho(\rho+2)-\rho\right)\left(-\hat m^2-3\rho+\rho_2+1\right)}{\rho} - \Big(2\hat m^8+\hat m^6(9-6\rho)+\hat m^4\left(6\rho^2-3\rho-10\right)+\hat m^2\left(-2\rho^3-5\rho^2+8\rho+2\right) - \rho\left(\rho^2-2\rho+2\right)\Big)\log\left(\frac{-\hat m^2-\rho+\rho_1+1}{2\rho}\right)\Big],$$

$$\frac{1}{\sigma_0^a}\frac{\mathrm{d}\sigma^{a,\bar\rho>0}_{\mathrm{rad,3C}}}{\mathrm{d}\rho} = \frac{\alpha_s C_F}{\pi(\rho-1)(\rho_3-1)(\rho_3-\rho)} \times\Big[(\rho-1)\Big(8\hat m^4(\rho-2\rho_3+1)+2\hat m^2(5\rho-2\rho_3+5)+3\rho^3-\rho^2(3\rho_3+2) - 2\rho-3\rho_3+3\Big)-\left(16\hat m^4+2\hat m^2\left(\rho^2-6\rho-1\right)+\rho^2+1\right) \times\left(-4\hat m^2-\rho^2+\rho\rho_3+\rho+\rho_3-1\right)\log\left(\frac{\rho_3-1}{\rho-\rho_3}\right)\Big],$$

$$\frac{1}{\sigma_0^a}\frac{\mathrm{d}\sigma^{a,\bar\rho>0}_{\mathrm{rad,3D}}}{\mathrm{d}\rho} = \frac{\alpha_s C_F}{2\pi(\rho-1)}\Big[2\rho_4\left(-8\hat m^2\rho+\rho^2+1\right) + 2\left(16\hat m^4+2\hat m^2\left((\rho-6)\rho-1\right)+\rho^2+1\right)\log\left(\frac{1-\rho_4}{1+\rho_4}\right)\Big]. \tag{B.1}$$

Appendix C

Distributions and Related Identities

C.1 Plus Distribution

In this appendix we will define the plus-distribution and give some useful relations.

The ordinary plus distribution can be defined as ($n > 0$) [12, 34]

$$\begin{aligned} \left[\frac{\Theta(x)\log^n x}{x}\right]_+ &:= \lim_{\beta\to 0}\frac{\mathrm{d}}{\mathrm{d}x}\left[\Theta(x-\beta)\int \mathrm{d}x\,\frac{\log^n x}{x}\right] \\ &= \lim_{\beta\to 0}\left[\Theta(x-\beta)\frac{\log^n x}{x} + \frac{1}{n+1}\log^{n+1}(\beta)\delta(x-\beta)\right], \end{aligned} \tag{C.1}$$

such that the integral with a test function $f(x)$ and $\Delta > 0$ reads

$$\int_0^\Delta \mathrm{d}x\,\left[\frac{\Theta(x)\log^n x}{x}\right]_+ f(x) = \int_0^\Delta \mathrm{d}x\,\frac{f(x)-f(0)}{x}\log^n x + f(0)\frac{\log^{n+1}\Delta}{n+1}, \tag{C.2}$$

and

$$\int_0^\Delta \mathrm{d}x\,\left[\frac{\Theta(x)\log^n x}{x}\right]_+ = \frac{\log^{n+1}\Delta}{n+1}. \tag{C.3}$$

An important scenario where plus distributions appear, is in ε expansions of the form

$$\frac{\Theta(x)}{x^{1+a\varepsilon}} = -\frac{1}{a\varepsilon}\delta(x) + \left[\frac{\Theta(x)}{x}\right]_+ - a\varepsilon\left[\frac{\Theta(x)\log x}{x}\right]_+ + \frac{(a\varepsilon)^2}{2}\left[\frac{\Theta(x)\log^2 x}{x}\right]_+ + \mathcal{O}(\varepsilon^3). \tag{C.4}$$

This shows clearly the reason we loose the term proportional to the delta function and obtain a $\bar{\rho}^{-1}$ term instead of a plus distribution for the 4-dimensional computation of the fixed order cross section in section 3.4.1.

Another important relation which is often used when manipulating plus distributions, is the rescaling identity [12]

$$\kappa\left[\frac{\Theta(x)\log^n(\kappa x)}{\kappa x}\right]_+ = \frac{\log^{n+1}\kappa}{n+1}\delta(x) + \sum_{k=0}^{n}\frac{n!}{(n-k)!\,k!}\log^{n-k}(\kappa)\left[\frac{\Theta(x)\log^k(x)}{x}\right]_+, \tag{C.5}$$

where κ is a dimensionless constant.

The “fractional plus distribution”, appearing in evolution kernels, is a generalization of the ordinary one and can be defined as [34, 54]

$$\begin{aligned}\left[\frac{\Theta(x)\log^n x}{x^{1+\omega}}\right]_+ &:= \lim_{\beta\to 0}\frac{\mathrm{d}}{\mathrm{d}x}\left[\Theta(x-\beta)\int \mathrm{d}x\,\frac{\log^n x}{x^{1+\omega}}\right]\\ &\to \lim_{\beta\to 0}\left[\Theta(x-\beta)\frac{1}{x^{1+\omega}}-\delta(x-\beta)\frac{1}{x^{\omega}\omega}\right]\qquad (n\to 0),\end{aligned}\tag{C.6}$$

where $\omega < 1$. Another way to define this distribution is via integrating $\frac{\Theta(x)\log^n x}{x^{1+\omega}}$ for values of ω where the integral converges, and analytically continue the result to other values.

To make some formulas more readable, we will use a notation similar to the one used in [9, 34]:

$$\begin{aligned}\mathcal{L}_n^{\mu}(\ell) &:= \frac{1}{\mu}\left[\frac{\Theta(\ell)\log^n\frac{\ell}{\mu}}{\ell/\mu}\right]_+,\\ \mathcal{L}_{n,\omega}^{\mu}(\ell) &:= \frac{1}{\mu}\left[\frac{\Theta(\ell)\log^n\frac{\ell}{\mu}}{(\ell/\mu)^{1+\omega}}\right]_+,\end{aligned}\tag{C.7}$$

where μ and ℓ can be dimensionful quantities of the same order. It is implied that the superscript can be dropped if $\mu = 1$.

C.2 Fourier Transforms of Distributions

The Fourier transform of the distributions defined in appendix C.1 can be obtained from the ε expansion of the expression

$$\mathcal{F}\left(\frac{\Theta(x)}{x^{1+a\varepsilon}}\right)(y) = \int \mathrm{d}x\;\mathrm{e}^{-ixy}\frac{\Theta(x)}{x^{1+a\varepsilon}},\tag{C.8}$$

where x and y are dimensionless quantities. The relevant results which are used in this thesis read

$$\begin{aligned}\mathcal{F}(\delta)(y) &= 1,\\ \mathcal{F}(\mathcal{L}_0)(y) &= -\log(iy\,\mathrm{e}^{\gamma_E}),\\ \mathcal{F}(\mathcal{L}_1)(y) &= \frac{\pi^2}{12}+\frac{1}{2}\log^2(iy\,\mathrm{e}^{\gamma_E}).\end{aligned}\tag{C.9}$$

C.3 Imaginary Part Identities

Finally, we summarize a set of useful relations between the plus distribution and the imaginary part of some analytic functions. These identities are used in the computation of the jet function calculation in appendix E.1. The relations read [12]

$$
\begin{aligned}
\mathrm{Im}\left\{\frac{1}{x+i0}\right\} &= -\pi\delta(x),\\
\mathrm{Im}\left\{\frac{\log(-x-i0)}{x+i0}\right\} &= -\pi\mathcal{L}_0(x),\\
\mathrm{Im}\left\{\frac{\log^2(-x-i0)}{x+i0}\right\} &= \frac{\pi^3}{3}\delta(x) - 2\pi\mathcal{L}_1(x),\\
\mathrm{Im}\left\{\frac{\mathrm{Li}_2\left(\frac{-x-i0}{y}\right)}{x+i0}\right\} &= -\pi\frac{\Theta(-x-y)\log\frac{-x}{y}}{x},\\
\mathrm{Im}\left\{\frac{y(y+2x)}{x(x+y)^2}\log\frac{y}{-x-i0}\right\} &= \pi\left[-\delta(x)\log y + \mathcal{L}_0(x) - \frac{\Theta(x)x}{(x+y)^2} + y\log\frac{y}{-x}\delta'(x+y)\right],\\
\mathrm{Im}\left\{\frac{\log\frac{y}{-x-i0}\log\left(1+\frac{x+i0}{y}\right)}{x+i0}\right\} &= \pi\left[\frac{1}{x}\log\frac{y}{-x}\Theta(-y-x) + \log\left(1+\frac{x}{y}\right)\mathcal{L}_0(x)\right].
\end{aligned}
\tag{C.10}
$$

Appendix D

Feynman Rules for SCET with Masses

In chapter 4 we derived the leading SCET Lagrangian (see Eq. (4.19)), and expressions for collinear and soft Wilson lines (see section 4.3). It is straightforward to derive the SCET Feynman rules from the corresponding Lagrangian and the momentum space representations of the Wilson lines [9, 36].

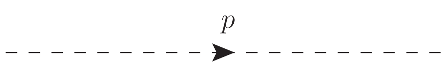

$$= \quad i\frac{\not{\bar{n}}}{2}\frac{p^-}{p^2-m^2+i0} \tag{D.1}$$

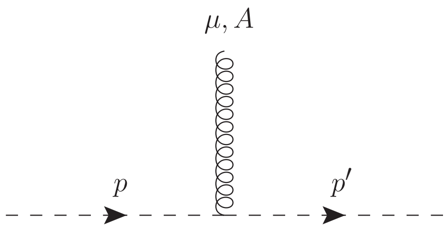

$$= \quad (ig_s T^A \tilde{\mu}^{\varepsilon}) n^{\mu} \frac{\not{\bar{n}}}{2} \tag{D.2}$$

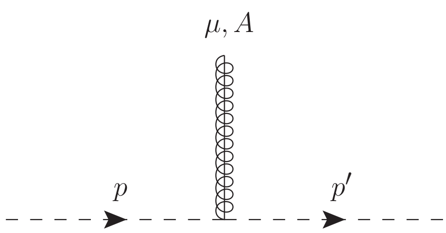

$$\begin{aligned} &= \quad (ig_s T^A \tilde{\mu}^{\varepsilon}) \left[n^{\mu} + \frac{\gamma_{\perp}^{\mu}\left(\not{p}_{\perp}+m\right)}{p^-} + \frac{\left(\not{p}'_{\perp}-m\right)\gamma_{\perp}^{\mu}}{p'^-} \right. \\ &\qquad \left. - \frac{\left(\not{p}'_{\perp}-m\right)\left(\not{p}_{\perp}+m\right)}{p^- p'^-}\bar{n}^{\mu} \right] \frac{\not{\bar{n}}}{2} \\ &=: \quad V^{\mu,A}(p,p',m) \end{aligned} \tag{D.3}$$

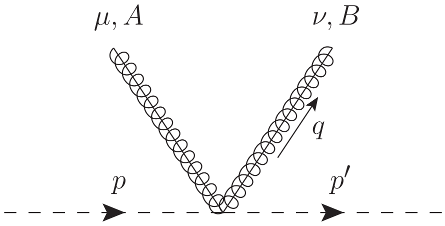

$$
\begin{aligned}
&= \quad \frac{i g_s^2 T^A T^B \tilde{\mu}^{2\varepsilon}}{p^- - q^-} \Bigg[\gamma_\perp^\mu \gamma_\perp^\nu - \frac{\gamma_\perp^\mu \left(\not{p}_\perp + m \right)}{p^-} \bar{n}^\nu \\
&\qquad - \frac{\left(\not{p}'_\perp - m \right) \gamma_\perp^\nu}{p'^-} \bar{n}^\mu + \frac{\left(\not{p}'_\perp - m \right) \left(\not{p}_\perp + m \right)}{p^- p'^-} \bar{n}^\mu \bar{n}^\nu \Bigg] \frac{\not{\bar{n}}}{2} \\
&\qquad + \frac{i g_s^2 T^B T^A \tilde{\mu}^{2\varepsilon}}{q^- + p'^-} \Bigg[\gamma_\perp^\nu \gamma_\perp^\mu - \frac{\gamma_\perp^\nu \left(\not{p}_\perp + m \right)}{p^-} \bar{n}^\mu \\
&\qquad - \frac{\left(\not{p}'_\perp - m \right) \gamma_\perp^\mu}{p'^-} \bar{n}^\nu + \frac{\left(\not{p}'_\perp - m \right) \left(\not{p}_\perp + m \right)}{p^- p'^-} \bar{n}^\mu \bar{n}^\nu \Bigg] \frac{\not{\bar{n}}}{2} \\
&=: \quad W^{\mu\nu\, AB}(p, p', q, m) \qquad \text{(D.4)}
\end{aligned}
$$

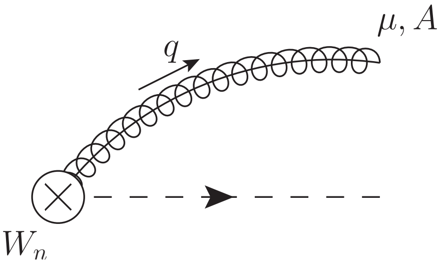

$$= \quad g_s \tilde{\mu}^\varepsilon \frac{\bar{n}^\mu T^A}{q^- + i0} \qquad \text{(D.5)}$$

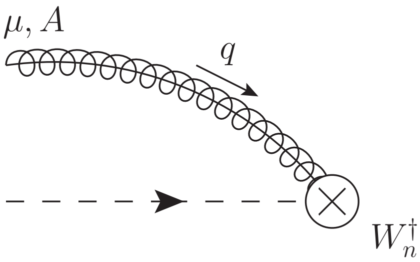

$$= \quad g_s \tilde{\mu}^\varepsilon \frac{\bar{n}^\mu T^A}{q^- - i0} \qquad \text{(D.6)}$$

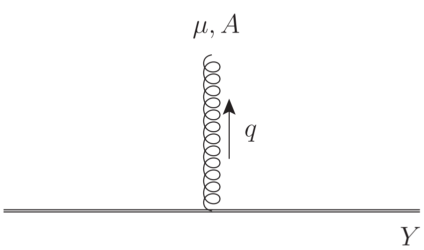

$$= \quad \begin{cases} g_s \tilde{\mu}^\varepsilon \frac{n^\mu T^A}{q^+ + i0} & (Y_n) \\ -g_s \tilde{\mu}^\varepsilon \frac{n^\mu T^A}{q^+ + i0} & (Y_n^\dagger) \\ g_s \tilde{\mu}^\varepsilon \frac{n^\mu \bar{T}^A}{q^+ + i0} & (\bar{Y}_n) \\ -g_s \tilde{\mu}^\varepsilon \frac{n^\mu \bar{T}^A}{q^+ + i0} & (\bar{Y}_n^\dagger) \end{cases} \qquad \text{(D.7)}$$

For $\bar{n}$-collinear Wilson lines one just has to swap $n \leftrightarrow \bar{n}$ and $q^+ \leftrightarrow q^-$ in the expressions (D.5) to (D.7).

Appendix E

Calculation of the Hard, Jet, and Soft Functions

In this appendix the calculations of the hard, jet, and soft functions used in sections 6.1, 6.2, and 6.3, are summarized. Note that spinors are omitted, and that the results and parts of the calculations can be found in [12].

E.1 Jet Function

If J is the sum of all jet function diagrams, the jet function is given by

$$J_{n,\bar{n}}(s,m,\mu) = \frac{1}{Q\pi}\mathrm{Im}\left\{i\mathrm{Tr}\left[\frac{\bar{\not{n}}}{4}J\right]\right\} =: \mathrm{Im}\{\hat{J}\}. \tag{E.1}$$

The first diagram we want to treat is J_a, where the subscript refers to the corresponding panel in Fig. 6.2. Using SCET Feynman rules we obtain

$$\begin{aligned} J_a = &\int \frac{\mathrm{d}^d q}{(2\pi)^d}\frac{i\not{n}}{2}\frac{\bar{n}\cdot p}{p^2-m^2+i0}V_\mu^A(p-q,p,m)\frac{-ig^{\mu\nu}\delta^{AB}}{q^2+i0}\frac{i\not{n}}{2}\frac{\bar{n}\cdot(p-q)}{(p-q)^2-m^2+i0}\tilde{\mu}^\varepsilon g_s\frac{T^B\bar{n}_\nu}{q^-+i0} \\ = &-4\pi\alpha_s C_F\not{n}\frac{p^-}{p^2-m^2+i0}\underbrace{\tilde{\mu}^{2\varepsilon}\int\frac{\mathrm{d}^d q}{(2\pi)^d}\frac{p^--q^-}{[(p-q)^2-m^2+i0]\,[q^-+i0]\,[q^2+i0]}}_{=:I_a}. \end{aligned} \tag{E.2}$$

After doing a light-cone coordinate transformation such that $\frac{\mathrm{d}^d q}{(2\pi)^d} = \frac{2^{-d}\pi^{-1-\frac{d}{2}}}{\Gamma\left(\frac{d-2}{2}\right)}(q_\perp)^{d-3}\mathrm{d}q^+\,\mathrm{d}q^-\,\mathrm{d}q_\perp$ the integral reads

$$\begin{aligned} I_a = \tilde{\mu}^{2\varepsilon}\frac{2^{-d}\pi^{-1-\frac{d}{2}}}{\Gamma\left(\frac{d-2}{2}\right)}\int_0^\infty \mathrm{d}q_\perp\int\mathrm{d}q^-\,q_\perp^{d-3}\frac{Q-q^-}{q^-+i0}\frac{-1}{(Q-q^-)q^-} \\ \times\int\mathrm{d}q^+\frac{1}{\left[q^+-\frac{q_\perp^2-i0}{q^-}\right]\left[q^+-\frac{s-q_\perp^2-p^+q^-}{Q-q^-}\right]}, \end{aligned} \tag{E.3}$$

with $s := p^2-m^2+i0$. Note that at leading order in the SCET power counting parameter λ, $p^- = Q$, and that $p_\perp = 0$ if the light-cone vector (4.1) is chosen to be aligned with the thrust axis.

The integral in the second line of (E.3) is only non-zero if the poles are located on different complex half planes. Using the residue theorem, the q^+ integral can be solved and the remaining expression is

$$I_a = -2\pi i \tilde{\mu}^{2\varepsilon} \frac{2^{-d}\pi^{-1-\frac{d}{2}}}{\Gamma\left(\frac{d-2}{2}\right)} \int\limits_0^Q \mathrm{d}q^- \int\limits_0^\infty \mathrm{d}q_\perp \, q_\perp^{d-3} \frac{Q-q^-}{q^- + i0} \frac{1}{q^-(s-p^+q^-) - Qq_\perp^2 + i0}, \tag{E.4}$$

which was solved by using `Mathematica`. Rewriting $Qp^+ = s + m^2$ and $d = 4 - 2\varepsilon$, the final result reads

$$\begin{aligned}
I_a =& -i2^{-4+2\varepsilon}\pi^{-1+\varepsilon} \frac{\Gamma(-\varepsilon)}{\Gamma(2-\varepsilon)\Gamma(1-\varepsilon)} \left(\frac{\tilde{\mu}^2}{-s}\right)^\varepsilon \csc\left((2-\varepsilon)\pi\right) {}_2F_1\left(\varepsilon, -\varepsilon; 2-\varepsilon; \frac{s+m^2}{s}\right) \\
=& -\frac{i}{16\pi^2}\Bigg[\frac{1}{\varepsilon^2} + \frac{1}{\varepsilon}\left(1 + \log\frac{\mu^2}{-s}\right) - \frac{m^2}{s+m^2}\log\frac{m^2}{-s} - \mathrm{Li}_2\left(\frac{s+m^2}{s}\right) + 2 + \frac{\pi^2}{12} + \log\frac{\mu^2}{-s} \\
&+ \frac{1}{2}\log^2\frac{\mu^2}{-s}\Bigg] + \mathcal{O}(\varepsilon) \\
=:& -\frac{i}{16\pi^2}\left(\frac{1}{\varepsilon^2} + \frac{1}{\varepsilon}\left(1 + \log\frac{\mu^2}{-s}\right) + G_{J_a}\right) + \mathcal{O}(\varepsilon).
\end{aligned} \tag{E.5}$$

which, inserting I_a back into Eq. (E.2), leads to (omitting $\mathcal{O}(\varepsilon)$ terms)

$$J_a = \frac{i\alpha_s C_F Q}{4\pi s}\not{n}\left[\frac{1}{\varepsilon^2} + \frac{1}{\varepsilon}\left(1 + \log\frac{\mu^2}{-s}\right) + G_{J_a}\right]. \tag{E.6}$$

To expand the hypergeometric function we used the `Mathematica` package `hypexp` [65].

It is easy to see that $J_b = J_a$, so the next diagram to consider is J_c which reads

$$\begin{aligned}
J_c =& \int \frac{\mathrm{d}^d q}{(2\pi)^d} \frac{i\not{n}}{2} \frac{p^-}{p^2 - m^2 + i0} V_\mu^A(p-q,p) \frac{i\not{n}}{2} \frac{p^- - q^-}{(p-q)^2 - m^2 + i0} \frac{-ig^{\mu\nu}\delta^{AB}}{q^2 + i0} V_\nu^B \frac{i\not{n}}{2} \frac{p^-}{p^2 - m^2 + i0} \\
=& \, g_s^2 C_F \frac{\not{n}}{2} \frac{Q^2}{s^2} \tilde{\mu}^{2\varepsilon} \int \frac{\mathrm{d}^d q}{(2\pi)^d} \frac{Q - q^-}{[q^2 + i0][(p-q)^2 - m^2 + i0]} \\
&\times \left(\frac{2dm^2}{Q(Q-q^-)} + (d-2)\frac{-q_\perp^2 - m^2}{(Q-q^-)^2} - (d-2)\frac{m^2}{Q^2}\right) + [\text{terms with even numbers of } \gamma\text{s}],
\end{aligned} \tag{E.7}$$

where the terms with an even number of gamma matrices are vanishing when the trace is taken at the end (see Eq. (E.1)). It is advisable to add diagram J_d before solving the integral in J_c, since the pole at $(Q - q^-) = 0$ cancels in the sum. J_d reads

$$\begin{aligned}
J_d =& \frac{1}{2} \int \frac{\mathrm{d}^d q}{(2\pi^d)} \frac{i\not{n}}{2} \frac{p^-}{s} W_{\mu\nu}^{AB}(p,p,q) \frac{-ig^{\mu\nu}\delta^{AB}}{q^2 + i0} \frac{i\not{n}}{2} \frac{p^-}{s} \\
=& -g_s^2 C_F (d-2) \frac{Q^2}{s^2} \frac{\not{n}}{2} \tilde{\mu}^{2\varepsilon} \int \frac{\mathrm{d}^d q}{(2\pi)^d} \frac{1}{[q^2 + i0]\,(Q - q^-)},
\end{aligned} \tag{E.8}$$

and therefore the sum of both diagrams reads

$$
\begin{aligned}
J_c + J_d = {}& g_s^2 C_F \frac{Q^2}{s^2}\frac{\not{n}}{2}\tilde{\mu}^{2\varepsilon}\int\frac{\mathrm{d}^d q}{(2\pi)^d}\frac{1}{[q^2+i0][(p-q)^2-m^2+i0]} \\
& \times\left[\frac{2dm^2}{Q}-(d-2)\frac{m^2(Q-q^-)}{Q^2}-(d-2)(p^+-q^+)\right]+[\#\gamma\ \text{even}] \\
= {}& -i\frac{\alpha_s C_F}{4\pi}\frac{Q}{s^2}\frac{\not{n}}{2}\left[\frac{1}{\varepsilon}(s-6m^2)+\frac{m^4(6m^2+7s)}{(m^2+s)^2}\log\frac{m^2}{-s}-(6m^2-s)\log\frac{\mu^2}{-s}\right. \\
& \left.-8m^2+\frac{s^2}{s+m^2}\right]+[\#\gamma\ \text{even}]\,. \qquad \text{(E.9)}
\end{aligned}
$$

Finally the mass counterterm J_e has to be computed. For simplicity we will renormalize the mass in the pole mass scheme, hence J_e reads

$$
\begin{aligned}
J_e &= \frac{i\not{n}}{2}\frac{Q}{s}\left(-i\frac{\not{\bar{n}}}{s}\frac{2m\,\delta m^{\text{pole}}}{Q}\right)\frac{i\not{n}}{2}\frac{Q}{s} \\
&= i\frac{\alpha_s C_F}{4\pi}\frac{Q}{s^2}\frac{\not{n}}{2}(-2m^2)\left(\frac{3}{\varepsilon}+4+3\log\frac{\mu^2}{m^2}\right). \qquad \text{(E.10)}
\end{aligned}
$$

Omitting the terms with even numbers of γ matrices, the sum of J_c, J_d, and J_e can be written as

$$
J_c+J_d+J_e = -i\frac{\alpha_s C_F}{4\pi}\frac{Q}{s}\frac{\not{n}}{2}\left[\frac{1}{\varepsilon}+\frac{s}{s+m^2}+\log\frac{\mu^2}{-s}-\frac{m^2(6s+5m^2)}{(m^2+s)^2}\log\frac{m^2}{-s}\right]. \qquad \text{(E.11)}
$$

Note that the mass scheme can be changed later. The zero-bins, as described in section 4.4, are scaleless for all jet function diagrams and therefore do not contribute to the result.

E.2 Hard Function

The first hard function diagram as seen in 6.1 gives

$$
\begin{aligned}
H_a = {}& \int\frac{\mathrm{d}^d q}{(2\pi)^d}V_\mu^A(p,p-q,m)\frac{i\not{n}}{2}\frac{p^- - q^-}{(p-q)^2-m^2+i0}\frac{-ig^{\mu\nu}\delta^{AB}}{q^2+i0}\Gamma_i^\alpha\left(g_s\frac{T^B\bar{n}_\nu}{q^-+i0}\tilde{\mu}^\varepsilon\right) \\
= {}& 2ig_s^2 C_F\Gamma_i^\alpha\tilde{\mu}^{2\varepsilon}\int\frac{\mathrm{d}^d q}{(2\pi)^d}\frac{Q-q^-}{[(p-q)^2-m^2+i0]\,[q^2+i0]\,[q^-+i0]} \\
= {}& 2ig_s^2 C_F\Gamma_i^\alpha I_a(s=0), \qquad \text{(E.12)}
\end{aligned}
$$

where the integral I_a is already defined in Eq. (E.2).

Using the same approach for I_a as in the jet function calculation it gives

$$
\begin{aligned}
I_a(s=0) = {}& -\frac{i2^{-d}\pi^{1-\frac{d}{2}}}{\Gamma\left(\frac{d-2}{2}\right)}\tilde{\mu}^{2\varepsilon}\csc\frac{d\pi}{2}\int_0^1\mathrm{d}x\,\frac{1-x}{x+i0}\left(-x\left(-p^+Qx\right)\right)^{\frac{d-4}{2}} \\
= {}& -\frac{i2^{-d}\pi^{1-\frac{d}{2}}}{\Gamma\left(\frac{d-2}{2}\right)}\csc\frac{d\pi}{2}\left(\frac{m^2}{\tilde{\mu}^2}\right)^{\frac{d-4}{2}}B(d-4,2), \qquad \text{(E.13)}
\end{aligned}
$$

with the beta function $B(x, y)$. Thus the full result of diagram H_a reads

$$H_a = \Gamma_i^\alpha \frac{\alpha_s C_F}{4\pi} \left[\frac{1}{\varepsilon^2} + \frac{1}{\varepsilon} \left(2 + \log \frac{\mu^2}{m^2} \right) + 4 + \frac{\pi^2}{12} + 2 \log \frac{\mu^2}{m^2} + \frac{1}{2} \log^2 \frac{\mu^2}{m^2} + \mathcal{O}(\varepsilon) \right]. \tag{E.14}$$

It is straightforward to show that $H_b = H_a$, so the last piece to consider is diagram c), for which the SCET Feynman rules lead to the scaleless integral

$$\begin{aligned} H_c = &\int \frac{\mathrm{d}^d q}{(2\pi)^d} \, (ig_s T^A \tilde{\mu}^\varepsilon) n_\mu \frac{\bar{\not n}}{2} \frac{i\not n}{2} \frac{p^- + q^-}{(p+q)^2 - m^2 + i0} \Gamma_i^\alpha \\ &\times \frac{i\bar{\not n}}{2} \frac{q^+ - p'^+}{(p'-q)^2 - m^2 + i0} (ig_s T^B \tilde{\mu}^\varepsilon) \bar{n}_\nu \frac{\not n}{2} \frac{-ig^{\mu\nu}\delta^{AB}}{q^2 + i0} \\ = {} & i8\pi\alpha_s C_F \Gamma_i^\alpha \tilde{\mu}^{2\varepsilon} \frac{2^{-d}\pi^{-1-\frac{d}{2}}}{\Gamma\left(\frac{d-2}{2}\right)} \int \mathrm{d}q^- \, \mathrm{d}q^+ \, \mathrm{d}q^\perp \left(q^\perp\right)^{d-3} \frac{1}{[q^+q^- - (q^\perp)^2 + i0] \, [q^+ + i0] \, [-q^- + i0]}, \end{aligned} \tag{E.15}$$

which does not contribute to the full result.

Therefore, expression H_a is the only SCET contribution to the hard function.

E.3 Soft Function

Using the Feynman rules for soft Wilson lines, diagrams S_a and S_b, shown in Fig. 6.3, give (already including all ingredients as seen in the soft function definition (5.17))

$$\begin{aligned} S_a = S_b = \delta(\ell^+)\delta(\ell^-) &\int \frac{\mathrm{d}^d q}{(2\pi)^d} \left(-g_s \frac{T^A n_\mu \tilde{\mu}^\varepsilon}{q^+ + i0} \right) \left(\frac{-i\delta^{AB} g^{\mu\nu}}{q^2 + i0} \right) \left(-g_s \frac{\bar{T}^B \bar{n}_\nu \tilde{\mu}^\varepsilon}{-q^- + i0} \right) \\ = & -2ig_s^2 C_F \tilde{\mu}^{2\varepsilon} \int \frac{\mathrm{d}^d q}{(2\pi^d)} \frac{1}{(q^+ + i0)(q^2 + i0)(q^- - i0)}, \end{aligned} \tag{E.16}$$

which is a scaleless integral and therefore not contributing.

To compute contribution S_c, it's useful to notice that the diagram is independent of perpendicular momenta such that the phase space integral reduces to

$$\int \frac{\mathrm{d}^d q}{(2\pi)^d} \, 2\pi\delta(q^2)\Theta(q^0) \quad \to \quad \frac{2^{2\varepsilon-4}\pi^{\varepsilon-2}}{\Gamma(1-\varepsilon)} \int \mathrm{d}k^+ \, \mathrm{d}k^- \, \Theta(k^+ + k^-)\Theta(k^+k^-) \left(k^+k^-\right)^{-\varepsilon}, \tag{E.17}$$

and we obtain

$$\begin{aligned} S_c = & \frac{2^{2\varepsilon-4}\pi^{\varepsilon-2}}{N_c\Gamma(1-\varepsilon)} \int \mathrm{d}k^+ \, \mathrm{d}k^- \, \Theta(k^+ + k^-)\Theta(k^+k^-) \left(k^+k^-\right)^{-\varepsilon} \\ & \times \left[\Theta(k^- - k^+)\delta(\ell^+ - k^+)\delta(\ell^-) + \Theta(k^+ - k^-)\delta(\ell^+)\delta(\ell^- - k^-) \right] \\ & \times \left(-g_s \frac{\bar{T}^A \bar{n}_\mu}{k^- + i0} \tilde{\mu}^\varepsilon \right) \left(g_s \frac{T^B n_\nu}{-k^+ + i0} \tilde{\mu}^\varepsilon \right) \left(-g^{\mu\nu}\delta^{AB} \right) \\ = & \frac{1}{2\pi} \frac{C_F \alpha_s \mu^{2\varepsilon} \, \mathrm{e}^{\gamma_E \varepsilon}}{\varepsilon\Gamma(1-\varepsilon)} \left(\delta(\ell^-)\Theta(\ell^+) \left(\ell^+\right)^{-1-2\varepsilon} + \delta(\ell^+)\Theta(\ell^-) \left(\ell^-\right)^{-1-2\varepsilon} \right). \end{aligned} \tag{E.18}$$

The last contribution to the soft function is diagram S_d, which gives the same result as S_c.

Appendix F

Evolutions

Here we discuss the renormalization group equations and the associated solutions for α_s, the hard, jet, and soft functions, the gap parameter, and the $\overline{\text{MS}}$ mass.

F.1 Running of α_s

For our numerical results we use 4-loop running of the strong coupling constant α_s. The renormalization group equation reads

$$\frac{\mathrm{d}\alpha_s(\mu)}{\mathrm{d}\log\mu} = \beta(\alpha_s) =: -\frac{\alpha_s^2}{2\pi}\sum_{i=0}^{\infty}\beta_i\left(\frac{\alpha_s}{4\pi}\right)^i, \tag{F.1}$$

where $\beta(\alpha_s)$ is the QCD beta function for which the perturbative coefficients are known up to β_3. They read [58]

$$\begin{aligned}
\beta_0 &= 11 - \frac{2}{3}n_f,\\
\beta_1 &= 102 - \frac{38}{3}n_f,\\
\beta_2 &= \frac{2857}{2} - \frac{5033}{18}n_f + \frac{325}{54}n_f^2,\\
\beta_3 &= \frac{149753}{6} + 3564\zeta_3 + \left(-\frac{1078361}{162} - \frac{6508}{27}\zeta_3\right)n_f + \left(\frac{50065}{162} + \frac{6472}{81}\zeta_3\right)n_f^2 + \frac{1093}{729}n_f^3.
\end{aligned} \tag{F.2}$$

Equation (F.1) can be solved iteratively which gives

$$\begin{aligned}
\frac{1}{\alpha_s(\mu)} &= \frac{\varphi}{\alpha_s(\mu_0)} + \frac{\beta_1\log\varphi}{4\pi\beta_0} + \frac{\alpha_s(\mu_0)}{\varphi}\frac{1}{(4\pi\beta_0)^2}\Big[(\beta_1^2-\beta_0\beta_2)(1-\varphi)+\beta_1^2\log\varphi\Big]\\
&\quad + \frac{\alpha_s^2(\mu_0)}{\varphi^2}\frac{1}{(4\pi\beta_0)^3}\left[\frac{\beta_0^2\beta_3}{2}(\varphi^2-1)+\beta_0\beta_1\beta_2(\log\varphi+\varphi-\varphi^2)+\frac{\beta_1^3}{2}\Big[(1-\varphi^2)^2-\log^2\varphi\Big]\right],
\end{aligned} \tag{F.3}$$

with $\varphi := 1 + \frac{\alpha_s(\mu_0)\beta_0}{2\pi}\log\frac{\mu}{\mu_0}$. This expression is used in our analysis.

F.2 Evolution Kernels

The evolution of the hard, jet, and soft functions derived in section 6.4 is governed by the functions ω and K, defined in Eq. (6.23), with the appropriate perturbative coefficients which are given in Eqs. (6.33) to (6.35).

The perturbative expansions of ω and K have the form [10]

$$\begin{aligned}\omega^{\mathrm{N^3LL}}(\mu,\mu_0,\Gamma,j) &= \frac{2}{j}\int_{\alpha_s(\mu_0)}^{\alpha_s(\mu)} \mathrm{d}\alpha\, \frac{\Gamma(\alpha)}{\beta(\alpha)} \\ &= \frac{\Gamma_0}{\beta_0 j}\Bigg[-\log r + \frac{\alpha_s(\mu_0)}{4\pi}\left(\frac{\beta_1}{\beta_0}-\frac{\Gamma_1}{\Gamma_0}\right)(r-1) + \frac{1}{2}\left(\frac{\alpha_s(\mu_0)}{4\pi}\right)^2\left(\frac{\beta_1\Gamma_1}{\beta_0\Gamma_0}-\frac{\Gamma_2}{\Gamma_0}-B_2\right)(r^2-1) \\ &\quad + \frac{1}{3}\left(\frac{\alpha_s(\mu_0)}{4\pi}\right)^3\left(\frac{\beta_1\Gamma_2}{\beta_0\Gamma_0}-B_2\frac{\Gamma_1}{\Gamma_0}-\frac{\Gamma_3}{\Gamma_0}-B_3\right)(r^3-1)\Bigg],\end{aligned} \tag{F.4}$$

and

$$\begin{aligned}K^{\mathrm{N^2LL}}(\mu,\mu_0,\Gamma,\gamma) - \omega^{\mathrm{NLL}}(\mu,\mu_0,\gamma,2) &= 2\int_{\alpha_s(\mu_0)}^{\alpha_s(\mu)} \mathrm{d}\alpha\,\frac{\Gamma(\alpha)}{\beta(\alpha)}\int_{\alpha_s(\mu_0)}^{\alpha}\mathrm{d}\alpha'\,\frac{1}{\beta(\alpha')} \\ = \frac{\Gamma_0}{2\beta_0^2}\Bigg\{\frac{4\pi}{\alpha_s(\mu_0)}\left(\frac{1}{r}+\log r-1\right) &+ \left(\frac{\Gamma_1}{\Gamma_0}-\frac{\beta_1}{\beta_0}\right)(r-1-\log r) - \frac{\beta_1}{2\beta_0}\log^2 r \\ + \frac{\alpha_s(\mu_0)}{4\pi}\Bigg[\left(\frac{\Gamma_1\beta_1}{\Gamma_0\beta_0}-\frac{\beta_1^2}{\beta_0^2}\right)(r-1-r\log r) &- B_2\log r + \left(\frac{\Gamma_2}{\Gamma_0}-\frac{\Gamma_1\beta_1}{\Gamma_0\beta_0}+B_2\right)\frac{r^2-1}{2} \\ &+ \left(\frac{\Gamma_2}{\Gamma_0}-\frac{\Gamma_1\beta_1}{\Gamma_0\beta_0}\right)(r-1)\Bigg]\Bigg\},\end{aligned} \tag{F.5}$$

with $B_2 := \left(\frac{\beta_1}{\beta_0}\right)^2 - \frac{\beta_2}{\beta_0}$, $B_3 := -\frac{\beta_1^3}{\beta_0^3} + 2\frac{\beta_1\beta_2}{\beta_0^2} - \frac{\beta_3}{\beta_0}$ and $r := \frac{\alpha_s(\mu)}{\alpha_s(\mu_0)}$.

F.3 R-Evolution

In section 6.7.1 we introduced the gap formalism to avoid the renormalon ambiguity in the soft function. As explained, we have to run the gap parameter $\bar{\Delta}(R,\mu)$ from the scale where the logs are small to the scale where we subtract the renormalon. A short overview considering the gap parameter running can be found in [10], and a detailed derivation is given in [54, 56, 57].

To obtain the running in μ one can use the fact that $\Delta = \bar{\Delta} + \delta$ is scale independent. Hence we deduce that

$$\mu\frac{\mathrm{d}}{\mathrm{d}\mu}\bar{\Delta}(R,\mu) = -\mu\frac{\mathrm{d}}{\mathrm{d}\mu}\delta(R,\mu) = -2R\,\mathrm{e}^{\gamma_E}\Gamma_s[\alpha_s] =: -R\gamma^{\mu}_{\bar{\Delta}}[\alpha_s(\mu)], \tag{F.6}$$

where $\Gamma_s[\alpha_s]$ is defined in Eq. (6.26), arising from the used gap scheme given in (6.56). Solving this differential equation is straightforward and gives

$$\bar{\Delta}(R,\mu) = \bar{\Delta}(R,\mu_0) - R\,\mathrm{e}^{\gamma_E}\omega_s(\mu,\mu_0,\Gamma_s,1), \tag{F.7}$$

with ω_s as defined in (6.23).

The RGE which governs the R-evolution is given by

$$R\frac{\mathrm{d}\bar{\Delta}(R,R)}{\mathrm{d}R} = -R\gamma^R_{\bar{\Delta}}[\alpha_s(R)],$$
$$\gamma^R_{\bar{\Delta}}[\alpha_s(R)] = \sum_{n=0}\gamma^R_{\bar{\Delta},n}\left(\frac{\alpha_s(R)}{4\pi}\right)^{n+1}. \tag{F.8}$$

and the solution reads [56]

$$\bar{\Delta}(R_1,R_1) = \bar{\Delta}(R_0,R_0) - \Lambda_{\mathrm{QCD}}\int\limits_{t(R_0)}^{t(R_1)} \mathrm{d}t\,\gamma^R_{\bar{\Delta}}(t)\frac{\mathrm{d}}{\mathrm{d}t}\,\mathrm{e}^{-G(t)}, \tag{F.9}$$

with

$$t(R) := -\frac{2\pi}{\beta_0\alpha_s(R)},$$
$$G(t) := -\int \mathrm{d}t\,\frac{2\pi}{\beta_0\beta(t)t^2},$$
$$\Lambda_{\mathrm{QCD}} = R\,\mathrm{e}^{G(t(R))} = R_0\,\mathrm{e}^{G(t(R_0))}, \tag{F.10}$$

where one should note that $\beta(t) \equiv \beta[\alpha_s]$ and $\gamma^R_{\bar{\Delta}}(t) \equiv \gamma^R_{\bar{\Delta}}[\alpha_s]$.

After using the μ running from Eq. (F.7), and expanding all ingedients to the appropriate order in α_s, one gets [54]

$$\begin{aligned}\left[\bar{\Delta}(R,\mu) - \bar{\Delta}(R_\Delta,\mu_\Delta)\right]^{\mathrm{N}^k\mathrm{LL}} &= -R_\Delta\,\mathrm{e}^{\gamma_E}\omega_s^{\mathrm{N}^{k-1}\mathrm{LL}}(R_\Delta,\mu_\Delta,\Gamma_s,1) - R\,\mathrm{e}^{\gamma_E}\omega_s^{\mathrm{N}^{k-1}\mathrm{LL}}(\mu,R,\Gamma_s,1)\\ &+ \Lambda^{(k)}_{\mathrm{QCD}}\sum_{j=0}^{k-1} S_j(-1)^j\left[\Gamma(-\hat{b}_1-j,t(R)) - \Gamma(-\hat{b}_1-j,t(R_\Delta))\right]\mathrm{e}^{i\pi\hat{b}_1},\end{aligned} \tag{F.11}$$

with

$$\hat{b}(t) := \frac{\mathrm{d}G(t)}{\mathrm{d}t} =: \sum_{j=0}\hat{b}_j t^{-j},$$
$$\hat{b}_0 = 1, \qquad \hat{b}_1 = \frac{\beta_1}{2\beta_0^2},$$
$$S(t) := -t\gamma^R_{\bar{\Delta}}(t)\hat{b}(t)\,\mathrm{e}^{-G(t)}\,\mathrm{e}^t(-t)^{\hat{b}_1} =: \sum_{j=0} S_j(-t)^{-j},$$
$$\Lambda^{(k)}_{\mathrm{QCD}} := R\exp\left(\sum_{j=0}^{k}\hat{b}_j\int \mathrm{d}t\,t^{-j}\right)\Bigg|_{t=t(R)}, \tag{F.12}$$

and the incomplete gamma function $\Gamma(s,x)$.

The S_i needed to obtain N^2LL accuracy are given by [54]

$$S_0 = 0,$$
$$S_1 = \frac{\gamma^R_{\bar{\Delta},1}}{(2\beta_0)^2} = \mathrm{e}^{\gamma_E}\frac{-C_F\pi^2\beta_0 + \gamma_{s,1}}{4\beta_0^2}. \tag{F.13}$$

F.4 Running of the $\overline{\mathrm{MS}}$ Mass

In section 6.7.2 we introduced the $\overline{\mathrm{MS}}$ mass which is, in contrast to the pole mass, free of the leading renormalon ambiguity. This short distance mass depends on the renormalization scale with the corresponding renormalization group equation [58]

$$\mu\frac{\mathrm{d}\overline{m}(\mu)}{\mathrm{d}\mu} = \overline{m}(\mu)\gamma_m[\alpha_s(\mu)] =: -2\overline{m}(\mu)\sum_{i=0}\gamma_{m,i}\left(\frac{\alpha_s}{4\pi}\right)^{i+1}, \tag{F.14}$$

with the perturbative coefficients

$$\begin{aligned}
\gamma_{m,0} &= 4,\\
\gamma_{m,1} &= \frac{202}{3} - \frac{20}{9}n_f,\\
\gamma_{m,2} &= 1249 - \left(\frac{2216}{27} + \frac{160}{3}\zeta_3\right)n_f - \frac{140}{81}n_f^2,\\
\gamma_{m,3} &= \frac{4603055}{162} + \frac{135680}{27}\zeta_3 - 8800\zeta_5 + \left(-\frac{91723}{27} - \frac{34192}{9}\zeta_3 + 880\zeta_4 + \frac{18400}{9}\zeta_5\right)n_f\\
&\quad + \left(\frac{5242}{243} + \frac{800}{9}\zeta_3 - \frac{160}{3}\zeta_4\right)n_f^2 + \left(-\frac{332}{243} + \frac{64}{27}\zeta_3\right)n_f^3.
\end{aligned} \tag{F.15}$$

Solving the differential equation in (F.14), the 4-loop evolution which is used in our analysis reads

$$\overline{m}(\mu) = \exp\left(-2\omega^{\mathrm{N^3LL}}(\mu,\mu_0,\gamma_m,2)\right)\overline{m}(\mu_0) =: \overline{m}(\mu_0)U_m(\mu_0,\mu). \tag{F.16}$$

Bibliography

[1] M. Dasgupta and G. P. Salam, "Event shapes in e^+e^- annihilation and deep inelastic scattering," *Journal of Physics G: Nuclear and Particle Physics* **30** no. 5, (2004) R143–R181, `arXiv:0312283 [hep-ph]`.

[2] S. Kluth, "Tests of quantum chromo dynamics at e^+e^- colliders," *Reports on Progress in Physics* **69** no. 6, (2006) 1771–1846, `arXiv:0603011 [hep-ex]`.

[3] C. W. Bauer, S. Fleming, and M. Luke, "Summing Sudakov logarithms in $B \to X_s\gamma$ in effective field theory," *Physical Review D* **63** no. 1, (2000) 014006, `arXiv:0005275 [hep-ph]`.

[4] C. W. Bauer, S. Fleming, D. Pirjol, and I. W. Stewart, "An effective field theory for collinear and soft gluons: Heavy to light decays," *Physical Review D* **63** no. 11, (2001) 114020, `arXiv:0011336 [hep-ph]`.

[5] C. W. Bauer and I. W. Stewart, "Invariant operators in collinear effective theory," *Physics Letters B* **516** no. 1-2, (2001) 134–142, `arXiv:0107001 [hep-ph]`.

[6] C. W. Bauer, D. Pirjol, and I. W. Stewart, "Soft-collinear factorization in effective field theory," *Physical Review D* **65** no. 5, (2002) 054022, `arXiv:0109045 [hep-ph]`.

[7] C. W. Bauer, S. Fleming, D. Pirjol, I. Z. Rothstein, and I. W. Stewart, "Hard scattering factorization from effective field theory," *Physical Review D* **66** no. 1, (2002) 014017, `arXiv:0202088 [hep-ph]`.

[8] T. Becher, A. Broggio, and A. Ferroglia, *Introduction to Soft-Collinear Effective Theory*, vol. 896 of *Lecture Notes in Physics*. Springer International Publishing, Cham, 2015. `arXiv:1410.1892 [hep-ph]`.

[9] C. W. Bauer and I. W. Stewart, "The Soft-Collinear Effective Theory." Online, 2014. Lecture Notes.

[10] R. Abbate, M. Fickinger, A. H. Hoang, V. Mateu, and I. W. Stewart, "Thrust at N^3LL with Power Corrections and a Precision Global Fit for $\alpha_s(m_Z)$," *Physical Review D* **83** no. 7, (2010) 074021, `arXiv:1006.3080 [hep-ph]`.

[11] S. Fleming, A. H. Hoang, S. Mantry, and I. W. Stewart, "Jets from massive unstable particles: Top-mass determination," *Physical Review D* **77** no. 7, (2008) 074010, `arXiv:0703207 [hep-ph]`.

[12] S. Fleming, A. H. Hoang, S. Mantry, and I. W. Stewart, "Top jets in the peak region: Factorization analysis with next-to-leading-log resummation," *Physical Review D* **77** no. 11, (2008) 114003, `arXiv:0711.2079 [hep-ph]`.

[13] Y.-t. Chien and M. D. Schwartz, "Resummation of heavy jet mass and comparison to LEP data," *Journal of High Energy Physics* **2010** no. 8, (2010) 58, `arXiv:1005.1644 [hep-ph]`.

[14] A. H. Hoang, D. W. Kolodrubetz, V. Mateu, and I. W. Stewart, “A Precise Determination of α_s from the C-parameter Distribution,” *Physical Review D* **91** no. 9, (2015) 094018, `arXiv:1501.04111 [hep-ph]`.

[15] M. Preisser, *C-Parameter with Massive Quarks.* Master’s thesis, University of Vienna, 2014.

[16] E. Farhi, “Quantum Chromodynamics Test for Jets,” *Physical Review Letters* **39** no. 25, (1977) 1587–1588.

[17] E. Gardi and J. Rathsman, “The thrust and heavy-jet mass distributions in the two-jet region,” *Nuclear Physics B* **638** no. 1-2, (2002) 243–287, `arXiv:0201019 [hep-ph]`.

[18] The MARK J Collaboration, D. Barber, *et al.*, “Physics with high energy electron-positron colliding beams with the MARK J detector,” *Physics Reports* **63** no. 7, (1980) 337–391.

[19] S. Catani, L. Trentadue, G. Turnock, and B. Webber, “Resummation of large logarithms in e^+e^- event shape distributions,” *Nuclear Physics B* **407** no. 1, (1993) 3–42.

[20] L. Clavelli, “Jet invariant mass in quantum chromodynamics,” *Physics Letters B* **85** no. 1, (1979) 111–114.

[21] L. Clavelli and D. Wyler, “Kinematical bounds on jet variables and the heavy jet mass distribution,” *Physics Letters B* **103** no. 4-5, (1981) 383–387.

[22] T. Chandramohan and L. Clavelli, “Consequences of 2nd order QCD for jet structure in e^+e^- annihilation,” *Nuclear Physics B* **184** (1981) 365–380.

[23] L. Clavelli and H. P. Nilles, “Jet-mass spectra in perturbative quantum chromodynamics,” *Physical Review D* **21** no. 5, (1980) 1242–1250.

[24] S. Catani, G. Turnock, and B. Webber, “Heavy jet mass distribution in e^+e^- annihilation,” *Physics Letters B* **272** no. 3-4, (1991) 368–372.

[25] A. G.-D. Ridder, T. Gehrmann, E. Glover, and G. Heinrich, “NNLO corrections to event shapes in e^+e^- annihilation,” *Journal of High Energy Physics* **2007** no. 12, (2007) 094, `arXiv:0711.4711 [hep-ph]`.

[26] J. Jersák, E. Laermann, and P. M. Zerwas, “Electroweak production of heavy quarks in e^+e^- annihilation,” *Physical Review D* **25** no. 5, (1982) 1218–1228.

[27] B. W. Harris and J. F. Owens, “Two cutoff phase space slicing method,” *Physical Review D* **65** no. 9, (2002) 094032, `arXiv:0102128 [hep-ph]`.

[28] J. C. Collins, *Renormalization.* Cambridge University Press, Cambridge, 1986.

[29] G. Kramer, G. Schierholz, and J. Willrodt, “Cross sections and angular distributions of three-jet final states in e^+e^- annihilation for heavy quarks,” *Zeitschrift für Physik C Particles and Fields* **4** no. 2, (1980) 149–152.

[30] B. Ioffe, “Associated production of gluonic jets and heavy mesons in e^+e^- annihilation,” *Physics Letters B* **78** no. 2-3, (1978) 277–280.

[31] H. P. Nilles, “Isolating Gluon Jets,” *Physical Review Letters* **45** no. 5, (1980) 319–322.

[32] K. Chetyrkin, J. Kühn, and A. Kwiatkowski, “QCD corrections to the e^+e^- cross-section and the Z boson decay rate: concepts and results,” *Physics Reports* **277** no. 4, (1996) 189–281.

[33] A. H. Hoang and I. W. Stewart, “Designing gapped soft functions for jet production,” *Physics Letters B* **660** no. 5, (2008) 483–493, `arXiv:0709.3519 [hep-ph]`.

[34] L. G. Almeida, S. D. Ellis, C. Lee, G. Sterman, I. Sung, and J. R. Walsh, "Comparing and counting logs in direct and effective methods of QCD resummation," *Journal of High Energy Physics* **2014** no. 4, (2014) 174, `arXiv:1401.4460 [hep-ph]`.

[35] S. Gritschacher, A. H. Hoang, I. Jemos, and P. Pietrulewicz, "Secondary heavy quark production in jets through mass modes," *Physical Review D* **88** no. 3, (2013) 034021, `arXiv:1302.4743 [hep-ph]`.

[36] A. K. Leibovich, Z. Ligeti, and M. B. Wise, "Comment on quark masses in SCET," *Physics Letters B* **564** no. 3-4, (2003) 231–234, `arXiv:0303099 [hep-ph]`.

[37] J. Chay, C. Kim, Y. G. Kim, and J.-P. Lee, "Soft Wilson lines in the soft-collinear effective theory," *Physical Review D* **71** no. 5, (2005) 056001, `arXiv:0412110 [hep-ph]`.

[38] A. V. Manohar and I. W. Stewart, "The zero-bin and mode factorization in quantum field theory," *Physical Review D* **76** no. 7, (2007) 074002, `arXiv:0605001 [hep-ph]`.

[39] C. C. Nishi, "Simple derivation of general Fierz-type identities," *American Journal of Physics* **73** no. 12, (2005) 1160, `arXiv:0412245 [hep-ph]`.

[40] C. W. Bauer, A. V. Manohar, and M. B. Wise, "Enhanced Nonperturbative Effects in Jet Distributions," *Physical Review Letters* **91** no. 12, (2003) 122001, `arXiv:0212255 [hep-ph]`.

[41] T. Becher and M. Neubert, "Toward a NNLO calculation of the $\bar{B} \to X_s + \gamma$ decay rate with a cut on photon energy: II. Two-loop result for the jet function," *Physics Letters B* **637** no. 4-5, (2006) 251–259, `arXiv:0603140 [hep-ph]`.

[42] T. Becher, M. Neubert, and B. D. Pecjak, "Factorization and momentum-space resummation in deep-inelastic scattering," *Journal of High Energy Physics* **2007** no. 01, (2007) 076, `arXiv:0607228 [hep-ph]`.

[43] A. Vogt, S. Moch, and J. Vermaseren, "The three-loop splitting functions in QCD: the singlet case," *Nuclear Physics B* **691** no. 1-2, (2004) 129–181, `arXiv:0404111 [hep-ph]`.

[44] B. Webber, "Renormalon phenomena in jets and hard processes," *Nuclear Physics B - Proceedings Supplements* **71** no. 1-3, (1999) 66–75, `arXiv:9712236 [hep-ph]`.

[45] Z. Ligeti, I. W. Stewart, and F. J. Tackmann, "Treating the b quark distribution function with reliable uncertainties," *Physical Review D* **78** no. 11, (2008) 114014, `arXiv:0807.1926 [hep-ph]`.

[46] V. Mateu, "Thrust and HJM distributions at N^{3}LL with power correnctions and precision determination of $\alpha_s(m_Z)$," 2011. `https://www.univie.ac.at/vienna.seminar/2011/talks/05_Mateu.pdf`. Talk at the Central European Seminar in Vienna.

[47] C. Lee and G. Sterman, "Momentum flow correlations from event shapes: Factorized soft gluons and soft-collinear effective theory," *Physical Review D* **75** no. 1, (2007) 014022, `arXiv:0611061 [hep-ph]`.

[48] G. P. Salam and D. Wicke, "Hadron masses and power corrections to event shapes," *Journal of High Energy Physics* **2001** no. 05, (2001) 061, `arXiv:0102343 [hep-ph]`.

[49] V. Mateu, I. W. Stewart, and J. Thaler, "Power corrections to event shapes with mass-dependent operators," *Physical Review D* **87** no. 1, (2013) 014025, `arXiv:1209.3781 [hep-ph]`.

[50] M. Beneke, "Renormalons," *Physics Reports* **317** no. 1-2, (1999) 1–142, arXiv:9807443 [hep-ph].

[51] I. I. Bigi, M. A. Shifman, N. G. Uraltsev, and A. I. Vainshtein, "Pole mass of the heavy quark: Perturbation theory and beyond," *Physical Review D* **50** no. 3, (1994) 2234–2246, arXiv:9402360 [hep-ph].

[52] a. H. Hoang, M. C. Smith, T. Stelzer, and S. Willenbrock, "Quarkonia and the pole mass," *Physical Review D* **59** no. 11, (1999) 114014, arXiv:9804227 [hep-ph].

[53] M. Beneke, "A quark mass definition adequate for threshold problems," *Physics Letters B* **434** no. 1-2, (1998) 115–125, arXiv:9804241 [hep-ph].

[54] A. H. Hoang and S. Kluth, "Hemisphere Soft Function at $\mathcal{O}(\alpha_s^2)$ for Dijet Production in e^+e^- Annihilation," arXiv:0806.3852 [hep-ph].

[55] S. Gritschacher, A. H. Hoang, I. Jemos, and P. Pietrulewicz, "Two loop soft function for secondary massive quarks," *Physical Review D* **89** no. 1, (2014) 014035, arXiv:1309.6251 [hep-ph].

[56] A. H. Hoang, A. Jain, I. Scimemi, and I. W. Stewart, "Infrared Renormalization-Group Flow for Heavy-Quark Masses," *Physical Review Letters* **101** no. 15, (2008) 151602, arXiv:0803.4214 [hep-ph].

[57] A. H. Hoang, A. Jain, I. Scimemi, and I. W. Stewart, "R-evolution: Improving perturbative QCD," *Physical Review D* **82** no. 1, (2009) 011501, arXiv:0908.3189 [hep-ph].

[58] K. Chetyrkin, J. Kühn, and M. Steinhauser, "RunDec: a Mathematica package for running and decoupling of the strong coupling and quark masses," *Computer Physics Communications* **133** no. 1, (2000) 43–65, arXiv:0004189 [hep-ph].

[59] A. H. Hoang, D. W. Kolodrubetz, V. Mateu, and I. W. Stewart, "C-parameter Distribution at $\mathrm{N^3LL'}$ including Power Corrections," *Physical Review D* **91** no. 9, (2014) 094017, arXiv:1411.6633 [hep-ph].

[60] R. W. L. Jones, M. Ford, G. P. Salam, H. Stenzel, and D. Wicke, "Theoretical uncertainties on α_s from event-shape variables in e^+e^- annihilations," *Journal of High Energy Physics* **2003** no. 12, (2003) 007, arXiv:hep-ph/0312016 [hep-ph].

[61] A. H. Hoang and I. W. Stewart, "Top Mass Measurements from Jets and the Tevatron Top-Quark Mass," *Nuclear Physics B - Proceedings Supplements* **185** no. C, (2008) 220–226, arXiv:0808.0222 [hep-ph].

[62] M. Butenschön, B. Dehnadi, A. Hoang, V. Mateu, M. Preisser, and I. Stewart, 2016. In Preparation.

[63] J. A. M. Vermaseren, "New features of FORM," arXiv:0010025 [math-ph].

[64] R. K. Ellis and G. Zanderighi, "Scalar one-loop integrals for QCD," *Journal of High Energy Physics* **2008** no. 02, (2008) 002, arXiv:0712.1851v4 [hep-ph].

[65] T. Huber and D. Maître, "HypExp, a Mathematica package for expanding hypergeometric functions around integer-valued parameters," *Computer Physics Communications* **175** no. 2, (2006) 122–144, arXiv:0507094 [hep-ph].

Acknowledgements

First I want to thank my supervisor Prof. André Hoang for his excellent introductory lectures and for giving me the opportunity to write this thesis in the particle physics group at the University of Vienna. Our discussions and his guidance provided an important basis for my understanding.

Very special thanks to Dr. Vicent Mateu Barreda who took the role of my unofficial co-supervisor and was always there to discuss unclear points. Working with him was always exciting as well as insightful, and I really appreciate that he invested so much time.

The members of the particle physics group were always very supportive and the familiar atmosphere is certainly something which should not be taken for granted. Especially I want to thank my office mates Moritz Preisser and Daniel Samitz for the countless discussions about nearly all topics occurring in this thesis as well as much more general topics including physics and non-physics. I also want to mention Bahman Dehnadi who was so kind to read through my thesis and who gave me many helpful comments. Additionally, I want to thank Prof. Helmut Neufeld for arousing my interest in particle physics and for promoting me from early on.

Of course, I want to thank all my colleagues and friends who contributed to my past exciting years. I could not think of a complete list, but I hope that the people I am writing about know how much I appreciate their friendship and support.

Last but not least I would like to thank my family and especially my parents, who always supported me in all thinkable ways, regardless of the types of my aims and how I wanted to pursue them. Thanks also to my girlfriend Astrid who was always there when I needed her and cheered me up at the points it was necessary.